AN INVESTIGATION OF COLOUR MEASUREMENT OF YARN DYED FABRICS BASED ON THE MULTISPECTRAL IMAGING SYSTEM

LUO LIN

Ph.D

The Hong Kong Polytechnic University

2015

The Hong Kong Polytechnic University

Institute of Textiles and Clothing

AN INVESTIGATION OF COLOUR MEASUREMENT OF YARN DYED FABRICS BASED ON THE MULTISPECTRAL IMAGING SYSTEM

LUO Lin

A Thesis Submitted in Partial Fulfilment of The Requirements for the Degree of Doctor Of Philosophy

June 2014

CERTIFICATE OF ORIGINALITY

I hereby declare that this thesis is my own work and that, to the best of my knowledge and belief, it reproduces no material previously published or written, nor material that has been accepted for the award of any other degree or diploma, except where due acknowledgement has been made in the text.

__________________________ (Signed)

______LUO Lin____________ (Name of student)

TO

MY FAMILY

Abstract

Commercial spectrophotometers and current state-of-the-art digital camera imaging systems are unable to measure the spectral reflectance of yarn dyed fabrics, the former can only measure the average reflectance of an area and the latter can only measure the tristimulus values derived from the camera's RGB responses. Multispectral imaging systems, on the other hand, have the potential to measure the reflectance of a multi-colour object, such as yarn dyed fabrics, since they can record both of the spectral and spatial information of a sample. In this thesis, colour measurement of yarn dyed fabrics based on the multispectral imaging technique is studied.

The major factor restraining multispectral imaging systems from application in textile is the difficulty of correlation the measurement results of a yarn dyed fabric to the true colours of the yarns. The spectral response of multispectral imaging systems to yarn dyed fabrics is dramatically affected by irregular 3D shapes of yarns, inter-reflection between neighbouring yarns, and interstices between weft and warp yarns. In this thesis, a novel reflection model is first proposed to estimate the interaction between light and a yarn dyed fabric surface. Surface texture, illumination occlusion and inter-reflection are taken into account. The reflection model is then verified by reducing the influence of texture on spectrophotometric colour. Derived from the proposed reflection model, reflectance and tristimulus values of yarn dyed fabrics with different texture structures are linear. The linear relationship in the reflectance space can be used to estimate a theoretical reflectance which discounts the influence of texture. Experimental results show that the impact of texture on colour for yarn dyed fabric samples in four colour centres and twenty-one texture structures can be reduced by 79%, 55%, 71% and 57%, respectively.

Based on the proposed reflection model, multispectral imaging colour measurement of yarn dyed fabrics are achieved through a series of image processing techniques, namely, colour region segmentation, solid-colour and multi-colour region detection, and weft and warp yarn segmentation. Firstly, a yarn dyed fabric image is partitioned into dominant colour regions by a Gaussian model. The Gaussian model is used to reconstruct the CIELAB colour histograms of dominant colour regions from those of yarns. A hierarchical segmentation structure is then devised to obtain dominant colour regions by combining histogram segmentation results in three colour channels. Experimental results shows the proposed approach has excellent performance for dominant colour region segmentation with high computational efficiency. Secondly, a dominant colour region is detected as solid-colour or multi-colour by CIExyY histogram distributions. Derived from the proposed reflection model, the CIExyY histogram of a multi-colour yarn dyed fabric accords with a combination of two Gaussian distributions, whereas for that of a solid-colour yarn dyed fabric, it correlated to one Gaussian distribution. Experiments on real yarn dyed fabric samples demonstrate that solid-colour and multi-colour yarn dyed fabric regions can be distinguished in terms of CIExyY histogram distribution. Finally, a multi-colour yarn dyed fabric is segmented to weft and warp yarns by a modified K-means clustering method. Experimental results indicate that the proposed method can segment weft and warp yarns in yarn dyed fabric images, with both high segmentation accuracy and fast processing speed.

In addition, the proposed reflection model can be utilized to accomplish multispectral imaging colour measurement of single yarns. Single yarns are the elemental weaving components of yarn dyed fabrics and have much simpler structures. The multispectral imaging colour of a single yarn is not affected by surface texture and inter-reflection. The colour measurement of single yarns is achieved by two steps. Firstly, a single yarn is segmented from backgrounds by an image difference method. Secondly, the reflectance of a single yarn can be specified by different weighting methods. Experimental results show that multispectral imaging colour measurement of single yarns can achieve a repeatability of 0.1185 CMC(2:1) units and a spatial reproducibility of 0.2827 CMC(2:1) units. Experimental results also show that single yarns measured by multispectral imaging systems can accomplish the similar colour matching results as solid-colour yarn dyed fabrics measured by spectrophotometers. Finally, an optical-based approach is proposed to explore the relation between the multispectral imaging colour of a single yarn and the spectrophotometric colour of the corresponding yarn card. A colour mapping equation between the single yarn and corresponding yarn card can be then found by the simplex optimal method. Experimental results show that colour difference between single yarns and corresponding yarn cards reduces from 2.97 to 1.20 CMC(2:1) units for 50 pairs of training samples and from 3.09 to 1.37 CMC(2:1) units for 50 pairs of testing samples.

List of Publications

The following journal and conference papers have been published based on the results generated from this work.

Journal papers:

1. **L. Luo**, S. J. Shao, H. L. Shen and J. H. Xin. An Unsupervised Method to Detect Dominant Colour Regions in Yarn Dyed Fabric Images. *Color. Technol.* 129(6), pp. 389-397. 2013
2. **L. Luo**, H. L. Shen, S. J. Shao and J. H. Xin. An efficient method to segment solid-colour and multi-colour regions in real yarn dyed fabric images. *Color. Technol.* (Accepted)
3. **L. Luo**, K. M. Tsang, H. L. Shen, S. J. Shao and J. H. Xin. An investigation of how the texture surface of a fabric influences its instrumental color. *Color Res. Appl.* (Accepted)
4. **L. Luo**, H. L. Shen, S. J. Shao and J. H. Xin. An effective method to segment weft and warp yarns in a multi-colour region of yarn dyed fabric images. *Color. Technol.* (Accepted)
5. **L. Luo**, H. L. Shen, S. J. Shao and J. H. Xin. Colour measurement and colour matching of single yarns based on a multispectral imaging system. *Color. Technol.* (Submitted)
6. **L. Luo**, H. L. Shen, S. J. Shao and J. H. Xin. A physically-based approach to color matching between single yarns and yarn cards. (Preparation)

Conference papers:

1. **L. Luo**, Hui-Liang Shen, Si-Jie Shao, John H. XIN. Colour matching comparison between spectrophotometric and multispectral imaging measurements. In Cross-Straits Conference on Textiles (CSTC'14). (Accpted)

2. **L. Luo**, K. M. Tsang, S. J. Shao and J. H. Xin. How the surface texture of a textile affects its colour. *Proceedings of AIC Colour 2013,12th Congress of the International Colour Association*, Newcastle, UK, pp. 1329- 1332, 2013.

3. K. M. Tsang, **L. Luo**, S. J. Shao and J. H. Xin. Texture effect on color difference evaluation by spectrophotometric and multi-spectral imaging measurement. *Proceedings of AIC Colour 2013, 12th Congress of the International Colour Association*, Newcastle, UK, pp. 1769-1772, 2013.

4. **L. Luo**, S. J. Shao, H. L. Shen and J. H. Xin. Color Representation Of Textile Fabric Using Multispectral Imaging Technology. *Proceedings of 2011 International Color Symposium in Autumn, Korea Society of Color Studies, Japan Society for the Promotion of Science*, pp.21-25, 2011.

5. J. H. Xin, S. J. Shao, **L. Luo** and H. L. Shen. Unsupervised Colour Segmentation of Textile Fabrics Constructed by Coloured Yarns. *Proceedings of AIC Colour 2011, 10th Congress of the International Colour Association*, Zurich, Switzerland, 2011.

Acknowledgements

I would like to take this opportunity to express my deepest appreciation and thanks to everyone who generously helped, supported and cared me.

First of all, I would like to express my special appreciation to my supervisor, Prof. John H. Xin. Without his supervision and constant help this dissertation would not have been possible. He has been a tremendous mentor for me. His advice on both research as well as on my career has been priceless. In addition, he generously supported me taking part in oversea exchange, which greatly opened my research horizon.

Secondly, I would like to express my heartfelt gratitude to my co-supervisor, Prof. Hui-liang Shen from Zhejiang University, China. He gave me a lot of valuable suggestions on my research and papers. His dedicated and religious attitudes to research work are always inspiring me.

Thirdly, I would like to express my gratitude towards Prof. David Clausi and Dr. Alexander Wong from University of Waterloo, Canada.

Prof. David Clausi was my supervisor when I was a visiting student in the Vision and Image Processing (VIP) Lab. Prof. David Clausi and Dr. Alexander Wong gave me great help and guidance in the research on fabric image segmentation.

Additionally, I would like to thank all my follows and colleagues in Prof. Xin's research group: Dr. Sijie Shao, Dr. Liang He, Ka Ma Tsang, Isabella Tang, YoungJoo, Shuk Yee Chiu, Wings Wang, Ka I Lee, Supannee, Vicky So, Yeeyee Kong, Huawen Hu, Jackie Lu, Xiaowei Wang, and Zongyue Yang. Thank you all for the helps on my research. In addition, I would like to thank my colleagues and friends in Prof. Shen's research group: Xiaohui Du, Wei Wang, Zhihuan Zheng, and Wei Dong. We had happy times together which I will treasure forever. Furthermore, I would like to thank all my colleagues in the VIP Lab: Fan Li, Lei Wang, Jiange Liu, Farnoud Kazemzadeh, and Shahid Haider. You gave me warm welcome and made me never feel lonely in Canada. The happy times we spent together will be my memories forever.

Finally, I would like to thank my family. Words cannot express how grateful I am to my mother, father, my mother-in law, father-in law, and my brother for all of the sacrifices that you have made on my behalf.

I would especially like to thank my beloved wife Sally. Your incredible support and being always with me motivate me to chase my dreams. I sincerely dedicate this thesis to you.

Table of Contents

List of Figures

List of Tables

Nomenclature

Abbreviations

3D	Three-Dimension
AA	Average of All Pixels
AC	Average of Pixels in the Central Area
AMCDM	Average of MCDM
CPU	Central Processing Unit
CMC	Color Measurement Committee
CIE	International Commission on Illumination
CLT	Central Limit Theorem
FCM	Fuzzy C-means Clustering
CRT	Cathode Ray Tube
ICM	Imaging Colour Measurement
LW	Lightness Weighting
MA	Maxima of All Pixels
MaxCDM	Maximum Colour Difference between each Measurement And the Mean of all Measurements
MeanCDM	Mean Colour Difference between each Measurement And the Mean of all Measurements
MinCDM	Minimum Colour Difference between each Measurement And the Mean of all Measurements
MSI	Multispectral imaging
NIST	National Institute of Standards and Technology
PC	Personal Computer
RAM	Random Access Memory
RMS	Rooted Mean Square
SCE	Specular Component Excluded
SNR	Signal-To-Noise Ratio
SPM	Spectrophotometer
std	Standard deviation
Std	Standard sample
TPI	Threads Per Inch
UV	Ultraviolet
WCD	Within-cluster Distance

Chapter 1 Introduction

This chapter first introduces the background to colour measurement of yarn dyed fabric. The objective and main contributions of this work are then addressed. Finally a general outline of the overall structure of this thesis is introduced.

1.1. Background

1.1.1. Colour Measurement of Yarn Dyed Fabrics

In textile and garment industries, accurate colour measurement is of paramount importance in quality control since colour is one of the most significant factors in causing rejection in the appeal and marketability of textile products. In general, there are two methods to measure yarn dyed fabric colour: visual evaluation and instrumental colour measurement [1]. The visual evaluation method assesses the colour of a fabric sample by human eyes, whereas the instrumental colour measurement method employs instruments to specify sample colour. The widely used instruments to measure colour of yarn dyed fabric include tristimulus colorimeters, spectrophotometers, camera imaging systems, and multispectral imaging (MSI) systems.

Traditionally, all colour assessments of fabric samples were carried out by the visual evaluation method. This method can be categorized into 'at desk' assessment and light cabinet assessment. Visual evaluation of a fabric sample is a subjective process. Inconsistent measurement results may exist among different quality inspectors.

Instrumental colours of fabric samples can be measured by two types of instruments. One is the device measuring the spectral reflectance of a fabric sample, such as a spectrophotometer and a MSI system. The other is the instrument which cannot provide spectral information but tristimulus values (a tristimulus colorimeter) or device-dependent colour (a RGB trichromatic camera imaging system). Compared with spectrophotometers and MSI systems, tristimulus colorimeters are cost-effective to conduct colour difference between standard and sample fabrics but they have limited usage in textile and garment industries [2]. For example, it is difficult to accurately identify colour match results under different light sources [3]. When colour measurements of fabric samples under different illuminants are needed, a spectral-based colour measurement system is preferred.

1.1.2. Sample-induced Effects

Sample-induced effects, such as translucency, fluorescence, and metallics, can hamper accurate colour measurement of a fabric sample [1]. There are four specific sample-induced effects when colour measurement of yarn dyed fabrics is involved. Firstly, weft and warp yarns in a yarn dyed fabric have irregular 3D shapes which cause significant colour variation among pixels. This non-uniformity leads to difficulty in yarn segmentation and colour specification. Another problem associated with 3D shape is pixels on the edge of a yarn would have extremely low luminance. Colours of these pixels may fluctuate dramatically because pixels with low luminance are extremely sensitive to noises. Secondly, there is inter-reflection between weft and warp yarns. As a consequence, the instrumental colour of a yarn changes when it is cross-woven by different coloured yarns. For example, the colour of a white yarn would be reddish when it is cross-woven by a red yarn but would be bluish when it is cross-woven by a blue yarn. Thirdly, fibers may protrude and overlap with cross-woven yarns. This would cause the colour of a yarn containing the colour information of its cross-woven yarns. Finally, there are interstices between weft and warp yarns. Colours of pixels on interstices are dramatically different from those of pixels on bulk of yarns.

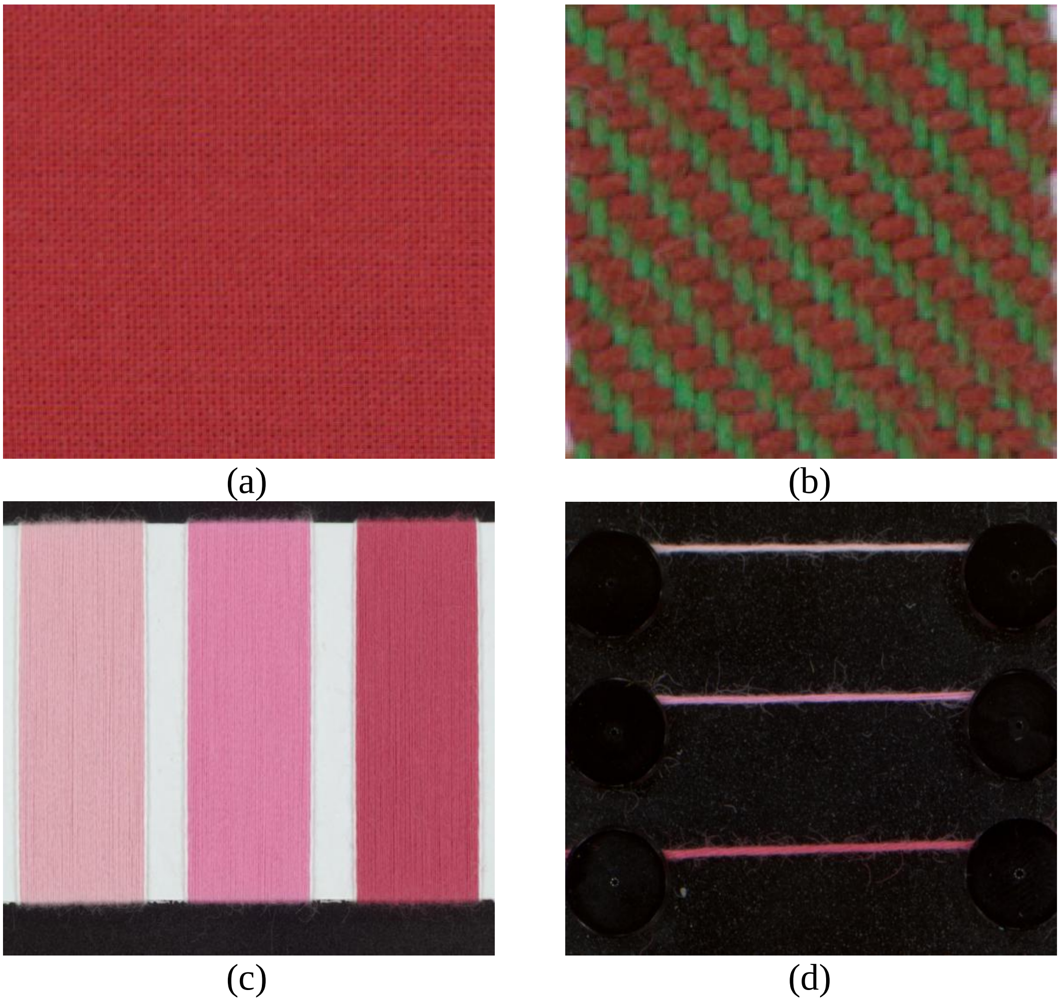

Figure 1.1 Four types of structures associated with yarn dyed fabrics: (a) solid-colour yarn dyed fabrics; (b) multi-colour yarn dyed fabrics; (c) yarn cards; (d) single yarns.

1.2. Research Objectives

As shown in Figure 1.1, there are four types of structures associated with yarn dyed fabrics: solid-colour yarn dyed fabrics, multi-colour yarn dyed fabrics, yarn cards, and single yarns. Solid-colour yarn dyed fabrics are cross-woven by same coloured weft and warp yarns. Multi-colour yarn dyed fabrics are interlaced by weft and warp yarns with different colours. A yarn card consists of single yarns weaving on a flat spool. For solid-colour yarn dyed fabrics and yarn cards, their colours can be precisely and accurately measured by a spectrophotometer. For multi-colour yarn dyed fabrics and single yarns, however, a spectrophotometer cannot directly measure their colours. One has to manually separate weft and warp yarns of a multi-colour yarn dyed fabric and then weave them on different yarn cards. Single yarns have to be carefully weaved on yarn cards before measuring their colours. Another limitation of spectrophotometers is the spatial resolution of a sample is lost. A spectrophotometer can only measure the average colour of a sample. While digital camera imaging systems can provide spatial information of a yarn dyed fabric, only the device-dependent colour, i.e., RGB colour, can be provided. Although attempts to estimate tristimulus values or reflectance from RGB values exist, the spectral information provided by a digital camera imaging system is not as accurate as that measured by a spectrophotometer. In contrast, a MSI system can provide both the spectral and spatial information of a sample. Up to present, there is no relevant work in exploring accurate colour measure of yarn dyed fabrics by MSI systems. Thus, the aim of this study is to investigate colour measurement of yarn dyed fabrics, especially multi-colour yarn dyed fabrics and single yarns, with a high degree of colour accuracy based on the multispectral imaging system.

To achieve colour measurement of multi-colour yarn dyed fabrics by a MSI system, the following image processing techniques are included:

1. To segment yarn dyed fabric images into dominant colour regions

2. To detect solid-colour and multi-colour yarn dyed fabric regions

3. To segment weft yarn and warp yarns in a multi-colour yarn dyed fabric region

To accomplish colour measurement of single yarns by a MSI system, the following methods are included:

1. To measure the colour of a single yarn

2. To map the colour of a single yarn measured by a MSI system to the colour of the corresponding yarn card measured by a spectrophotometer

The above mentioned methods to measure colours of multi-colour yarn dyed fabrics and single yarns are based on a reflection model which estimates the interaction between light and yarn dyed fabric surface. The reflection model is verified by estimating the influence of texture on colour.

1.3. Research Significance and Value

The outcome of this study would make a significant contribution to colour measurement of yarn dyed fabrics. The details are as follows:

1. The study would contribute to accurate reproduction, simulation and visualization of fabrics, especially multi-coloured ones, and hence assisting e-communication, e-commerce in textile and garment industries.

2. The study would contribute to colour quality control of yarn dyed fabrics in textile and garment industries.

3. The segmentation results of colour regions and weft and warp yarns would facilitate computer-aid structure analysis of yarn dyed fabrics.

4. The findings of this study would assist interpreting how the texture structures of fabrics and inter-reflection between yarns influence colours.

5. The colour specification methods of single yarns can be applied to specifying the colour of a 3-dimensional object captured by camera imaging systems.

6. Colour measurement results of single yarns and colour mapping between single yarns and yarn cards would assist colour reproduction based on single yarns.

1.4. Outline of the Work

This thesis has been divided into 9 chapters as outlined as follows.

Chapter 1 (this chapter) gives a brief introduction about the thesis, including the background to colour measurement of yarn dyed fabrics, objectives, significance and value of the research, and the structure of the thesis.

Chapter 2 provides a literature review related to colour measurement of yarn dyed fabrics.

In Chapter 3, the methodology of colour measurement of yarn dyed fabric is first introduced. Secondly, a new reflection model is proposed to estimate the light reflected by yarn dyed fabric surfaces. The model takes the surface texture, illuminant occlusion and inter-reflection between neighbouring yarns into account. Finally, the reflection model is verified by reducing the influence of texture on colour measured by a spectrophotometer.

Chapter 4 investigates the method to detect dominant colour regions standing out conspicuously in yarn dyed fabric images. A probabilistic model is proposed to associate the colour of a dominant colour region with colours of yarns. Based on this model, the colour histograms of a dominant colour region are first estimated from those of yarns in a yarn dyed fabric image. Then, a hierarchical segmentation structure is devised to detect dominant colour regions in the image.

Chapter 5 explores the approach to efficiently segment solid-colour and multi-colour regions in a real yarn dyed fabric image. According to the reflection model introduced in Chapter 3., the chromaticity histograms of a solid-colour region accord with one Gaussian distribution whereas those of a multi-colour region highly agree with a combination of two Gaussian distributions.

Chapter 6 studies the method to segment weft and warp yarns in multi-colour yarn dyed fabric images. Interstices between weft and warp yarns are firstly detected. A modified K-means clustering approach is then utilized to separate weft and warp yarns.

In Chapter 7, the method to accurately measure the colour of a single yarn is investigated. A single yarn is firstly segmented from background by image difference method. The colour of the single yarn is then specified by different weighting methods.

In Chapter 8, the colour mapping method between single yarns and yarn cards is studied. The spectral response of a spectrophotometer to a yarn card is firstly introduced. Secondly, the relationship between the colour of a yarn card measured by a spectrophotometer and the colour of the corresponding single yarn measured by a MSI system is modeled. Thirdly, colour mapping between single yarns and corresponding yarn cards is converted to an optimization problem. Finally, the simplex method is used to find the optimal solution.

Finally, Chapter 9 closes the thesis with a summary of the main work performed and the directions for further studies.

Chapter 2 Literature Review

A detailed literature survey is given in this chapter to provide the background information related to colour measurement of yarn dyed fabrics.

2.1. Colour Measurement Methods of Yarn Dyed Fabrics

2.1.1. Visual colour evaluation methods

There are two methods to conduct visual colour evaluation in textile and garment industries. The earliest one is so-called 'at desk' assessment, in which people evaluate fabrics at the desk or the place of manufacture. This measurement method cannot obtain reliable results owing to inconsistent viewing condition and ambient light. Another limitation of this method is that assessment results are subjective, which implies evaluation results by an inspector may be different from those by another one.

In order to eliminate the influence of inconsistent illumination on colour assessment, light cabinets [4,5] are utilized to evaluate samples in textile and garment industries. Standardized light sources, such as CIE Standard Illuminant D65 stimulators, Light source A, and Light source F [6], are applied. Consistent viewing conditions are achieved by a sloping board inside a light cabinet. However, colour assessment in a light cabinet is also a subjective process, which indicates that inconsistent measurement results may exist among different quality inspectors.

2.1.2. Tristimulus Colorimeters

A tristimulus colorimeter is the simplest instrument to measure the objective colour of a fabric [2]. Typically, a tristimulus colorimeter consists of a light source, three filters (red, green and blue) and a data processor. The light source provides consistent light to illuminate a fabric sample at the 45° angle to its normal. The three filters are specially designed to match the response of human eyes to colours. The data processor directly calculates the tristimulus values of a sample from the output of three filters.

Colorimeters are cost-effective to measure colour difference between samples. However, the absolute accuracy is limited because the light source and filters just approximately match the CIE (International Commission on Illumination) definitions [3]. Another limitation is incapacity to metamerism [3]. Metamerism can be defined as a pair of colours having the same tristimulus values but different spectral stimuli [7]. Metamerism can be also termed that the visual match of two samples is reached for an observer under specified viewing conditions but their spectral stimuli are different [8]. Metamerism problem implies that tristimulus values of a fabric sample measured by a colorimeter under one illuminant cannot be utilized to predict tristimulus values of the sample illuminated by other illuminants.

2.1.3. Spectrophotometers

Spectrophotometers are the most widely used instruments to measure instrumental colours of fabric samples in textile and garment industries. A spectrophotometer primarily consists of four parts: a light source, a spectral analyzer, a detector array and a data post-processing system. The light source provides consistent illumination at a CIE-recommended illuminating and viewing geometry[9]. The spectral analyzer splits the light reflected by a sample into spectral components. The splitting accuracy of a spectral analyzer determines the performance characteristics of a spectrophotometer. The detector array is composed of a number of photosensitive diodes placed side by side and insulated from one another. They record the spectral components of the light reflected by a sample. The data post-processing system is responsible for data processing tasks such as colour conversion from reflectance to CIE colour spaces and colour difference calculation.

A spectrophotometer can provide accurate and precise spectral resolution for fabric samples. The spectral reflectance is independent of characteristics of acquisition systems and illuminants, i.e., the measurement results of a spectrophotometer can be transformed to any colour space and can be interpreted for any other illuminants.

However, there are three limitations when spectrophotometers are employed to measure colours of yarn dyed fabrics. Firstly, spectrophotometers assume the colour of a yarn dyed fabric is solid, i.e., weft and warp yarns have the same colour. In order to measure the colour of a multi-colour yarn dyed fabric, one needs to manually separate weft and warp yarns. It is time and energy consuming, and prone to error because of inconsistency in preparing yarn samples. Secondly, the size of a measured sample is limited. In general, the aperture size of a spectrophotometer is 3mm to 26mm. As a consequence, spectrophotometers cannot be utilized to measure colours of samples with size smaller than 3mm. Finally, spectrophotometers cannot provide the spatial resolution of a sample. A spectrophotometer yields a result of the averaged reflection within its aperture. Thus, the texture information is lost when a spectrophotometer is used.

A large number of spectrophotometers are commercially available, such as products provided by Datacolor International, X-Rite, Hunter Lab, and Konica Minolta. The widely used spectrophotometers in textile and garment industries include ColorEye 7000A from X-Rite Colour Management Co. Ltd and Datacolor 600 and 650 from Datacolor International.

2.1.4. Digital camera imaging systems

Digital camera imaging systems are developed to obtain the spatial information of a sample when measuring its colour. A digital camera imaging system stimulates the colour vision response of human eyes to a sample just as a tristimulus colorimeter does [10]. However, the three filters and the data processor are replaced by a digital camera. The camera is used to output the colour image of a sample in the red (R), green (G), and blue (B) channels. Each pixel of the image is a vector in a three dimensional space, made up from the red, green and blue channels [11]. A light source box with one or more standard illuminants is used to provide controlled and consistent illumination.

Digital camera imaging systems can conduct colorimetric measurement on samples with complicated patterns, texture structures and multi-colour components, a task which is impossible for spectrophotometers [12,13]. Camera imaging systems are non-contact systems which do not destruct samples unlike spectrophotometers do. They do not limit the size of a sample and can measure solid-colours and multi-colours.

However, camera imaging systems suffer from three limitations. Firstly, the output of a digital camera is device-dependent colour, i.e., the colours measured by different camera imaging systems are not identical [14]. In order to employ a camera imaging system as a tristimulus colorimeter, the RGB output data must be transformed into device-independent coordinates, usually the tristimulus values. This transformation process is called camera characterisation which determines the overall measurement accuracy of a digital camera imaging system [12]. Different camera characterisation methods have been proposed by Berns *et al.* [15,16] , Mullikin *et al.* [17], Pointer *et al.* [18], Hong *et al.* [19], Barnard and Funt [20], Green [21],Verdu *et al.* [22], Cheung *et al.* [23], Ji *et al.* [24]. Secondly, the measurement results of a sample under one illuminant cannot be used to predict the colour illuminated by other illuminants [3,14]. In order to detect the instrumental colours of a sample illuminated by different lighting sources, several standard illuminants are needed in a digital camera imaging system. Finally, the ability of a digital camera imaging system to detect eye-camera metamerism is insufficient. Eye-camera metamerism is defined as colours of two samples appearing the same to human eyes but being different by digital camera imaging systems [17,25]. A digital camera imaging system may detect the eye-camera metamerism for one set of training samples but may not for other testing samples [12]. The results from characterisation methods are derived to perform best for just training samples. Some testing samples may yield bad eye-camera metamerism. While characterised digital camera imaging systems have been used in colour appearance assessment [26] and colour fastness evaluation [27,28,29,30], its spectral accuracy hampers increasing applications in the textile and garment industries.

Three digital camera imaging systems are commercially available, DigiEye system from VeriVide Limited [31], CAM 500 system from Tintometer Group [32], and Viewport system from Datacolor [33]. DigiEye can output the tristimulus values and spectral data which are recovered from RGB values. CAM 500 can measure the surface colour of textiles and assess their visual appearance. Datacolor Viewport™ can capture the RGB images of non-solid samples and conduct color matching.

2.1.5. Multispectral imaging systems

In order to fully understand the colour of a fabric, both of the spatial information and spectral information are important. The spectral information can avoid illuminant metamerism and yield illuminant-independent colour. The spatial information can help understand important knowledge of the sample, such as texture and gloss which have great impacts on how human beings interpret colours. Multispectral imaging (MSI) systems can provide both the spectral and spatial information of a sample [34,35,36,37,38]. MSI systems were initially developed for remote sensing, astrophysics and military applications [39] but rapidly used in other fields, such as medicine [40], agriculture [41], art conservation [42], and skin analysis [43].

Typically, a MSI system consists of four parts: an illuminating system, a monochrome digital camera, a filter system including several filters (more than 3), and a data post-processing software. The illuminating system is responsible for providing controlled and consistent light. The monochrome digital camera captures sample images in different bandwidths. The filter system allows light passing though in a particular bandwidth. The powerful data post-processing software exploits the information contained in the spectral and spatial data. One of challenges for a MSI system is to reconstruct reflectance of samples from the response of a monochrome digital camera. Several reflectance reconstruction techniques have been proposed. These methods include Wiener estimation [44,45,46,47,48], pseudoinverse method [23,35,49], finite-dimensional modeling [23], and hybrid-based method [50]. Another challenge is the volume spectral and spatial data which are difficult to handle, view and interpret [51]. For example, one classical task is to group pixels with similar characteristics into regions by their spectral signatures.

One MSI system is commercially available, can:scan and can:view from Caddon printing & imaging GmbH [52]. Can: scan can capture the spectral colours of samples with complex coloured patterns and structured surfaces. Can:view can display the sample images measured by can:scan.

While multispectral imaging systems can accurately provide both of the spectral and spatial information of yarn dyed fabrics, they cannot be directly used to conduct colour matching and colour reproduction of yarn dyed fabrics. The spectral response of a MSI system to a fabric sample can be vastly influenced by many factors, such as texture, glossy, areal density and linear density. The major factor restraining MSI systems from application in textile is how to correlate the measurement results of a fabric sample to its true colour. There is no physical model which can estimate the influence of the above mentioned factors on the colour of a yarn dyed fabric measured by a MSI system, i.e., the reflection from the yarn dyed fabric cannot be estimated.

2.2. The Employed Multispectral Imaging System

A MSI system, namely Imaging Colour Measurement (ICM), was developed to measure colours of yarn dyed fabrics. The ICM system was composed by a monochrome digital camera, a filter wheel with 16 narrowband filters, an autofocus step motor and a circular light source. The monochrome digital camera captured an image with 1040*1392 pixels. The filter wheel split the spectrum of visible light into 16 bands. The step motor controlled the focus of the camera by rotating its aperture. The circular light source provided a 45°/0° CIE D65 illumination which can eliminate the influence of gloss on colour.

The focus of the monochrome camera was auto-adjusted by the algorithm proposed by Shen *et al.* [53]. The optimal focus position maximizes the symmetry of the focus measure distribution and is determined by distance metrics. The reflectance of a yarn dyed fabric sample was reconstructed by the adaptive Wiener estimation algorithm [48]. The proposed reflectance reconstruction method adaptively selected training samples for the autocorrelation matrix calculation in

Wiener estimation, without a prior knowledge of the spectral information of the samples being imaged [48].

Table 2.1 The technical specification of the ICM system

Repeatability (NIST White Tiles)	Average: 0.03 CMC(2:1) units
Uniformity of illumination (NIST White Tiles)	Maximum: 0.1 CMC(2:1) units
	Average: 0.01 CMC(2:1) units
Inter-instrument agreement between ICM system and benchmark reflection spectrophotometers	Average spectral reflectance accuracy: 0.0024 RMS errors
	Maximum spectral reflectance accuracy: 0.0089 RMS errors
	Average colorimetric accuracy: 0.23 CMC(2:1) units
	Maximum colorimetric accuracy: 0.62 CMC(2:1) units
Measurement time	Less than 25 seconds
Spectral wavelength accuracy	Less than 1 nm
Optical configuration	$45^0/0^0$
Spectral range	400 nm - 700 nm
Measurement sizes	5.5 cm*7.5 cm

As shown in Table 2.1, the repeatability of the ICM system on measuring the National Institute of Standards and Technology (NIST) white tiles is 0.03 CMC(2:1) units. When the ICM system is used to measure the NIST white tiles, the maximum and average colorimetric errors of uniformity are 0.1 and 0.01 CMC(2:1) units. The inter-instrument agreements between the ICM system and a benchmark reflection spectrophotometer (Datacolor 650) are 0.0089 and 0.0024

RMS (rooted mean square) with the maximum and average spectral reflectance accuracy errors when the Digital Colorchecker SG from Gretagmacbeth were used. The maximum and average colorimetric accuracy are 0.62 and 0.23 CMC(2:1) units compared to the benchmark spectrophotometer.

2.3. Reflection Models

2.3.1. Dichromatic Reflection Model

The dichromatic reflection model [54] is proposed to estimate the reflection from inhomogeneous dielectric surfaces, such as paints, wood, papers and plastics. According to the dichromatic reflection model, reflection from an inhomogeneous dielectric surface can be decomposed into two additive parts: body reflection and interface reflection [54]. Body reflection occurs due to interaction between incident light and pigment particles within a material. Interface reflection arises at the interface between two materials with different refractive indexes. Body reflection modifies the spectral distribution of the light and reflects in random directions. Body reflection is also called diffuse reflection and represents the characteristics of materials. Interface reflection is also called specular reflection, i.e., it is highly directional. Interface reflection only depends on incident light. Body and interface reflections can be further separated into two independent components [54]: a wavelength factor and a geometric term.

In order to reveal the true colour of a sample, the interface reflection component should be removed from the measured colour because this component only contains the colour information of light source. A large number of attempts to separate body and interface reflections have been studied by Artusi *et al.* [55], Mallick *et al.* [56], Shen *et al.* [57, 58,59], Tan and Ikeuchi [60], Yang *et al.* [61].

2.3.2. Phong Reflection Model

The Phong reflection model proposed by Phong [62] is an empirical model to estimate the local illumination of points on a surface. The Phong reflection model is widely used computer graphics software to shade surfaces [63,64,65,66,67]. The Phong reflection model describes the reflected light by a surface as a combination of ambient light, diffuse reflected light, and specular reflected light:

$$I_p = k_a i_a + \sum_{m \in lights} (k_d < \hat{L}_m, \hat{N} > i_{m,d} + k_s < \hat{R}_m, \hat{V} >^{\alpha} i_{m,s}) \quad (2\text{- }1)$$

where I_p, i_a, $i_{m,d}$, and $i_{m,s}$ denote the intensities of a surface point, ambient lighting, diffuse and specular components of the light source m, k_a, k_d, and k_s represent the ambient reflection, diffuse reflection, and specular reflection constants, $\hat{L}_m$ and $\hat{R}_m$ express the illuminant direction and the direction of the perfectly reflected ray related to the light source, $\hat{N}$, $\hat{V}$ and α are the normal at the point, the viewer direction, and the shininess constant for the surface, $< \hat{A}, \hat{B} >$ denotes the dot product of vectors $\hat{A}$ and $\hat{B}$.

2.3.3. Oren–Nayar Reflectance Model

The Oren–Nayar reflectance model [68] is proposed by Oren and Nayar to estimate the diffuse reflection from rough surfaces. The Oren–Nayar reflectance model is widely used to predict the appearance of natural surfaces, such as concrete [69] and sand [70,71]. According to the Oren–Nayar reflectance model, the radiance of the reflected light L_r can be modeled as :

$$L_r = \frac{\rho}{\pi} \cdot \cos\theta_i \cdot \{A + B \cdot \max[0, \cos(\phi_i - \phi_r)] \cdot \sin\alpha \cdot \tan\beta]\} \cdot L_i \quad (2\text{- }2)$$

where L_i and ρ denote the radiance of the incoming light and the albedo of the surface, (θ_i, ϕ_i) and (θ_r, ϕ_r) represent the directions of incident light and viewing. A, B, α, and β are determined by the following equations:

$$\begin{cases} A = 1 - 0.5 \cdot \dfrac{\sigma^2}{\sigma^2 + 0.33} \\ B = 0.45 \cdot \dfrac{\sigma^2}{\sigma^2 + 0.09} \\ \alpha = \max(\theta_i, \theta_r) \\ \beta = \min(\theta_i, \theta_r) \end{cases} \tag{2- 3}$$

where the measure of the roughness of the surface, determined as the variance of a Gaussian slope distribution of the surface.

When a surface is flat, i.e., $\sigma = 0$, we have $A = 1$ and $B = 0$. The Nayar reflectance model is simplified to the Lambertian model [72]:

$$L_r = \frac{\rho}{\pi} \cdot \cos\theta_i \cdot L_i \tag{2- 4}$$

2.4. Influence of Texture on Colour

The surface texture of a fabric is one of the most important factors to influence its colour. A number of studies have been conducted to explore how the texture of a fabric affects its colour. These studies can be divided into three directions: the influence of texture on colour difference [73,74,75,76,77,78,79,80], the influence of texture on colour attributes [117,81], and the relationship between texture descriptors and colours [114,115,116,82].

Kuehni and Marcus [73] were the pioneers in studying the effect of texture structures of fabrics on their visual colour difference. They found the minimum value to perceive a colour difference between different fabric texture structures under standardized laboratory conditions was one CIELAB unit. Xin *et al.* [74] investigated the effect of texture structures on visual colour difference using 15 texture images captured by a high performance scanner and simulated on CRT. They found the visual colour difference of the textured pairs reduced around 35% to 43% compared with the solid colour pair. Han *et al.* [75] explored the influence of texture structures of fabrics on their colours using real fabric samples and their reproduced CRT pairs. They found the visual colour difference of textured sample pairs accorded with that of physical samples better than no-textured colour pairs. Kandi and Tehran [76] explored the impact of surface texture on visual and instrumental colour difference using knitted polyester fabrics with eight different texture structures. The visual colours were assessed by the greyscale method [83]. The instrumental colour difference were calculated by formulas CIEDE2000 (2:1), CMC (2:1), CIE94 (2:1) and CIELAB. They found the texture structures had a significant influence on the performance of colour difference formulae and the CIEDE2000 (2:1) formula had the best ability to predict the visual colour difference for the textured textiles. Montag and Berns [77] employed simulated texture of thread wound on a card to explore the influence of texture on suprathreshold lightness tolerances. They found lightness tolerances were larger when the lightness values of the samples increased. They concluded that the factor of the effect of texture on tolerance thresholds was almost 2 for textured samples as compared to the uniform samples. Huertas *et al.* [78,79,80] studied the influence of texture structures on the visual suprathreshold colour tolerances of lightness, chroma and hue by simulated randomly distributed dots over homogeneous samples. They found the random-dot textures increased the lightness tolerance more than the chroma and hue ones.

In order to fully understand the influence of texture structures on colour, the lightness, chroma and hue difference of textured fabrics were analyzed. Shao *et al.* [117] investigated the influence of texture structures on instrumental and visual colours using knitted fabrics. They found that there was strong inconsistency between instrumental and visual colours. The absolute difference between textured and jersey samples in the lightness, chroma and hue attributes was also evaluated. They concluded that texture structures had an impact on lightness, chroma and hue. Luo *et al.* [81] investigated how the surface texture of a fabric influences its luminance and chromaticity coordinates. They concluded that colour difference between fabrics with different texture structures was mainly caused by luminance rather than chromaticity.

To explore how texture structures affect colours, the relationship between textures of fabrics and their instrumental and visual colours was studied. In general, a group of fabric samples with different texture structures are first collected to conduct an experiment. These samples are then measured by a spectrophotometer to obtain their instrumental colours. The visual difference between a standard sample and batch samples is assessed by subjects to study the influence of texture on visual colour. The greyscale method [83] is commonly used to perform this visual assessment. The textures of these samples are quantified by different texture descriptors. Finally, the relationship between the instrumental or visual colour difference and the texture are established. Xin *et al.* [114] employed the half-width of histogram as the texture descriptor and found there was high correlation between the visual colour difference and the texture feature. Kandi *et al.* [115] investigated the relationship between the instrumental and visual colour difference of fabrics and their texture parameters described by Gabor functions. They found there was good correlation between the visual colour difference and Gabor function values. Kitaguchi *et al.* [116] studied the relationship between the visual assessment results and several texture descriptors such as the co-occurrence matrices, run length, grey level difference and neighbouring grey level dependence statistics. They concluded that there was good relationship between visual assessment results and texture features from co-occurrence and grey level difference but poor correlation between perceptual results and textures described by run length and neighbouring grey level dependence statistics. Trussell *et al.* [82] investigated the mathematical model associating visual colour and texture. The model was based on a combination of the optical transfer function of the human eye and its interaction with the power distribution of the texture pattern in the frequency domain.

The influence of texture on instrumental colour measured in different geometries was also studied by Kandi *et al.* [84]. Colour changes with texture structures for the d/8 and 45/0 geometries were evaluated. It was found that the influences of texture on instrumental colour measured in d/8 geometry and 45/0 are similar.

2.5. Colour Region Segmentation of Fabrics

Two approaches have been investigated to segment colour regions in fabric images. One approach applied clustering algorithms and the other was based on classical image segmentation methods of still images.

2.5.1. Clustering Algorithms

Clustering is a method to divide data into classes so that items in the same class are as similar as possible and items in different classes are as dissimilar as possible [85]. Clustering methods can be categorized into hard clustering and fuzzy clustering [85]. In the hard clustering method, a hard partition is determined to divide each data element into exactly one class. In the fuzzy clustering method, data elements can belong to more than one class and a set of membership functions are used to indicate the strength of data elements associating with particular classes. One of the most widely used fuzzy clustering algorithms is the fuzzy C-means clustering (FCM) algorithm [85, 86]. Some researchers have employed the FCM algorithm to segment fabric colour. Pan *et al.* [87,88] used the FCM algorithm to obtain the number of yarn colours and layouts of yarns. Kuo *et al.* [89] employed the FCM algorithm in the RGB colour space to achieve colour segmentation of printed fabrics.

2.5.2. Segmentation Methods of Still Images

The colour region segmentation of a fabric image can be viewed as a particular application of still image segmentation techniques in textile and garment fields. The segmentation methods of still images can be mainly categorized into: histogram-based methods [90,91], region-based methods [92,93,94,95,96], edge-based methods [97,98,99], hybrid-based methods [100,101,102], and graph-based methods [103,104].

Histogram-based segmentation methods

The histogram of an image is a discrete function which counts the number of pixels with the same value in the image [105]. Histogram-based segmentation methods assume that pixels whose values are within a certain range belong to the same class, i.e., an object and its background would correspond to different peaks of the histogram [106]. A threshold can be chosen as the valley between two peaks to segment an object from its background.

Histogram-based segmentation methods are computationally efficient. Good segmentation results can be achieved for images including distinct objects. However, histogram-based segmentation methods neglect the spatial information of an image. As a result, it cannot guarantee that segmentation results are contiguous. Another limitation of histogram-based segmentation method is the difficulty to automatically determine segmentation thresholds from a complicated histogram.

Region-based segmentation methods

Region-based segmentation methods group pixels into different regions by defined properties. Two approaches are included: region growing approaches [92,93] and region split-merge approaches [94,95,96]. Region growing approaches start from some seed points, and examine their neighbouring pixels, then attach pixels to the region provided attributes of these pixels are within a predefined range. The process is iterated until all pixels in an image have been assigned to a region. In contrast, region split-merge approaches start from the root of a tree which represents the whole image. A parent node of the tree is split into four son nodes if the parent node is non-uniform (the splitting process). Inversely, son nodes are merged if they are homogeneous (the merging process). The splitting and merging process continues recursively until no further splitting or merging are possible.

Region-based methods take spatial information into account during segmentation and can correctly separate regions that have the same defined properties. However, the segmentation performance of region-based methods depends on the manually tuned thresholds and initial seeds. Another disadvantage is the heavy computation.

Edge-based segmentation methods

Image segmentation can also be achieved by detecting object edge. Edge-based segmentation methods measure the dissimilarity, or sharp changes, between neighbouring pixels. Sharp change between pixels is believed corresponding to discontinuities in depth and surface orientation, changes in material properties and variation in scene illumination [107]. Ideally, edge detection results in a set of connected points that indicate the boundaries of objects. However, Over-segmentation would occur in edge-based segmentation methods if edges are ill-defined [108].

Hybrid-based segmentation methods

Hybrid-based segmentation methods combine region-based methods and edge-based methods to obtain good segmentation results. Unfortunately, it still remains problematic to fuse region and edge features. `

Graph-based segmentation methods

Graph-based image segmentation techniques view an image as a graph in which each node corresponds to a pixel and edges link neighbouring pixels. Each edge is valued as a weight to show the relation strength between pixels it connects [104]. The objective of segmentation result is to find minimum cuts in the graph. Graph-based methods suffer from high computational complexity.

2.6. Colour Reproduction of Yarn Dyed Fabrics

In textile and garment industries, the recipe to dye yarns constructing a yarn dyed fabric is predicted by the colorant formulation system based on spectrophotometric measurements [109]. Five steps are included to estimate the dye recipe accurately matching for a standard solid-colour yarn dyed fabric or yarn card. Firstly, a dye calibration database is built for different dyes based on the Kubelka-Munk model [110]. The dye calibration database finds the relationship between dye concentrations and sample K/S values. Dyestuffs with different concentrations are used to dye yarns. The reflectance values of these dyed samples are then measured by a spectrophotometer, followed by K/S calculation. The relation between the dyestuff concentrations and the K/S values can be found by regression methods. Based on the dye database, secondly, several recipe candidates to match the colour of a standard sample are predicted by the colorant formulation system. Thirdly, a batch sample is carefully dyed based on the best recipe among others. Fourthly, computer colour matching experiments between the standard and batch samples are conducted to verify the recipe accuracy. Finally, a recipe is corrected when the coloration results are not satisfied, i.e., the colour difference between the standard and a batch sample is larger than a tolerance.

2.7. Conclusion

In this chapter, a detailed literature survey is given to provide the background information related to colour measurement of yarn dyed fabrics. Firstly, methods to conduct colour measurement of yarn dyed fabrics and the employed multispectral imaging system are introduced. Secondly, reflection models to estimate the interaction between light and sample surfaces are briefly presented. Thirdly, detail reviews of the influence of texture on colour are given. Fourthly, colour region segmentation algorithms are detailed reviewed. Finally, colour reproduction of yarn dyed fabrics is described.

Chapter 3 Methodology of Colour Measurement of Yarn Dyed Fabrics

This chapter first introduces the methodology of colour measurement of yarn dyed fabrics based on the multispectral imaging technique. Secondly, a novel reflection model is proposed to estimate the light reflected by a yarn dyed fabric surface. Finally, the reflection model is then verified by reducing the influence of texture on colour measured by spectrophotometers.

3.1. Colour Measurement of Yarn Dyed Fabrics

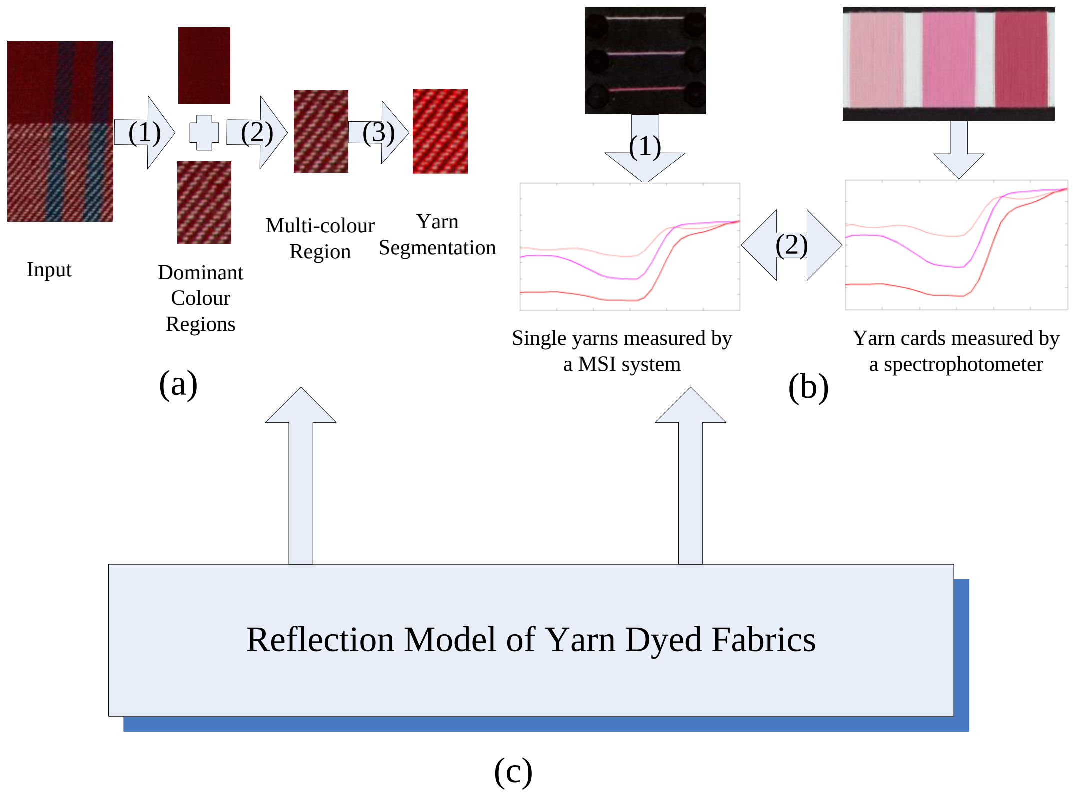

(a)-(1): dominant colour region segmentation

(a)-(2): solid-colour and multi-colour region detection

(a)-(3): weft and warp yarn segmentation

(b)-(1): colour measurement of single yarns

(b)-(2): colour mapping between single yarns and yarn cards

Figure 3.1 The colour measurement schematic of yarn dyed fabrics: (a) colour measurement of multi-colour yarn dyed fabrics; (b) colour measurement of single yarns; (c) reflection model of yarn dyed fabrics.

This thesis focuses on colour measurement of multi-colour yarn dyed fabrics and yarn cards based on the multispectral imaging technique since colours of solid-colour yarn dyed fabrics and yarn cards can be acquired by spectrophotometers. A novel reflection model is proposed to estimate the light reflected by a yarn dyed fabric surface. Based on the reflection model, colour measurement of multi-colour yarn dyed fabrics includes three steps: dominant colour region segmentation, solid-colour and multi-colour region detection, and weft and warp yarn segmentation, as shown in Figure 3.1a. Figure 3.1b shows that two steps are included in colour measurement of single yarns: single yarn segmentation and colour mapping between single yarns and yarn cards. The following sections of this chapter introduce the proposed reflection model. The following chapters investigate the methods for colour measurement of multi-colour yarn dyed fabrics and single yarns.

3.2. Reflection Model of Yarn Dyed Fabrics

According to the dichromatic reflection model [54], reflection from an inhomogeneous dielectric surface is composed by body reflection $I_b(\lambda)$, and interface reflection $I_i(\lambda)$, which can be modeled as:

$$\begin{aligned} L(\lambda) &= I_b(\lambda) + I_i(\lambda) \\ &= m_b E(\lambda) R_1(\lambda) + m_i E(\lambda) \end{aligned} \tag{3.1}$$

where $L(\lambda)$ and λ denote the radiance of a sample and the wavelength, $E(\lambda)$ and $R_1(\lambda)$ represent the illuminant spectrum and the nominal reflectance of the sample, m_b and m_i are the geometric terms for body and interface reflections. m_b and m_i are determined by the geometry between the illuminant and the sample.

As mentioned in Section 2.3, the body reflection component relates to the colour of a yarn dyed fabric. The body and interface reflection components can be separated by different methods. Consequently, only the body reflection component is considered in the proposed reflection model. For a yarn dyed fabric with only diffuse reflection, the radiance at the surface position (p_Y, q_Y), $L(\lambda, p_Y, q_Y)$, is a product of a geometric term $m_b(p_Y, q_Y)$ and a wavelength factor $E(\lambda, p_Y, q_Y)R_1(\lambda)$:

$$L(\lambda, p_Y, q_Y) = m_b(p_Y, q_Y)E(\lambda, p_Y, q_Y)R_1(\lambda) \tag{3.2}$$

where $E(\lambda, p_Y, q_Y)$ and $R_1(\lambda)$ denote the irradiance at (p_Y, q_Y) and the nominal reflectance of the measured yarn.

As shown in Figure 3.2, two illuminants shine light on (p_Y, q_Y) [111]: a system illuminant and an ambient illuminant. The system illuminant is the light source of a colour measurement instrument, yielding beams $E_D(\lambda, p_Y, q_Y)$ as illustrated by the red lines in Figure 3.2.

The ambient illuminant stems from light reflected by neighbouring yarns, $E_A(\lambda, p_Y, q_Y)$, as plotted by the blue line in Figure 3.2.

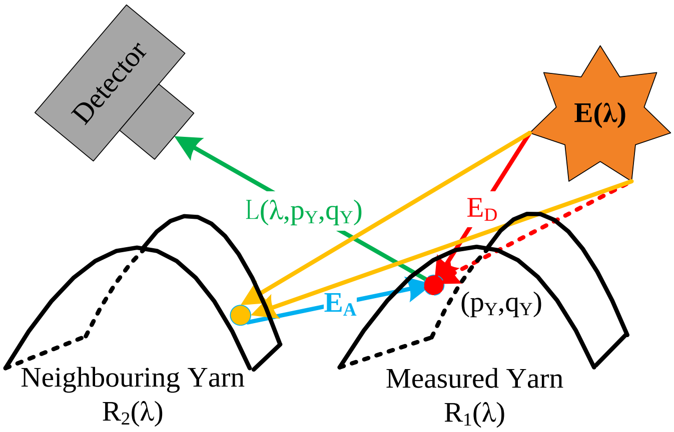

Figure 3.2 The reflection schematic in a yarn dyed fabric.

The light from the system illuminant may be masked and shadowed, as shown by the dotted red line in Figure 3.2. An occlusion term $H(p_Y, q_Y) \in [0,1]$ is used to indicate the percent of the light reaching (p_Y, q_Y):

$$E_D(\lambda, p_Y, q_Y) = H(p_Y, q_Y)E(\lambda) \tag{3.3}$$

where $E(\lambda)$ denotes the system illuminant spectrum. $H(p_Y, q_Y) = 0$ represents that the light is completely occluded. In contrast, $H(p_Y, q_Y) = 1$ refers to no occlusion.

The light from the ambient illuminant are integrated over the entire hemisphere $\Omega(p_Y, q_Y)$:

$$E_A(\lambda, p_Y, q_Y) = \int_{\Omega(p_Y, q_Y)} m_b(\vec{i}) E(\lambda, \vec{i}) R_2(\lambda) d\vec{i} \tag{3.4}$$

where $\vec{i}$ denotes the incident angle of ambient light, $m_b(\vec{i})$ and $E(\lambda, \vec{i})$ represent the geometric term and reflected light from the direction $\vec{i}$, $R_2(\lambda)$ is the nominal reflectance of the neighbouring yarn.

$E(\lambda, \vec{i})$ is also composed by two parts, light from the system illuminant $E_{DA}(\lambda, \vec{i})$ and light from ambient illuminant $E_{AA}(\lambda, \vec{i})$. $E_{DA}(\lambda, \vec{i})$ may be also masked and occluded. We have:

$$\begin{aligned} E_A(\lambda, p_Y, q_Y) &= \int_{\Omega(p_Y, q_Y)} m_b(\vec{i}) R_2(\lambda) [E_{DA}(\lambda, \vec{i}) + E_{AA}(\lambda, \vec{i})] d\vec{i} \\ &= E(\lambda) R_2(\lambda) \int_{\Omega(p_Y, q_Y)} m_b(\vec{i}) H(\vec{i}) d\vec{i} \\ &+ R_2(\lambda) \int_{\Omega(p_Y, q_Y)} m_b(\vec{i}) E_{AA}(\lambda, \vec{i}) d\vec{i} \end{aligned} \tag{3.5}$$

where $H(\vec{i})$ represents the percentage of beams from the system illuminant reaching the corresponding position on the neighbouring yarn.

Substituting Eqn (3.3) and Eqn (3.5) into Eqn (3.2), we get:

$$\begin{aligned} L(\lambda, p_Y, q_Y) &= m_b(p_Y, q_Y) R_1(\lambda) [E_D(\lambda, p_Y, q_Y) + E_A(\lambda, p_Y, q_Y)] \\ &= m_b(p_Y, q_Y) H(p_Y, q_Y) E(\lambda) R_1(\lambda) \\ &+ m_b(p_Y, q_Y) E(\lambda) R_1(\lambda) R_2(\lambda) \int_{\Omega(p_Y, q_Y)} m_b(\vec{i}) H(\vec{i}) d\vec{i} \\ &+ m_b(p_Y, q_Y) R_1(\lambda) R_2(\lambda) \int_{\Omega(p_Y, q_Y)} m_b(\vec{i}) E_{AA}(\lambda, \vec{i}) d\vec{i} \end{aligned} \tag{3.6}$$

According to the one-bounce model [112], inter-reflection diminishes dramatically with each bounce. Therefore, the last term of Eqn (3.6) can be assumed to be negligible since it represents two bounces of inter-reflection. If we represent the ambient integral in the second term of Eqn (3.6) as an ambient coefficient $A(p_Y, q_Y)$, i.e., $A(p_Y, q_Y) = \int_{\Omega(p_Y, q_Y)} m_b(\vec{i}) H(\vec{i}) d\vec{i}$, we have:

$$\begin{aligned} L(\lambda, p_Y, q_Y) = {} & m_b(p_Y, q_Y) H(p_Y, q_Y) E(\lambda) R_1(\lambda) \\ & + m_b(p_Y, q_Y) A(p_Y, q_Y) E(\lambda) R_1(\lambda) R_2(\lambda) \end{aligned} \tag{3.7}$$

Eqn (3.7) expresses that the light reflected by a yarn dyed fabric is influenced by a yarn surface coefficient $m_b(p_Y, q_Y)$, a system illuminant occlusion coefficient $H(p_Y, q_Y)$ and an inter-reflection coefficient $A(p_Y, q_Y)$. These three coefficients change with surface positions of a yarn dyed fabric. According to the Oren–Nayar reflectance model [113], the yarn surface parameter can be specified as $m_b(p_Y, q_Y) = \cos(\theta)$, where θ is the incident angle at (p_Y, q_Y). Consequently, the surface texture of a yarn dyed fabric can significantly influence $m_b(p_Y, q_Y)$. $H(p_Y, q_Y)$ and $A(p_Y, q_Y)$ represent effects of the system light source and neighbouring yarns on the light reflected by a yarn dyed fabric.

3.3. Reflection Model Verification

The proposed reflection model is verified by estimating how the texture of a yarn dyed fabric dictates its instrumental colour measured by a spectrophotometer.

3.3.1. Background

Texture is one of the most important factors in affecting the colour of a fabric in textile and garment industries [114,115,116,117]. While fabric samples normally have different texture structures, the underlying assumption is that fabrics are flat when a piece of equipment is used to measure their colours [118]. The most widely used instruments in textile and garment industries to achieve colour measurement are spectrophotometers. A spectrophotometer can be considered as a combination of two subsystems: an optical subsystem and a detection subsystem. The optical subsystem generates light to illuminate a sample. It is composed of light source, integrating sphere, and lenses. The detection subsystem measures the radiant flux of the light reflected by a sample. It consists of detector array and spectral analyzer. Generally, there are two sets of optical and detection subsystems within a spectrophotometer: a set of sample subsystem and a set of reference subsystem. The sample subsystem illuminates a fabric sample and detects its reflected radiant flux. The reference subsystem generates and detects a reference beam. The ratio of the radiant flux reflected by the sample to that of the reference beam is defined as the spectral reflectance of the sample. According to the proposed reflection model in Section 3.1, the surface texture of a yarn dyed fabric has a great impact on both its instrumental and perceived colors. Thus, yarn dyed fabrics with different texture structures but cross-woven by same coloured yarns have different colours when a spectrophotometer is used.

While the impact of texture on colour has been studied for more than three decades, quantitative relationships, such as linearity or correlation, between texture and instrumental colour, including colour difference, lightness, chroma and hue, are found difficult to be established.

3.3.2. Influence of Texture on Colour

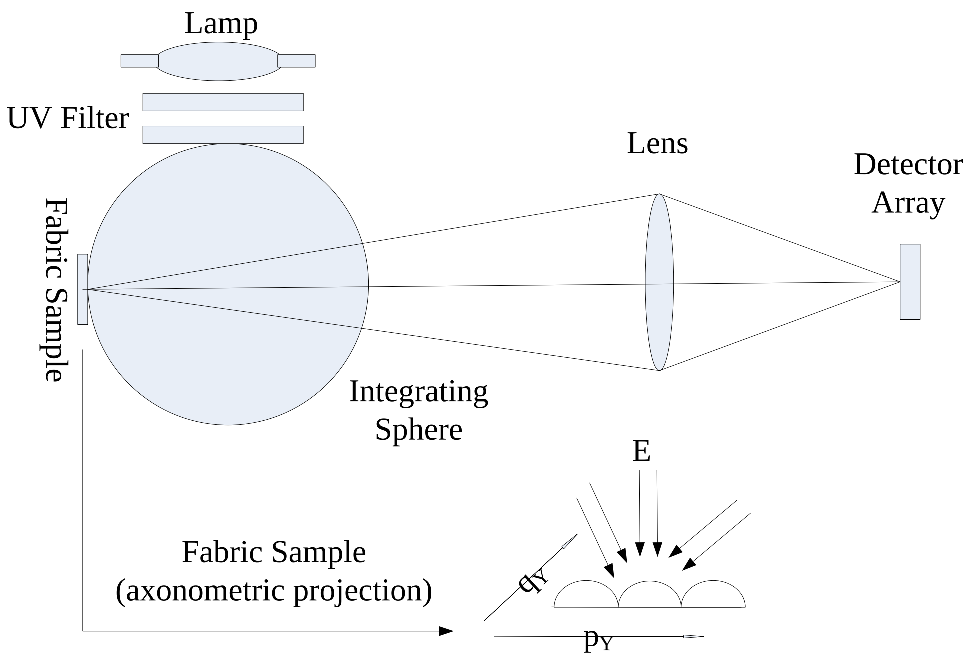

Figure 3.3 The basic optics within a spectrophotometer

Figure 3.3 shows the basic optics within a spectrophotometer. Given the detector area A_d, the optical system efficiency τ, and the maximum aperture diameter of the lens system F, the contribution of the surface position (p_Y, q_Y) to the flux at the detector, $\Phi(\lambda, p_Y, q_Y)$, is given by [119,120]:

$$\Phi(\lambda, p_Y, q_Y) = \pi \frac{A_d \tau}{4F^2} L(\lambda, p_Y, q_Y) \tag{3.8}$$

where $L(\lambda, p_Y, q_Y)$ and λ denote the radiance at (p_Y, q_Y) and the wavelength, respectively.

For yarn dyed fabrics with different textures in a colour centre, $R_1(\lambda) = R_2(\lambda)$ in Eqn (3.7) as the weft and warp yarns have the same colour. $R_1(\lambda)$ and $R_2(\lambda)$ can be abbreviated as $R(\lambda)$. Substituting Eqn (3.7) into Eqn (3.8), the total radiant flux at the detector is:

$$\begin{aligned}
\Phi_S(\lambda) &= \iint_{p_Y, q_Y} \Phi(\lambda, p_Y, q_Y) dp_Y dq_Y \\
&= \pi \frac{A_d \tau}{4F^2} E(\lambda) R(\lambda) \iint_{p_Y, q_Y} m_b(p_Y, q_Y) H(p_Y, q_Y) dp_Y dq_Y \\
&+ \pi \frac{A_d \tau}{4F^2} E(\lambda) R^2(\lambda) \iint_{p_Y, q_Y} m_b(p_Y, q_Y) A(p_Y, q_Y) dp_Y dq_Y \\
&= \left(1 + \frac{\iint_{p_Y, q_Y} m_b(p_Y, q_Y) A(p_Y, q_Y) dp_Y dq_Y}{\iint_{p_Y, q_Y} m_b(p_Y, q_Y) H(p_Y, q_Y) dp_Y dq_Y} R(\lambda)\right) \pi \frac{A_d \tau}{4F^2} E(\lambda) R(\lambda) \iint_{p_Y, q_Y} m_b(p_Y, q_Y) H(p_Y, q_Y) dp_Y dq_Y
\end{aligned} \tag{3.9}$$

Eqn (3.9) expresses that the radiant flux at the detector of a spectrophotometer is determined by three parameters: the geometric term $m_b(p_Y, q_Y)$, the occlusion coefficient $H(p_Y, q_Y)$ and the inter-reflection coefficient $A(p_Y, q_Y)$. These three parameters change with surface positions. According to the Oren–Nayar reflectance model [113], the geometric term can be specified as $m_b(p_Y, q_Y) = \cos(\theta)$, where θ is the incident angle at (p_Y, q_Y). In peak areas of a surface, the contribution of $m_b(p_Y, q_Y) A(p_Y, q_Y)$ to the total radiant flux is insignificant compared to $m_b(p_Y, q_Y) H(p_Y, q_Y)$ because the occlusion coefficient and geometric term are close to 1 but the inter-reflection coefficient is near to 0. However, the contribution of $m_b(p_Y,q_Y)H(p_Y,q_Y)$ is slightly in valley areas because the incident angles are large, i.e., $m_b(p_Y,q_Y)$ is close to 0. In the transition areas between peak and valley areas, both of $m_b(p_Y,q_Y)A(p_Y,q_Y)$ and $m_b(p_Y,q_Y)H(p_Y,q_Y)$ contribute to the measured colours. The contribution of $m_b(p_Y,q_Y)H(p_Y,q_Y)$ becomes less with positions more approaching valley areas.

While the surface of a yarn dyed fabric can be divided into peak, valley and transition areas, the possibility of pixels locating in peak areas is much larger than valleys and transition areas since the real yarn cross-sectional shape approximates race-track [121], lens [122] or shoulder squareness [123] rather than ideal circle, as shown in Figure 3.4. In addition, the integrating sphere of a spectrophotometer would cause the intensity of light from the direct illuminant larger than light from the ambient illuminant. Hence, the term $\iint_{p_Y,q_Y} m_b(p_Y,q_Y)A(p_Y,q_Y)dp_Y dq_Y \,/$ $\iint_{p_Y,q_Y} m_b(p_Y,q_Y)H(p_Y,q_Y)dp_Y dq_Y$ can be assumed to be negligible for a yarn dyed fabric sample when a spectrophotometer is used to measure its colour:

$$\Phi_S(\lambda) = \pi \frac{A_d \tau}{4F^2} E(\lambda) R(\lambda) \iint_{p_Y, q_Y} m_b(p_Y, q_Y) H(p_Y, q_Y) dp_Y dq_Y \qquad (3.10)$$

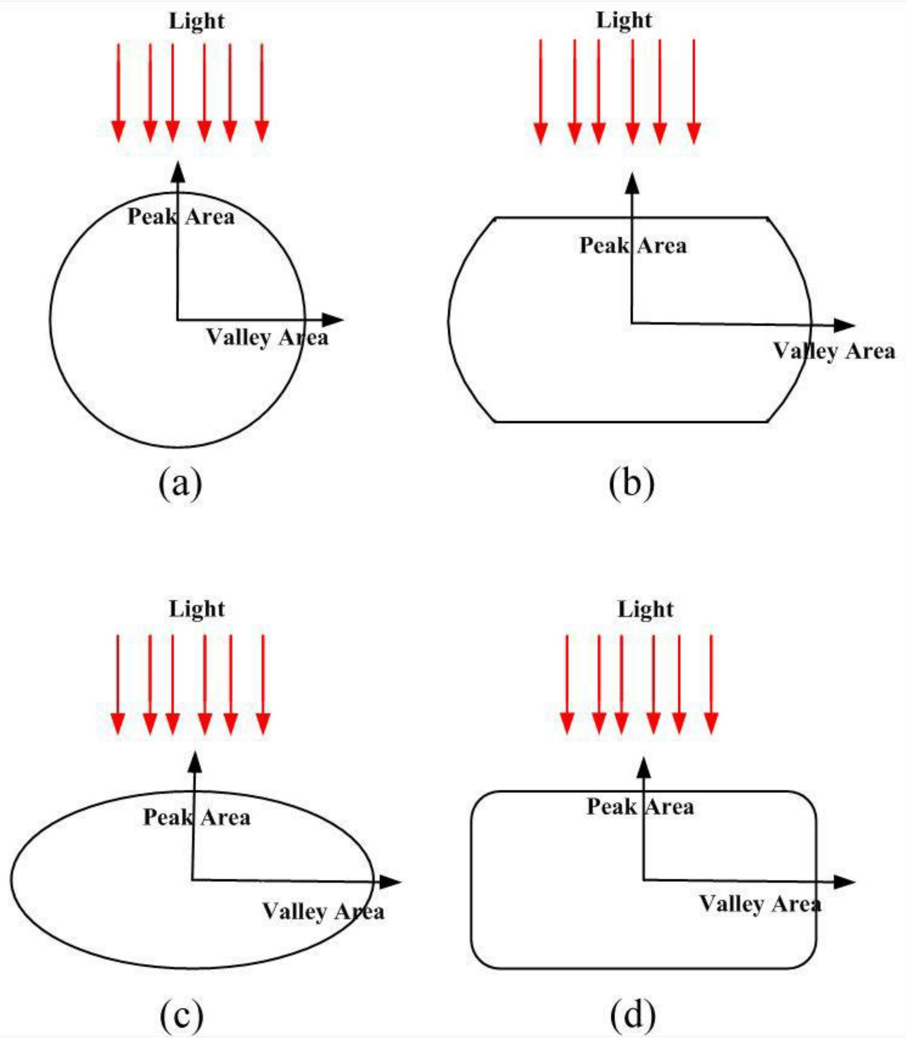

Figure 3.4 The ideal and real yarn cross-sectional shapes of fabrics: (a) ideal yarn cross-sectional shape: circle; (b) real yarn cross-sectional shape: race-track; (c) real yarn cross-sectional shape: lens; (d) real yarn cross-sectional shape: shoulder squareness

The reference subsystem within a spectrophotometer measure the colour of the beam reflected by the sphere wall, which give a measure of the light incident on the fabric sample [124]. The flux at the detector of the reference subsystem is:

$$\Phi_R(\lambda) = \pi \frac{A_d \tau}{4F^2} E(\lambda) A_r \tag{3.11}$$

where A_r denotes the aperture area of the spectrophotometer.

Combining Eqn (3.10) and Eqn (3.11), the spectral response of a spectrophotometer to a yarn dyed fabric can be modeled as:

$$\begin{aligned} R_b(\lambda) &= \frac{\Phi_S(\lambda)}{\Phi_R(\lambda)} \\ &= \frac{\iint\limits_{p_Y,q_Y} m_b(p_Y,q_Y) H(p_Y,q_Y) dp_Y dq_Y}{A_r} R(\lambda) \\ &= \frac{\iint\limits_{p_Y,q_Y} m_b(p_Y,q_Y) H(p_Y,q_Y) dp_Y dq_Y}{A_r} |R(\lambda)| \bar{R}(\lambda) \end{aligned} \tag{3.12}$$

where $|R(\lambda)| \iint\limits_{p_Y,q_Y} m_b(p_Y,q_Y) H(p_Y,q_Y) dp_Y dq_Y / A_r$ is termed as the magnitude of the measured reflectance, $\bar{R}(\lambda)$ denotes the spectral direction in the reflectance space.

The expression in Eqn (3.12) defines a set of lines with identical direction but different magnitudes in the reflectance space. The direction of the lines is determined by the spectral direction of the nominal reflectance of fabrics, $\bar{R}(\lambda)$. The magnitudes depend on the geometric terms $m_b(p_Y,q_Y)$, the occlusion coefficient $H(p_Y,q_Y)$, and the magnitude of the nominal reflectance $|R(\lambda)|$. $m_b(p_Y, q_Y)$ and $H(p_Y, q_Y)$ change with surface positions of textured fabrics.

The normalized reflectance is defined as:

$$\bar{R}_b(\lambda) = \frac{R_b(\lambda)}{\int_\lambda R_b(\lambda) d\lambda} = \frac{\dfrac{\iint_{p_Y, q_Y} m_b(p_Y, q_Y) H(p_Y, q_Y) dp_Y dq_Y}{A_r} R(\lambda)}{\dfrac{\iint_{p_Y, q_Y} m_b(p_Y, q_Y) H(p_Y, q_Y) dp_Y dq_Y}{A_r} \int_\lambda R(\lambda) d\lambda} = \frac{R(\lambda)}{\int_\lambda R(\lambda) d\lambda} \quad (3.13)$$

Eqn (3.13) expresses the normalized reflectance curves of fabrics with different texture surfaces are identical which only depend on the nominal reflectance of these samples, i.e., $R(\lambda)$.

Given the CIE colour matching functions $\bar{x}(\lambda)$, $\bar{y}(\lambda)$, $\bar{z}(\lambda)$, the tristimulus values of these fabric samples can be specified as [125]:

$$\begin{cases} X = k\int_{\lambda} R_b(\lambda)E(\lambda)\bar{x}(\lambda)d\lambda = k\dfrac{\iint_{p_Y,q_Y} m_b(p_Y,q_Y)H(p_Y,q_Y)dp_Y dq_Y}{A_r}\int_{\lambda} E(\lambda)R(\lambda)\bar{x}(\lambda)d\lambda \\ Y = k\int_{\lambda} R_b(\lambda)E(\lambda)\bar{y}(\lambda)d\lambda = k\dfrac{\iint_{p_Y,q_Y} m_b(p_Y,q_Y)H(p_Y,q_Y)dp_Y dq_Y}{A_r}\int_{\lambda} E(\lambda)R(\lambda)\bar{y}(\lambda)d\lambda \\ Z = k\int_{\lambda} R_b(\lambda)E(\lambda)\bar{z}(\lambda)d\lambda = k\dfrac{\iint_{p_Y,q_Y} m_b(p_Y,q_Y)H(p_Y,q_Y)dp_Y dq_Y}{A_r}\int_{\lambda} E(\lambda)R(\lambda)\bar{z}(\lambda)d\lambda \end{cases} \tag{3.14}$$

where k is a normalising factor given by $k = 100/\int_{\lambda} E(\lambda)\bar{y}(\lambda)d\lambda$.

The expression in Eqn (3.14) reveals that fabric samples with different texture structures define a line in the CIEXYZ colour space. The direction of the line is defined as $[\int_{\lambda} E(\lambda)R(\lambda)\bar{x}(\lambda)d\lambda,$ $\int_{\lambda} E(\lambda)R(\lambda)\bar{y}(\lambda)d\lambda,$ $\int_{\lambda} E(\lambda)R(\lambda)\bar{z}(\lambda)d\lambda]^T$.

The chromaticity coordinates of these fabric samples are computed as [125]:

$$\begin{cases} x = \dfrac{X}{X+Y+Z} = \dfrac{\int_\lambda E(\lambda)R(\lambda)\bar{x}(\lambda)d\lambda}{\int_\lambda E(\lambda)R(\lambda)(\bar{x}(\lambda)+\bar{y}(\lambda)+\bar{z}(\lambda))d\lambda} \\ y = \dfrac{Y}{X+Y+Z} = \dfrac{\int_\lambda E(\lambda)R(\lambda)\bar{y}(\lambda)d\lambda}{\int_\lambda E(\lambda)R(\lambda)(\bar{x}(\lambda)+\bar{y}(\lambda)+\bar{z}(\lambda))d\lambda} \\ z = \dfrac{Z}{X+Y+Z} = \dfrac{\int_\lambda E(\lambda)R(\lambda)\bar{z}(\lambda)d\lambda}{\int_\lambda E(\lambda)R(\lambda)(\bar{x}(\lambda)+\bar{y}(\lambda)+\bar{z}(\lambda))d\lambda} \end{cases} \tag{3.15}$$

Eqn (3.15) reveals that the chromaticity coordinates of fabric samples with different texture structures are identical.

The CIELAB colours of these fabric samples can be transformed from their tristimulus values [125], we have:

$$\begin{cases} L* = 116f(Y/Y_n) - 16 \\ a* = 500[f(X/X_n) - f(Y/Y_n)] \\ b* = 200[f(Y/Y_n) - f(Z/Z_n)] \end{cases} \tag{3.16}$$

where

$$f(t) = \begin{cases} t^{1/3} & t > (\frac{6}{29})^3 \\ \frac{1}{3}(\frac{29}{6})^2 t + \frac{4}{29} & \text{otherwise} \end{cases} \tag{3.17}$$

Eqn (3.16) and Eqn (3.17) show the colour transformation from CIEXYZ to CIELAB space is non-linear. As a consequence, the linearity in the reflectance space (Eq.(2.12)) and CIEXYZ space (Eq.(2.14)) is lost in the CIELAB space for fabric samples with different texture structures. Assuming linear dependence of spectral reflectance with texture, therefore, it is messy to estimate the influence of texture structures of fabric samples on their colors in the CIELAB space.

3.3.3. Results and Discussion

Preparation of Samples

84 knitted cotton yarn dyed fabric samples were prepared for the experiment. These samples were in four colour centres recommended by the CIE [126]: green, gray, red and blue (Figure 3.5a). In each colour centre, the single jersey structure, i.e., the plain structure, was defined as the standard texture (Figure 3.5b-Std.). The batch texture structures in each colour centre included 20 different textures widely used in knitwear structures (Figure 3.5b-2~21). The standard and batch samples in each color center were knitted by one same colored yarn using a Shima Seiki Knitting Machine.

The MACBETH Color-Eye 7000A Spectrophotometer was used to measure the instrumental colours of these samples. The specular component excluded (SCE) and UV excluded modes were applied to eliminate the influence of specular light and UV on samples.

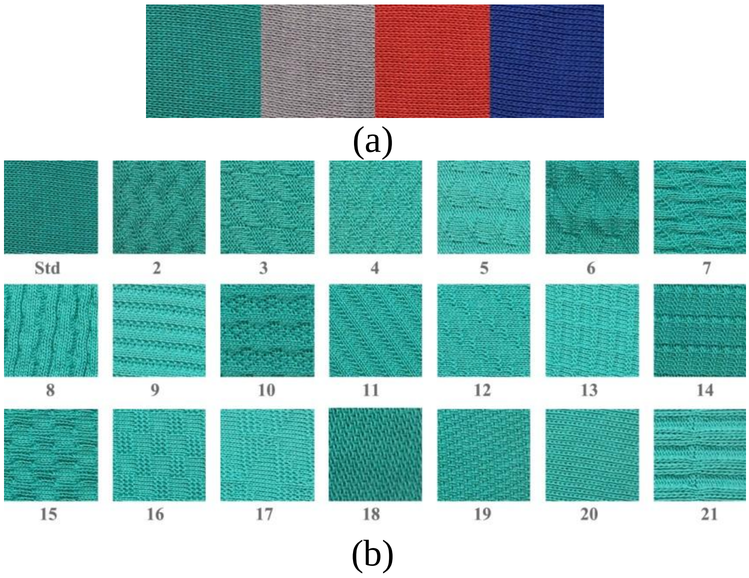

Figure 3.5 The prepared physical knitted yarn dyed fabric samples: (a) samples in 4 colour centres: green, gray, red and blue; (b) the used 21 texture structures.

Reflectance Space

The first experiment analyzed how texture structure affects measured reflectance. Figure 3.6 shows the reflectance and normalized reflectance curves of all the samples. As shown in Figure 3.6a, the reflectance curves of samples in each colour centre have the same direction (the shape of curves) but slightly different magnitudes. Figure 3.6b shows the normalized reflectance curves of samples in each colour centre are approximately the same. The results shown in Figure 3.6 demonstrate that fabric samples with different texture surfaces define a set of lines with identical direction but different magnitudes in the reflectance space. The normalized reflectance of these samples is identical.

In order to check the degree of similarity among the normalized reflectance curves of samples in each color center, the angle between the normalized reflectance curves of batch samples and the standard sample in each color center is calculated [127]:

$$\begin{aligned}\theta &= \cos^{-1}\left(\frac{\overline{R}_b^B(\lambda)\bullet\overline{R}_b^S(\lambda)}{\left\|\overline{R}_b^B(\lambda)\right\|\left\|\overline{R}_b^S(\lambda)\right\|}\right) \\ &= \cos^{-1}(\overline{R}_b^B(\lambda)\bullet\overline{R}_b^S(\lambda))\end{aligned} \quad (3.18)$$

where $\overline{R}_b^B(\lambda)$ and $\overline{R}_b^S(\lambda)$ denote the normalized reflectance of a batch sample and the corresponding standard sample in each colour centre. The normalized reflectance curves between the batch and standard samples are identical when the angle is equal to 0°. The dispersion of two normalized reflectance curves is larger with increasing angles.

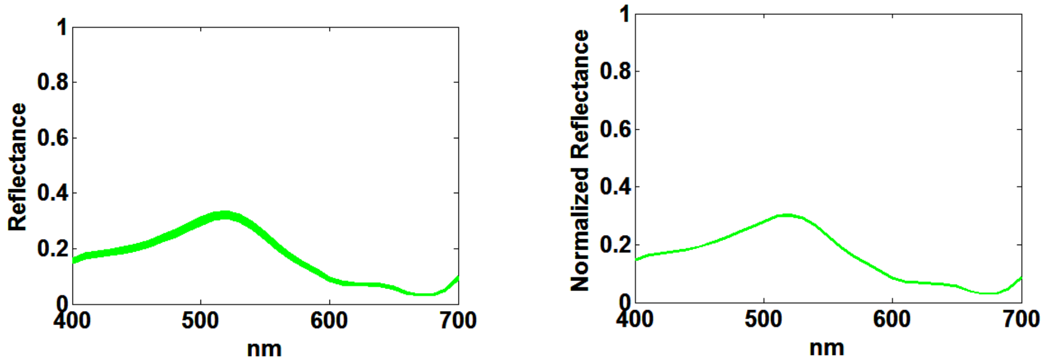

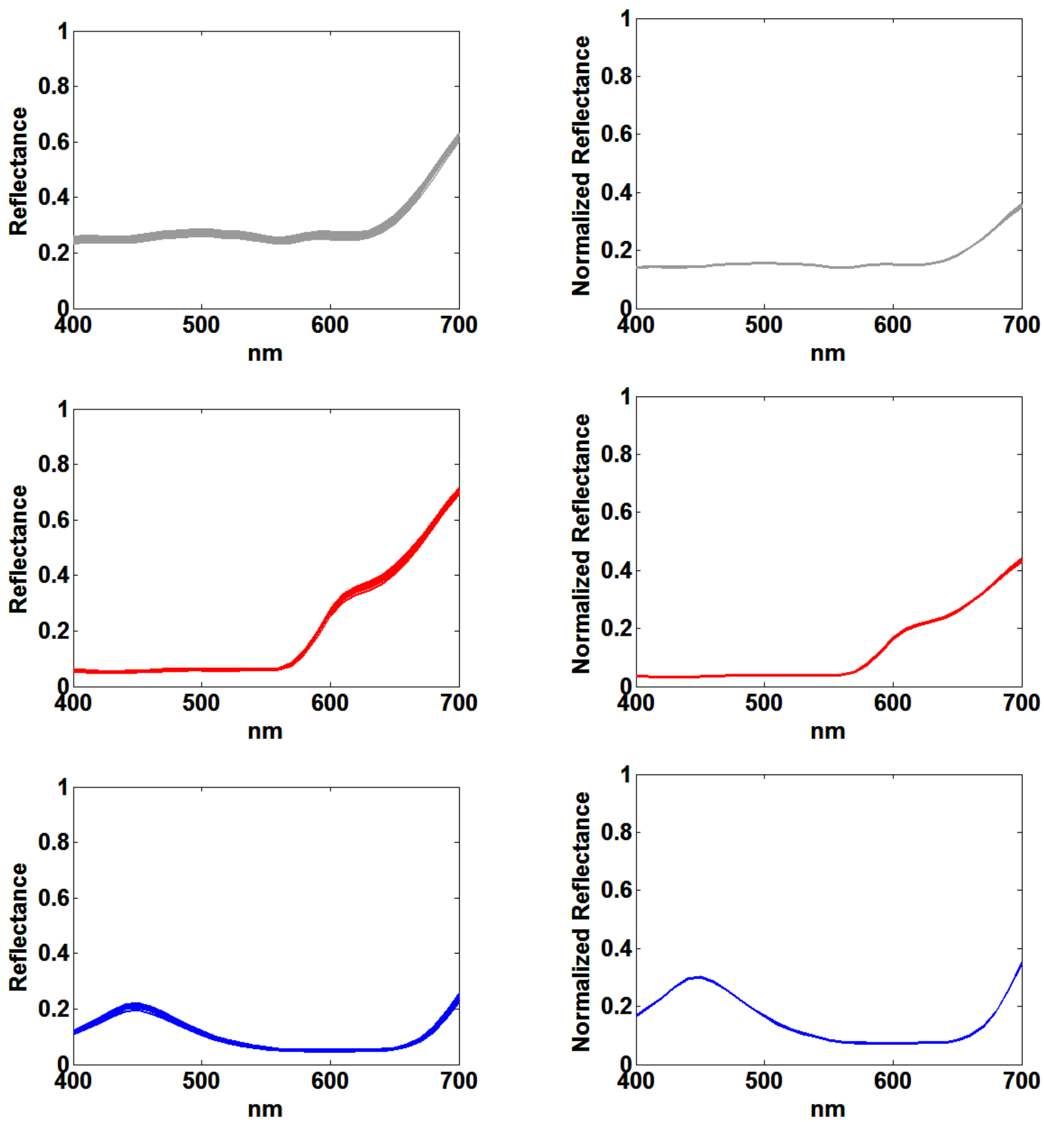

(a) (b)

Figure 3.6 The reflectance and normalized reflectance curves of all samples: (a) the reflectance curves of samples in green, gray, red and blue colour centres (from top to bottom); (b) the normalized reflectance curves of samples in green, gray, red and blue colour centres (from top to bottom). Noted that all the curves in (a) and (b) are drawn with the same scale.

Figure 3.7 shows the angles between the normalized reflectance curves of batch and standard samples in each colour centre. The angles of samples with texture No. 20 are smallest, i.e., 0.16°, 0.16°, 0.08°, and

0.40° for the green, gray, red, and blue samples. This stems from that texture Std and texture No.20 are visually similar, as shown in Figure 3.5b. Samples with texture No.18, No.7, and No.21 produce the largest, second largest and third largest angles for all of the samples, i.e., 1.01°, 0.86°, and 0.86°. This result highly agrees with the large perceived differences between texture Std and texture No.18, No.7, and No.21. The average angles are 0.51°, 0.41°, 0.66°, and 0.80° for the samples in green, gray, red and blue. The small angles between the normalized reflectance curves of the batch and standard samples in each color center demonstrate that their normalized reflectance curves resemble in the normalized reflectance space, which echoes the results shown in Figure 3.6b.

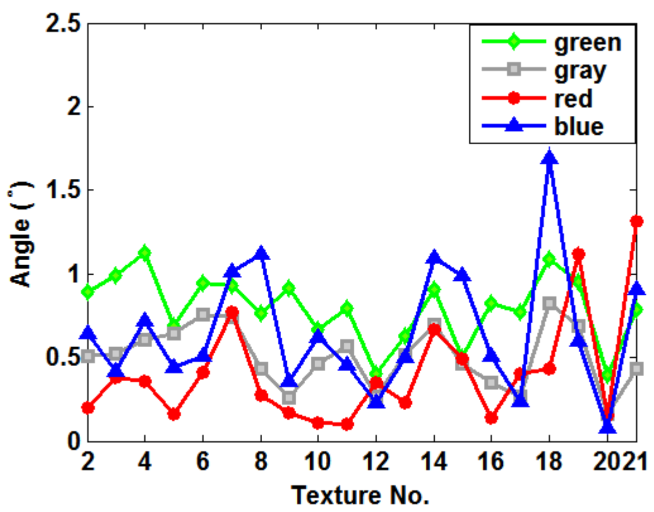

Figure 3.7 The angles of the normalized reflectance curves of batch and standard samples in green, gray, red and blue.

Besides the normalized reflectance, the magnitude of measured reflectance was also analyzed. Given a measured reflectance of a sample $R=[r_1,r_2,\cdots r_n]$, the magnitude of the reflectance is defined as [128]:

$$|R|=\sqrt{\sum_{i=1}^{n} r_i^{\,2}} \tag{3.19}$$

where n denotes the number of spectral bands.

Figure 3.8 shows the magnitudes of measured reflectance of samples in each colour centre. The reflectance magnitudes is in the ranges [1.01, 1.11], [1.66, 1.81], [1.57, 1.66] and [0.64, 0.73] for samples in green, gray, red and blue. It can be observed that the texture structure of a fabric would cause its reflectance magnitude fluctuation, which coheres the results shown in Figure 3.6a.

When considering a reflectance curve as a vector, reflectance can be expressed as a combination of direction (normalized reflectance) and magnitude. With Figure 3.7 showing that fabrics with different texture structures have approximately identical normalized reflectance, whereas Figure 3.8 showing that their reflectance magnitude values vary with texture structures, it can be concluded that the texture surface of a fabric sample dominantly influences the magnitude of reflectance rather than its direction.

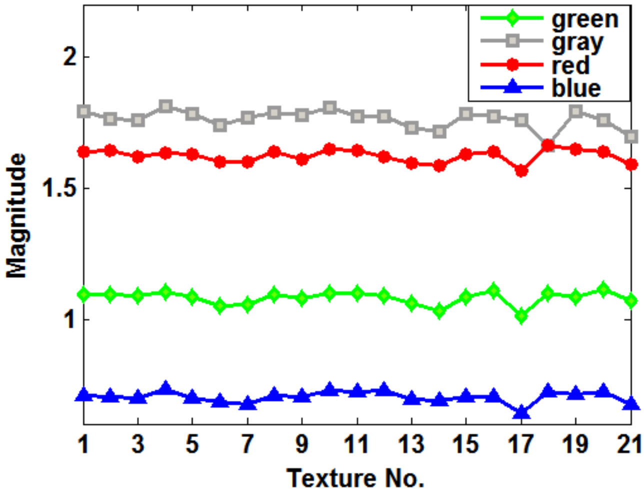

Figure 3.8 The reflectance magnitudes of samples in green, gray, red and blue.

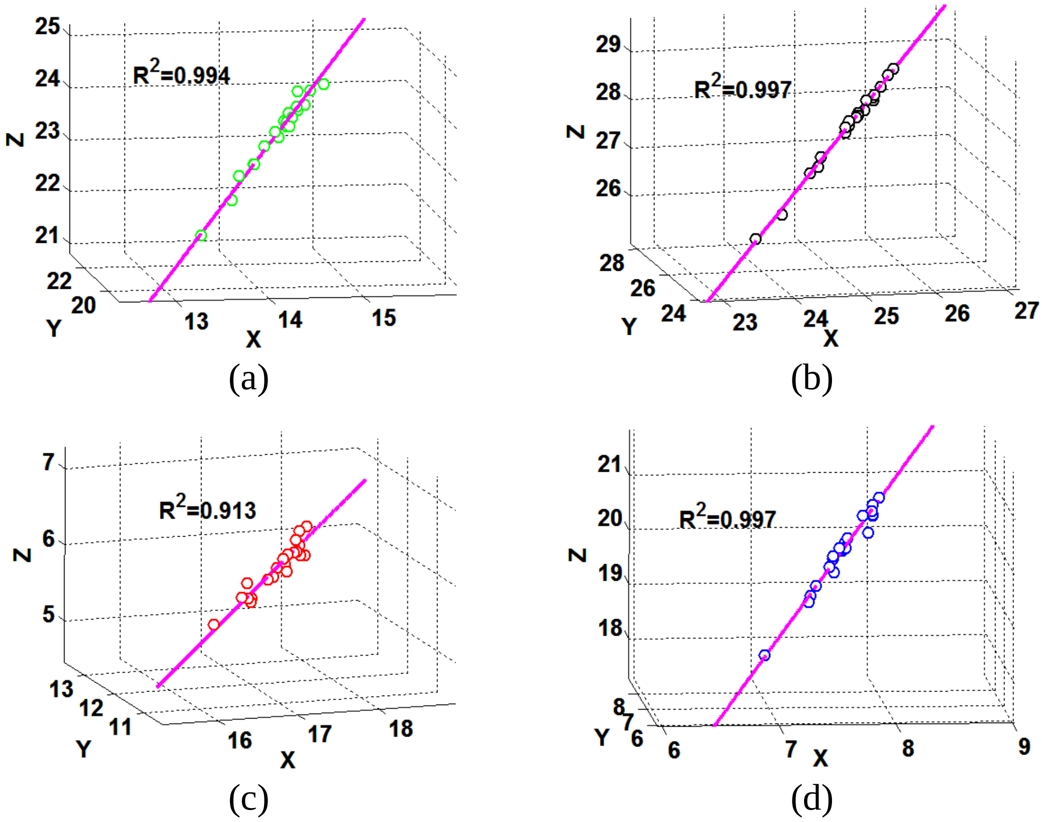

Figure 3.9 The colour distributions of samples in the CIEXYZ space. (a)-(d) tristimulus distributions of green, gray, red and blue samples.

CIEXYZ colour space

The second experiment examined how the texture structure of a fabric sample affects its tristimulus and chromaticity coordinates. Figure 3.9 shows colour distributions of all the samples in the CIEXYZ space. Least squares regress method [129] was used to fit tristimulus values to a line. The correlation values between tristimulus values and regressed lines are 0.994, 0.997, 0.913 and 0.997 for the green, gray, red and blue samples. The high correlation values demonstrate that colours of fabric samples with different texture structures approximately define a line in the CIEXYZ colour space.

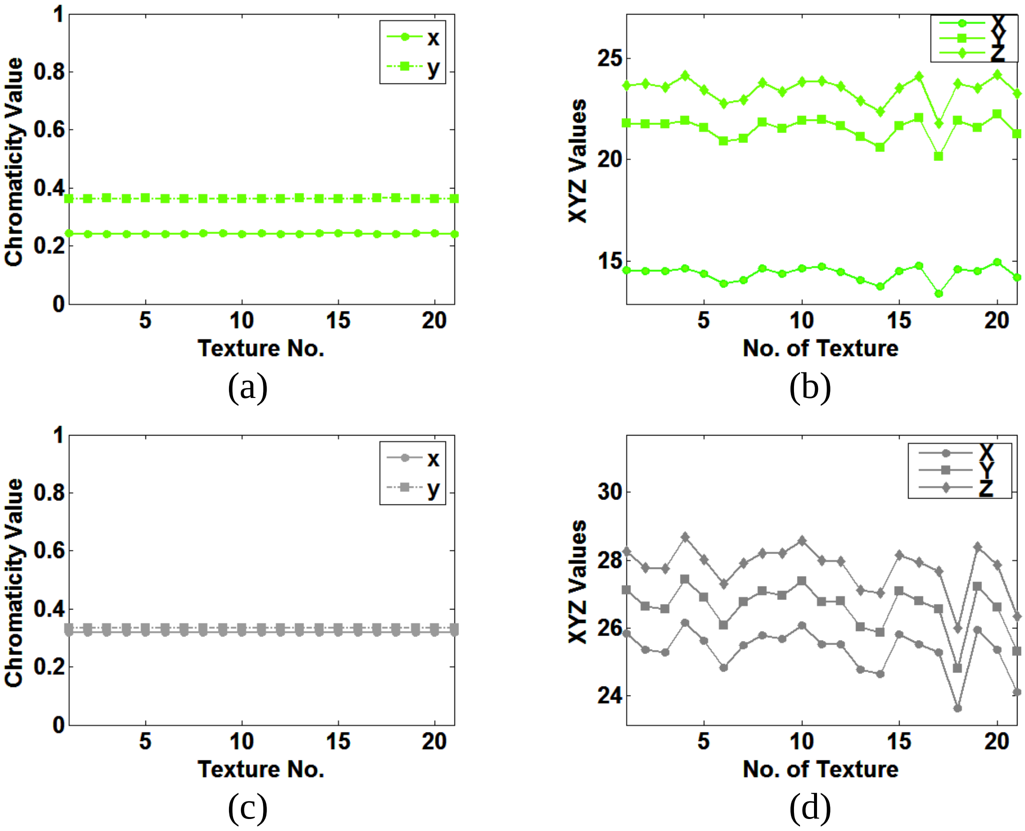

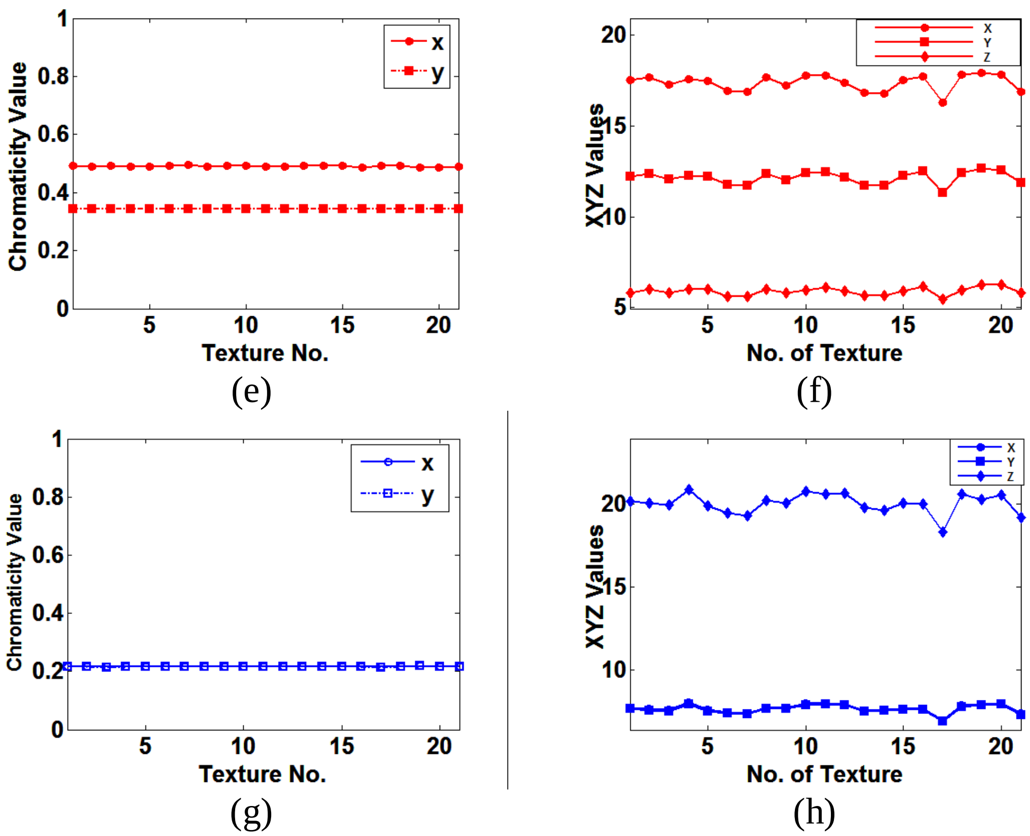

Figure 3.10 The chromaticity coordinates and tristimulus values of all samples: (a), (c), (e), and (g) the chromaticity coordinates of green, gray, red and blue samples; (b), (d), (f), and (h) the tristimulus values of green, gray, red and blue samples.

Table 3.2 The standard deviation (std) of chromaticity coordinates and tristimulus values of all samples.

	std of x	std of y	std of X	std of Y	std of Z
Green Samples	0.0007	0.0009	0.3750	0.5175	0.5952
Gray Samples	0.0000	0.0004	0.6305	0.6644	0.6770
Red Samples	0.0022	0.0002	0.4410	0.3427	0.2209
Blue Samples	0.0008	0.0012	0.2578	0.2645	0.6128

Figure 3.10 depicts chromaticity coordinates and tristimulus values of samples in green, gray, red and blue. It can be observed that the chromaticity coordinates of samples in each colour centre are approximately identical. However, their tristimulus values dramatically

vary with texture structures. The standard deviation [130] was used to quantify chromaticity and tristimulus difference between samples with different textures in each colour centre. As shown in Table 3.2, the standard deviations of chromaticity coordinates are less than 0.0012 for all samples. However, the standard deviations of tristimulus values for these samples are more than 0.2..

CIELAB colour space

The third experiment analyzed the CIELAB colours of these samples. Least squares regress method [129] was utilized to fit CIELAB colours to a line. As shown in Figure 3.11, the correlation values between the CIELAB colours and the regressed lines are 0.081, 0.161, 0.044 and 0.372 for samples in green, gray, red and blue. Comparing Figure 3.11 with Figure 3.9, we can conclude that colour distributions are much less linear in the CIELAB space than the CIEXYZ space.

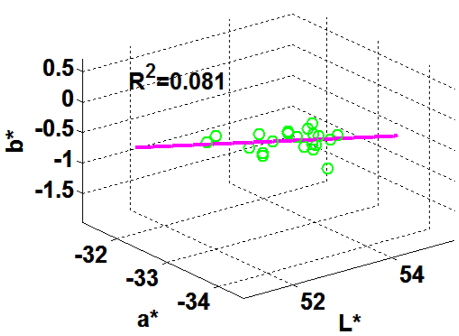

(a)

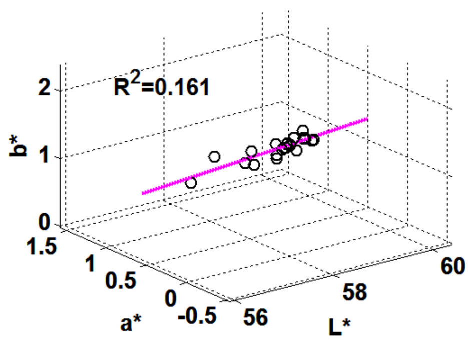

(b)

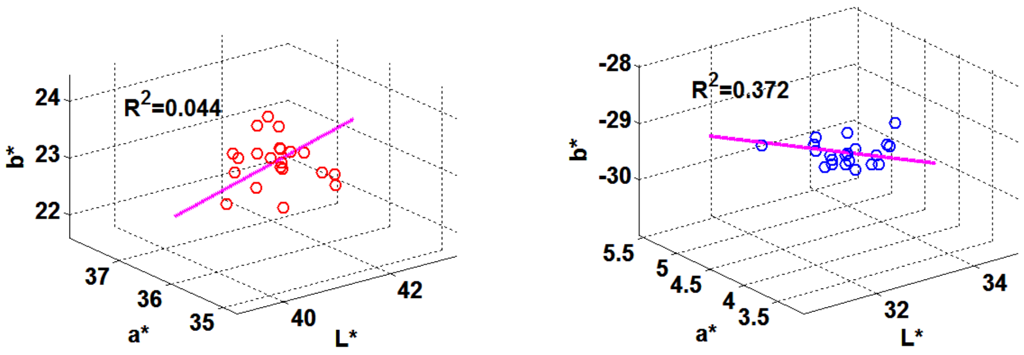

(c) (d)

Figure 3.11 The colour histograms in the CIELAB space. (a)-(d) the CIELAB colour histograms of the green, gray, red and blue samples.

Removing the effect of texture on colour

The linear relationship between the measured reflectance of fabrics with different textures can be utilized to estimate a theoretical reflectance which discounts the influence of texture on colour. For a fabric sample with the j-th texture in the colour centre C_i, its theoretical reflectance $R^j_{T,i}(\lambda)$ can be expressed as:

$$R^j_{T,i}(\lambda) = \left|R^j_{T,i}(\lambda)\right| \bar{R}^j_{T,i}(\lambda) \tag{3.20}$$

where $\left|R^j_{T,i}(\lambda)\right|$ and $\bar{R}^j_{T,i}(\lambda)$ denote the magnitude and the normalized reflectance of $R^j_{T,i}(\lambda)$.

As shown in Eqn (3.12), the magnitude $\left|R^j_{b,i}(\lambda)\right|$ is determined by the surface variable ($\iint_{p_Y,q_Y} m_b(p_Y,q_Y)H(p_Y,q_Y)dp_Y dq_Y$), the aperture size (A_r)

and the nominal reflectance magnitude ($|R_i(\lambda)|$). A reasonable assumption is that the surface variable is approximately identical for two samples with same texture but in different colour centres C_1 and C_2 ($R^j_{b,1}(\lambda)$ and $R^j_{b,2}(\lambda)$). Comparing to the corresponding samples with standard texture in C_1 and C_2 ($R^s_{b,1}(\lambda)$ and $R^s_{b,2}(\lambda)$), as a consequence, multiple relationships $|R_{b,1}(\lambda)|/|R^s_{b,1}(\lambda)|$ and $|R_{b,2}(\lambda)|/|R^s_{b,2}(\lambda)|$ can approximate to be identical. For a sample with measured reflectance $R^j_{b,i}(\lambda)$, we can estimate its multiple relationship of reflectance magnitude compared to the corresponding standard sample ($M_j = |R^j_{b,i}(\lambda)| / |R^s_{b,i}(\lambda)|$) as the mean of multiple relationship of reflectance magnitudes among samples in all the colour centres:

$$M_j = \frac{1}{N}\sum_{i=1}^{N}\frac{|R^j_{b,i}(\lambda)|}{|R^s_{b,i}(\lambda)|} \tag{3.21}$$

where N denotes the number of colour centres, here, $N = 4$.

Given the measured reflectance $R^j_{b,i}(\lambda)$ for the sample with *j*-th texture in the colour centre C_i , the magnitude of theoretical reflectance $|R^j_{T,i}(\lambda)|$ can be estimated as:

$$\left|R_{T,i}^{j}(\lambda)\right| = \frac{\left|R_{b,i}^{j}(\lambda)\right|}{M_j} \tag{3.22}$$

The normalized reflectance $\bar{R}_{T,i}^{j}(\lambda)$ can be estimated as $\bar{R}_{b,i}^{j}(\lambda)$ because samples with different texture structures in a colour centre have the same normalized reflectance (Eqn (3.14) and Figure 3.7).

Figure 3.12 shows the multiple relationships of reflectance magnitude for the green, gray, red and blue samples. In each colour centre, the sample with single jersey (Figure 3.5-Std) was chosen as the standard texture. It can be observed that samples with same texture in different colour centres have approximately identical multiple relationship in terms of reflectance magnitude. Some outliers exist in Figure 3.12, such as samples with No. 17 texture structure, yet the deviation is high, which may be caused by non-uniformity during preparing samples. The color differences between batch and standard samples before and after removing texture effect were calculated by the CMC(2:1) formula, which is one of the color difference formulas widely adopted in textile. The standard sample in each color center is the one with the standard texture. Figure 3.13 shows colour difference before and after removing texture effect for each sample. The standard samples in each colour centre are the ones with the standard texture. As shown in Figure 3.13, the colour difference after removing texture effect is much smaller. The average colour difference values before texture effect removal are 0.39, 0.30, 0.31, 0.32 CMC(2:1) units for samples in green, gray, red and blue. The average colour difference values after removing texture effect are 0.08, 0.13, 0.09 and 0.14 CMC(2:1) units for these samples. The influence of texture on colour is reduced by 79%, 55%, 71% and 57% for the green, gray, red, and blue samples respectively.

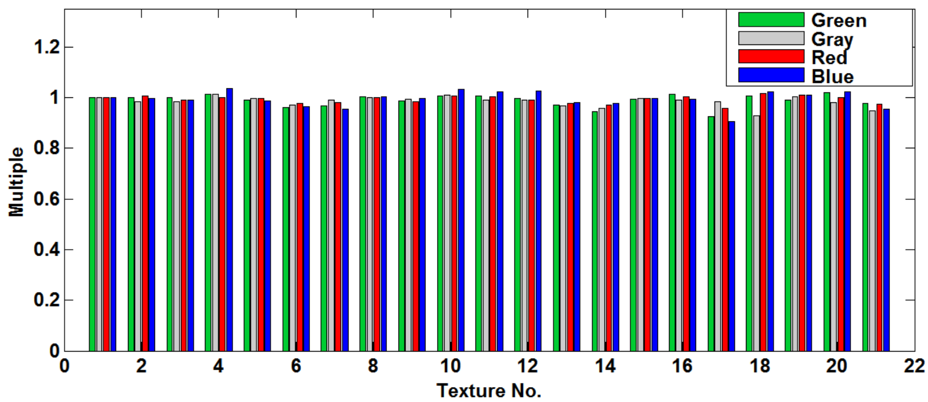

Figure 3.12 The multiple relationships of samples in terms of reflectance magnitude. In each colour centre, samples with single jersey (Figure 3.5-Std) are chosen as standards.

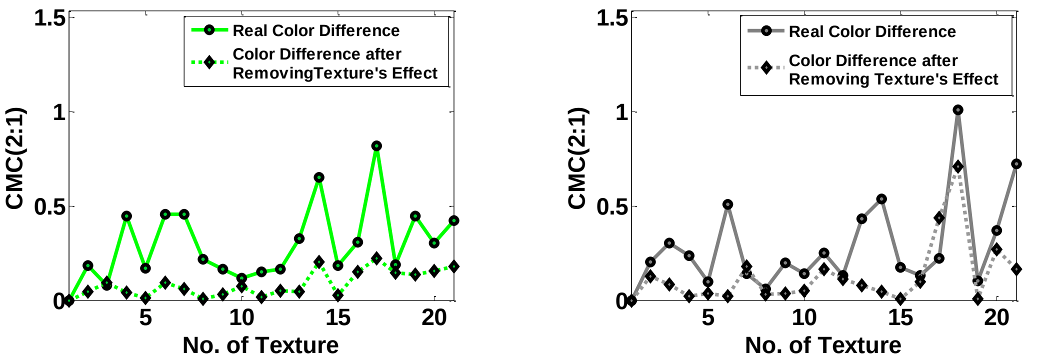

(a) (b)

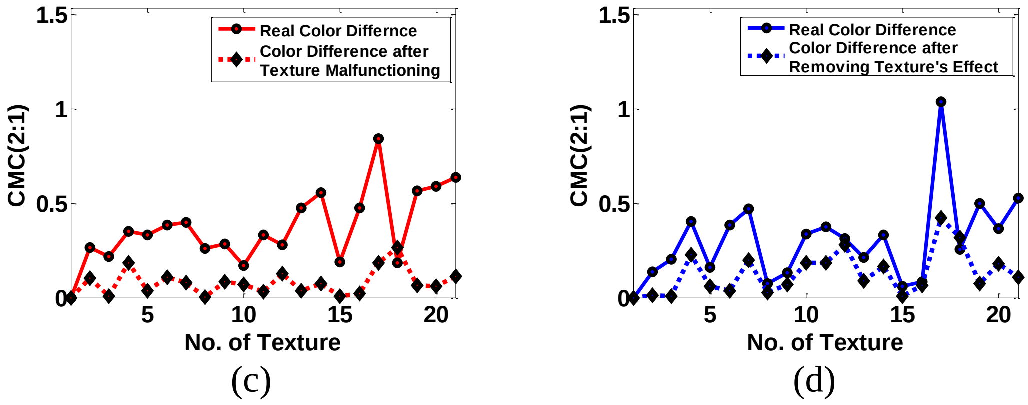

Figure 3.13 The colour difference between samples with different texture structures and the stand texture structure before and after removing texture effect.

3.4. Conclusion

The methodology of colour measurement of yarn dyed fabrics is first introduced in this chapter. A novel reflection model is then proposed to estimate the light reflected by a yarn dyed fabric. The model expressed that the light reflected by a fabric surface is composed by two parts: the occluded light from the system illuminant and the light reflected by neighbouring yarns. In addition, three parameters influence the light reflected by a fabric surface: surface texture, inter-reflection between yarns and illuminant occlusion. Finally, the reflection model is verified by estimating the influence of texture on colour measured by spectrophotometers. Based on the reflection model, the texture of a yarn dyed fabric dominantly influences the magnitude of reflectance rather than its direction. In the CIEXYZ space, yarn dyed fabrics with different texture structures define a line which implies that their chromaticity coordinates are identical. An approach is proposed to reduce the influence of texture on colour. Experimental results show that the influence of texture on colour for yarn dyed fabric samples in four colour centres (green, gray, red and blue) can be reduced by 79%, 55%, 71% and 57% respectively comparing to the real measured colour difference.

Chapter 4 Dominant Colour Region Segmentation

In this chapter, a novel unsupervised approach to detect dominant colour regions standing out conspicuously in yarn dyed fabric images is presented. A probabilistic model is proposed to associate the colour of a dominant colour region with colours of its yarns. Based on this model, colour histograms of a dominant colour region are first estimated from those of yarns. A hierarchical segmentation structure is then devised to detect dominant colour regions. Experimental results show that the proposed approach achieves satisfactory performance for dominant colour region segmentation in yarn dyed fabric images, with high computational efficiency.

4.1. Background

Traditionally, a spectrophotometer is used to measure solid colours of fabrics. However, for a multi-coloured object, such as a yarn dyed fabric, prior to measuring the colour of yarns by a spectrophotometer, it is necessary to separate them. This is time and energy consuming, and prone to error owing to inconsistency in preparing yarn samples. With the development of digital imaging technology, image analysis techniques are adopted to extract colour information from fabrics. To measure the colour of a yarn dyed fabric by image analysis techniques, it is necessary initially to detect colour regions standing out conspicuously in the image. These regions are called dominant colour regions, and their colours are referred to dominant colours (Figure 4.1c). For a dominant colour region of a yarn dyed fabric, however, its colour cannot easily be measured owing to three-dimensional (3D) shapes of yarns, which results in a significant colour difference among pixels of a yarn (Figure 4.1d). This non-uniformity leads to difficulty in segmenting dominant colour regions.

As mentioned in Section 2.5, colour region segmentation in fabric images can be achieved by cluster-based approaches and automatic segmentation algorithms of still images. However, it is difficult to directly utilize cluster-based approaches to segment colour regions in yarn dyed fabric images since colours are more scattered and uneven in yarn dyed fabrics than textile prints. While automatic segmentation of still images has been investigated for many years in the field of image processing, it is difficult to segment colour regions in yarn dyed fabric images by directly applying any of these segmentation methods. Sample-induced effects of yarn dyed fabrics introduced in Chapter 1 cause difficulties to finding a global threshold for histogram-based and region-based segmentation methods, as shown in Figure 4.1b. It is also difficult to employ edge-based segmentation methods because of intermittent and winding boundaries of yarns.

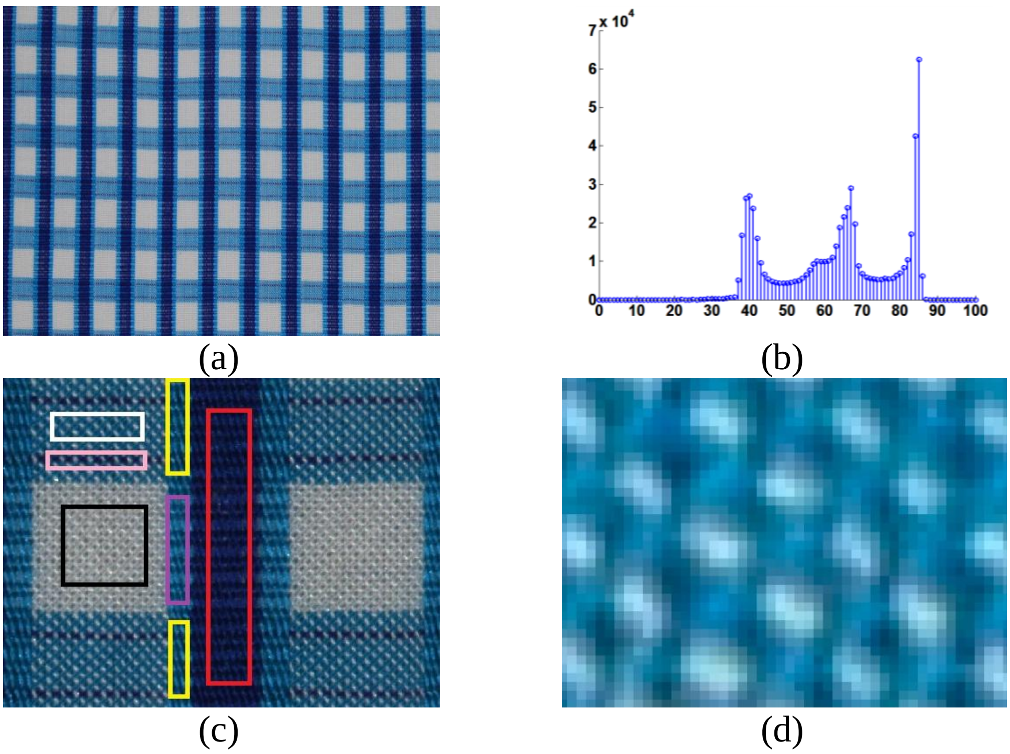

Figure 4.1 Example of dominant colour regions in a yarn dyed fabric image: (a) the yarn dyed fabric image; (b) the lightness histogram of the image; (c) its dominant colour regions include six regions (shown as white, black, red, yellow, pink, and purple rectangles); (d) pixels in the dominant colour region shown as the white rectangle in (c).

4.2. Dominant Colour Region Segmentation

For a yarn dyed fabric image, appearance colours of its yarns and dominant colour regions are denoted as $I_M(x)$ and $I_T(x)$. The deviation of $I_M(x)$ from $I_T(x)$ depends on several factors, such as fineness and strength of fibres, physical shape of fibers, yarn structure, and thread density. According to the central limit theorem (CLT) [131], almost any measured quantity that depends on several underlying factors has a Gaussian probability density function. When a sufficiently large number of data are considered (the number of pixels is 1040*1392), the probability that $I_M(x)$ associates with $I_T(x)$ can be hypothesised to follow the Gaussian distribution [132]:

$$\rho = (2\pi)^{-3/2}|\Sigma|^{-1/2}\exp\left\{-\frac{1}{2}(I_T(x)-I_M(x))^T\Sigma^{-1}(I_T(x)-I_M(x))\right\} \tag{4.1}$$

where $I_T(x), I_M(x) \in R^3$, and $\sum$ is the covariance matrix of colours.

According to the study of Kurugollu [133], it is not always feasible to obtain a reliable image segmentation from 3D histograms owing to data insufficiency. The adopted CIELAB colour space in this study, meanwhile, is a 3D colour space with three independent variables L*, a*, and b*. Therefore, the probability of $I_M(x)$ associating with $I_T(x)$ in each colour channel is modeled independently.

Given the dominant colours $I_T^i(x)(i=1,2,3)$ and the colours of yarns $I_M^i(x)(i=1,2,3)$ in a yarn dyed fabric image, the probability of $I_M^i(x)$ associating with $I_T^i(x)$ can be modeled as:

$$\rho = \min(\rho_1, \rho_2, \rho_3) \tag{4.2}$$

where ρ_i is the probability that $I_M^i(x)$ associates with $I_T^i(x)$ in ***i***-th colour channel:

$$\rho_i = (2\pi\sigma_i{}^2)^{-1/2} \exp(-\frac{1}{2}(I_T^i(x) - I_M^i(x))^2 / \sigma_i{}^2) \tag{4.3}$$

where $\sigma_i{}^2$ is the variance of the probability distribution in each colour channel.

A threshold D is set to determine whether two yarns with colours $I_M(x_1)$ and $I_M(x_2)$ belong to one dominant colour region [its colour is $I_T(x_0)$]. The probabilities that $I_M(x_1)$ and $I_M(x_2)$ associate with $I_T(x_0)$ are denoted as ρ^{01} and ρ^{02}, respectively. If $\min(\rho^{01}, \rho^{02}) > D$, these two yarns are determined to belong to the same dominant colour region, and *vice versa*.

It is of low efficiency to compare all the pairs of $I_M^i(x_1)$ and $I_M^i(x_2)$ in an image to determine whether they belong to one dominant colour region. Instead, an implicit solution based on histogram analysis is proposed to detect dominant colour regions. Firstly, colour histograms of yarns are employed to estimate σ_i in Eqn (4.3). Secondly, colour histograms of dominant colours are reconstructed by the estimated $\hat{\sigma}_i$. Finally, reconstructed colour histograms of dominant colours are explored to calculate the segmentation threshold D.

4.2.1. Estimate Parameters in the Model

The standard deviation of the histogram of yarns [$I_M^i(x)$] is employed to estimate σ_i in Eqn (4.3):

$$\hat{\sigma}_i = \left(\frac{1}{n-1}\sum_{i=1}^{n}(x_i - \bar{x})^2\right)^{\frac{1}{2}} \tag{4.4}$$

where $\bar{x}$ is the mean value of x.

As ρ_i is monotonically decreasing in the domain $\left\| I_T^i(x) - I_M^i(x) \right\|$, the histograms of yarns [$I_M^i(x)$] are divided into several segments by its local valleys before applying Eqn (4.4) to estimate σ_i.

4.2.2. Reconstruct Colour Histograms of Regions

The colour histograms of dominant colours [$I_T(x)$] can be directly reconstructed from the colour histograms of yarns [$I_M^i(x)$] by the equation:

$$f(r_k) = \sum_{i=0}^{N} h(r_i)\rho_i \tag{4.5}$$

where $f(r_k)$ denotes the r_k-th level of the reconstructed colour histogram of dominant colours [$\hat{I}_T^i(x)$], $h(r_i)$ is r_i-th level of the colour histogram of yarns [$I_M^i(x)$], ρ_i is the probability of the colour of yarns [$I_M^i(x) = r_i$] associating with the colour of dominant colour regions [$\hat{I}_T^i(x) = r_k$] in the image, which can be calculated from Eqn (4.3) and Eqn (4.4), and N is the total number of segments of the colour histograms of yarns [$I_M^i(x)$].

Figure 4.2 illustrates reconstruction of the colour histogram of dominant colours (Figure 4.2c) from the colour histogram of yarns (Figure 4.2b) in the lightness channel. Eqn (4.4) was firstly employed to estimate σ_i from the lightness histogram of yarns (Figure 4.2b). Secondly, Eqn (4.3) was used to calculate the probability of colours of yarns associating with colours of dominant colour regions. Finally, Eqn (4.5) was used to reconstruct the histograms of dominant colours (Figure

4.2c). Two key points can be derived from Figure 4.2b and Figure 4.2c. Firstly, the local maxima in the colour histograms of $\hat{I}_T^i(x)$ and $I_M^i(x)$ are almost identical. Specifically, the local maxima in Figure 4.2b locate at 40, 58, 67 and 85. In Figure 4.2c, the local maxima locate at 40, 57, 66, and 83. Secondly, the reconstructed colour histograms of $\hat{I}_T^i(x)$ is more separable than those of $I_M^i(x)$. In Figure 4.2b, it is very difficult to determine whether the local maximum at 58 represents a dominant colour, whereas it becomes convincing in Figure 2c. These two key points are extremely helpful in segmenting dominant colour regions in yarn dyed fabric images.

By identifying local minima of the reconstructed colour histogram of dominant colours as the segmentation thresholds in *i*-th colour channel, dominant colour region segmentation could be achieved in each colour channel:

$$T_i(x_k) = LMin(x), i = 1,2,3, k = 1,2,\cdots \qquad (4.6)$$

where $LMin(x)$ denotes the points of the local minima x_k of the reconstructed colour histogram of $\hat{I}_T^i(x)$.

Figure 4.2d shows the segmentation result of Figure 4.2a in the lightness L* channel using the thresholds $T_1(x_k)$.

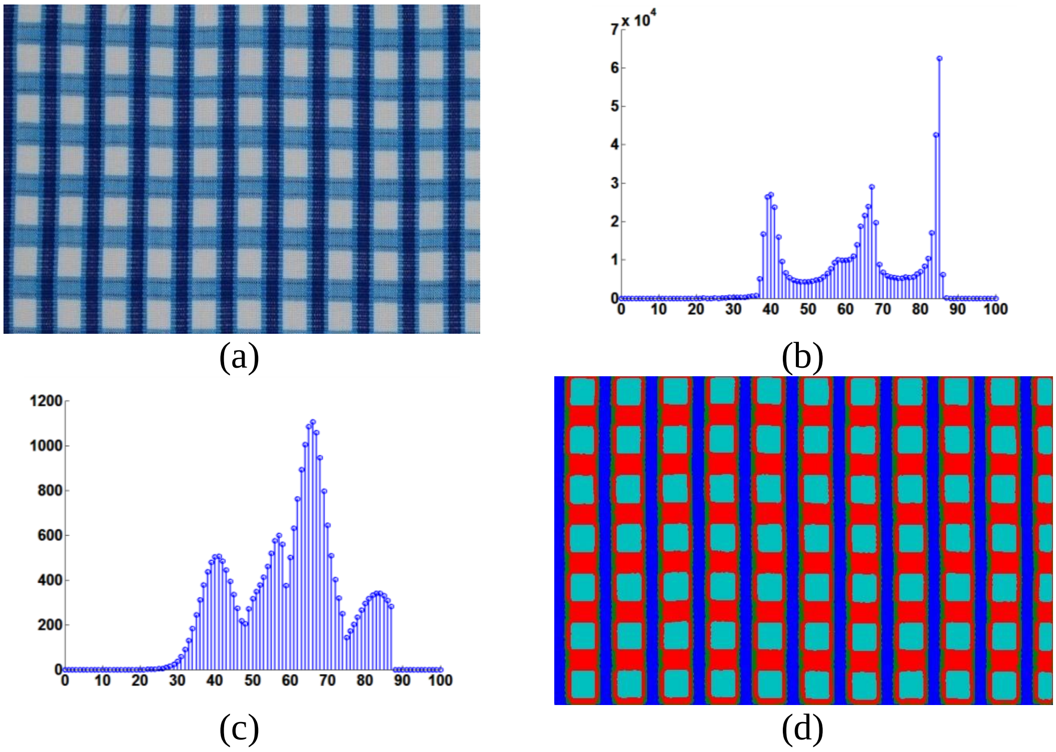

Figure 4.2 Example of dominant colour region segmentation in the lightness L* channel: (a) the yarn dyed image; (b) the colour histogram of $I_M^1(x)$; (c) the reconstructed colour histogram of $\hat{I}_T^1(x)$; (d) the segmentation result of dominant colour regions in the lightness L* channel.

4.2.3. Estimate Segmentation Thresholds

It is non-trivial to obtain a threshold D to determine whether two yarns belong to one dominant colour region. Instead, an implicit approach based on a hierarchical segmentation structure is proposed in this study to find the final segmentation of dominant colour regions.

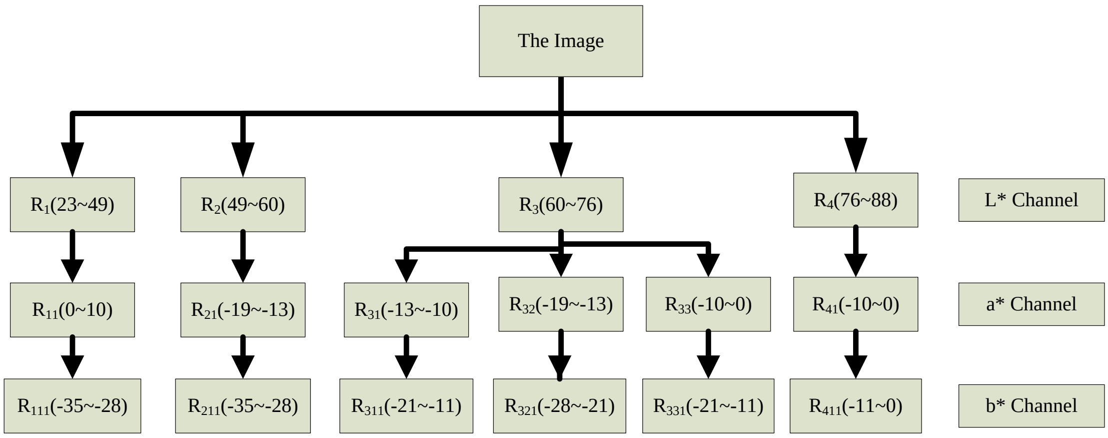

Figure 4.3 Example of the hierarchical segmentation structure to obtain the final segmentation result of dominant colour regions

Firstly, a yarn dyed fabric image is segmented into several regions R_i by the thresholds $T_1(x_k)$. Secondly, pixels in R_i are divided into one or more subregions R_{ij} by the thresholds $T_2(x_k)$. Finally, R_{ij} are split into one or more subregions R_{ijk} by the thresholds $T_3(x_k)$. Figure 4.3 shows an illustration of this procedure. For the yarn dyed image shown in Figure 4.2a, its segmentation thresholds in L*, a* and b* channels are $T_1(x_k) = 23,\ 49,\ 60,\ 76,\ 88\ \ (k = 1,\ 2,\ \cdots\ 5)$, $T_2(x_k) = -19,\ -13,\ -10,\ 0\ \ (k = 1,\ 2,\ 3,\ 4)$ and $T_3(x_k) = -35,\ -28,\ -21,\ -11,\ 0\ (k = 1,\ 2,\ \cdots\ 5)$. In the L* channel, the image is segmented into four regions $R_i\ (i = 1,2,3,4)$ by the thresholds $T_1(x_k)$. In the a* and b* channels, R_1, R_2 and R_4 cannot be divided into subregions by $T_2(x_k)$ and $T_3(x_k)$. However, R_3 can be split into 3 subregions $R_{3j}(j=1,2,3)$ by the thresholds $T_2(x_k)$. Thus, the final segmentation is 6 dominant colour regions, i.e., R_{111}, R_{211}, R_{311}, R_{321}, R_{331} and R_{411}.

In fact, the hierarchical segmentation structure is an implicit estimation of the threshold D. Given two yarns with colours $I_M^i(x_1)$, $I_M^i(x_2)$, one dominant colour $I_T^i(x)$ of a yarn dyed fabric image, and its segmentation thresholds $T_i(x_k)$ in three channels, segmentation in each colour channel can be formulated as:

$$\begin{cases} \min(\rho_i^{01},\rho_i^{02}) \ge D_i & (I_M^i(x_1)-T_i(x_k))\times(I_M^i(x_2)-T_i(x_k))>0 \\ \min(\rho_i^{01},\rho_i^{02}) < D_i & (I_M^i(x_1)-T_i(x_k))\times(I_M^i(x_2)-T_i(x_k))<0 \end{cases} \tag{4.7}$$

where $(I_i(x_1)-T_i(x_k))\times(I_i(x_2)-T_i(x_k))>0$ indicates $I_M^i(x_1)$ and $I_M^i(x_2)$ belong to $I_T^i(x)$ in the view of *i*-th colour channel, and *vice versa*. $\rho_i^{0j}(j=1,2)$ and D_i are defined as:

$$\rho_i^{0j}=(2\pi\hat{\sigma}_i^{\,2})^{-1/2}\exp(-\frac{1}{2}\left\|I_M^i(x_j)-T_i(x)\right\|^2/\hat{\sigma}_i^{\,2})(j=1,2) \tag{4.8}$$

$$D_i=(2\pi\hat{\sigma}_i^{\,2})^{-1/2}\exp(-\frac{1}{2}\left\|\Delta T_i(x)\right\|^2/\hat{\sigma}_i^{\,2})(j=1,2) \tag{4.9}$$

where $\Delta T_i(x)=T_i(x_k)-T_i(x_{k-1})$, $\rho_i^{0j}(j=1,2)$ denotes the probability that $I_M^i(x_j)$ associates with the dominant colour $I_T^i(x)=T_i(x_k)$, and D_i denotes the probability that the yarn with colour $T_i(x_k)$ associates with the dominant colour region with colour $T_i(x_{k-1})$.

Given a threshold D, which is set to determine whether two yarns with colours $I_M^i(x_1)$ and $I_M^i(x_2)$ belong to one dominant colour region its colour is $I_T^i(x)$) in the proposed model (Eqn (4.1)), $\min(\min(\rho_1^{01}, \rho_1^{02}),$ $\min(\rho_2^{01}, \rho_2^{02}),$ $\min(\rho_3^{01}, \rho_3^{02})) \geq D$ indicates that these two yarns belong to a dominant colour region in the view of all three colour channels. An example is the subregion R_{111} in Figure 4.3. If $\min(\rho_i^{01}, \rho_i^{02}) < D$ but $\min(\rho_j^{01}, \rho_j^{02}) > D$, however, these two yarns belong to a dominant colour region in the view of *j*-th colour channel but do not in the view of *i*-th colour channel. The segmentation results obtained by $T_j(x_k)$ can be partitioned more precisely into subregions by $T_i(x_k)$. As shown in Figure 4.3, the colour region R_3 segmented by the threshold $T_1(x_k)$ can be partitioned into three subregions by the threshold $T_2(x_k)$. Thus, segmentation based on the hierarchical segmentation structure estimates the threshold D as:

$$D = \min(D_i) \tag{4.10}$$

4.2.4. Summary of the Segmentation Algorithm

With a yarn dyed fabric image captured by a multispectral imaging system, the follow steps will be carried out:

(1) Convert the reflectance space of the image to the CIELAB colour space.

(2) Create the histograms of the image for L*, a* and b* colour channels.

(3) Divide the histograms of each colour channel into several segments by their local valleys.

(4) Estimate σ_i of each segment of the histograms of each colour channel by Eqn (4.4)

(5) Reconstruct the histograms of each colour channel by Eqn (4.5).

(6) Calculate the dominant colour segmentation thresholds in the reconstructed histogram of each colour channel by Eqn (4.6).

(7) Obtain the dominant colour segmentation results in each colour channel by these thresholds.

(8) Combine the segmentation results in each colour channel into final segmentation results by the hierarchical structure shown in Figure 4.3.

4.3. Results and Discussion

In order to evaluate the proposed approach, it was implemented on a PC with 2.80 GHz CPU and 8 GB RAM. Cotton yarn dyed fabric samples were used. The image captured by ICM was converted into data in CIELAB colour space. In order to reduce the influence of noises, images in CIELAB colour space were preprocessed by a Gaussian filter with a radius of 7 pixels.

4.3.1. Verification of the Probability Model

The first experiment looked at the probabilistic distribution of colour in the dominant colour region of a yarn dyed fabric image. Figure 4.4b plots the lightness histogram of the dominant colour region shown as a yellow rectangle in Figure 4.4a. The shape of the histogram shown in Figure 4.4b agrees with the Gaussian distribution.

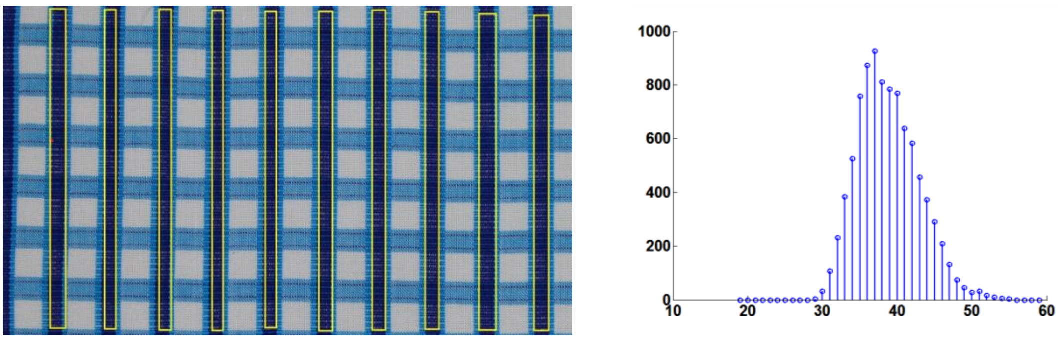

(a) (b)

Figure 4.4 Example of dominant colour regions and their lightness histogram: (a) dominant colour regions (The yellow rectangles show the selected dominant colour regions); (b) the corresponding lightness histogram.

4.3.2. Experiments Using Macro and Telephoto Lenses

A macro lens with a 25 mm focal length was used to evaluate the proposed method. Test samples were classified into two groups: a simple group and a complex group. In the simple group, dominant colour regions had distinct colours and consisted of regular patterns, such as thick stripes and rectangles. On the other hand, dominant colour regions in the complex group were not easily identified. Images in this group had patterns with different sizes, and colours were quite analogous to one another. Figure 4.5 and Figure 4.6 show the dominant colour region segmentation results of images in the simple and complex groups respectively. The dominant colour regions in the simple and complex groups are both separated correctly compared with the actual fabric samples.

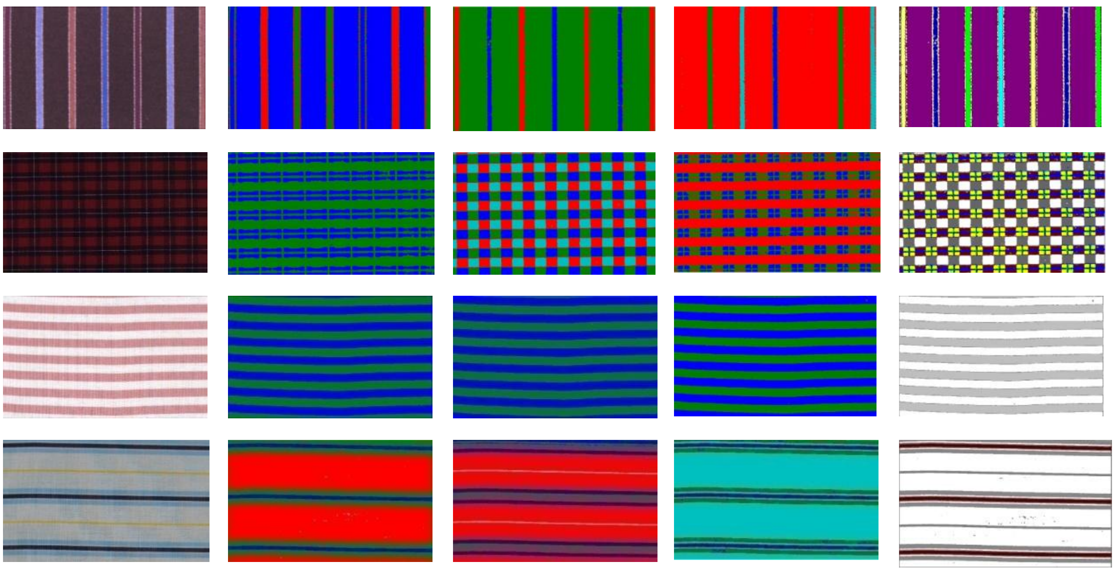

(a) (b) (c) (d) (e)

Figure 4.5 Experimental results in the simple group: (a) source images; (b-d) segmentation results in the L*, a* and b* channels; (e) final segmentation results of dominant colour regions.

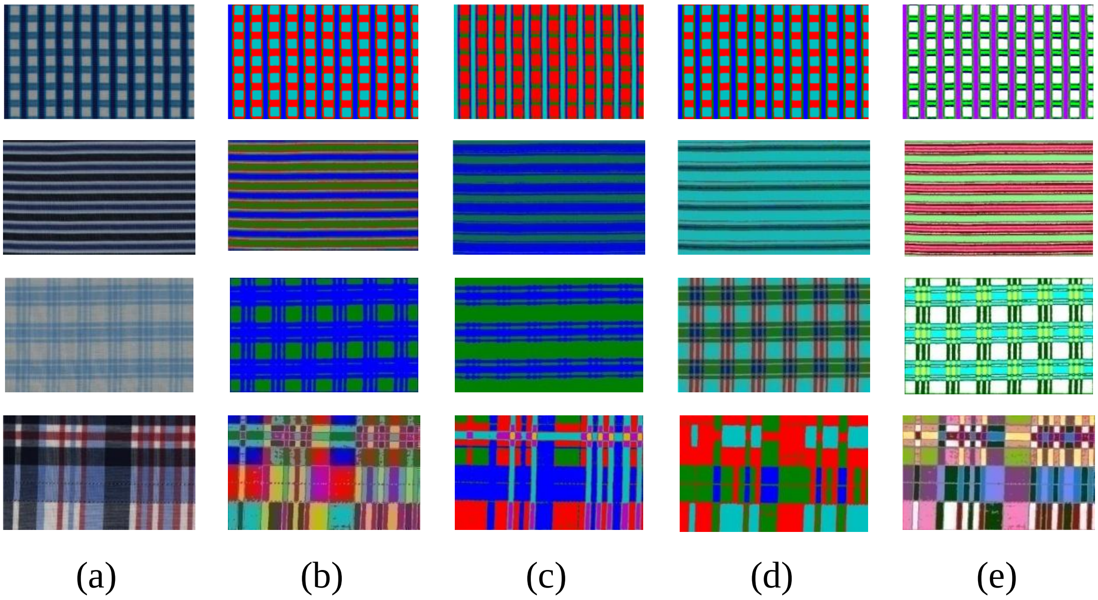

Figure 4.6 Experimental results in the complex group: (a) source images; (b-d) segmentation results in the L*, a* and b* channels; (e) final segmentation results of dominant colour regions.

A telephoto lens with a 100 mm focal length was also used to evaluate the proposed method. As the imaging areas from a telephoto lens are smaller than those from a macro lens, only parts of the images in Figure 4.6 can be captured by the telephoto lens, shown in Figure 4.7. These images and the experimental results are shown in Figure 4.8. It is also demonstrated that the proposed method segments dominant colour regions of these yarn dyed fabric images successfully. Comparing the segmentation results in Figure 4.6 and Figure 4.8, the proposed method performs better with the macro lens than with the telephoto lens. When the telephoto lens is used, the spatial structure of yarns is much clearer.

Thus, it is more difficult to cluster the yarns of a yarn dyed fabric as one dominant colour region.

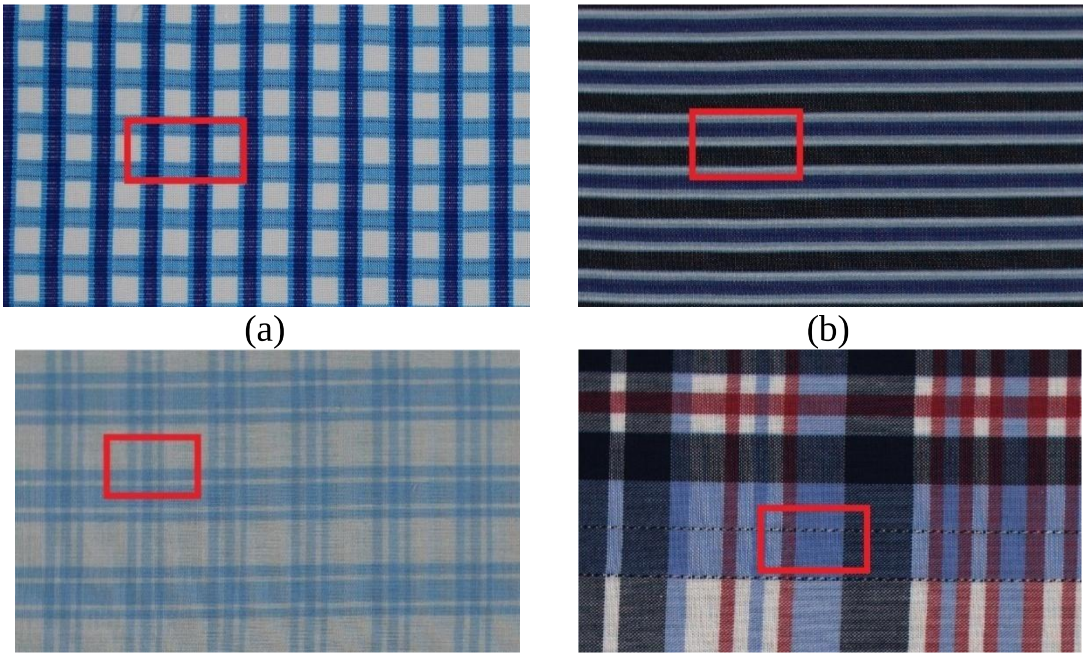

Figure 4.7 The areas of fabrics (shown in Figure 4.6) captured by the telephoto lens.

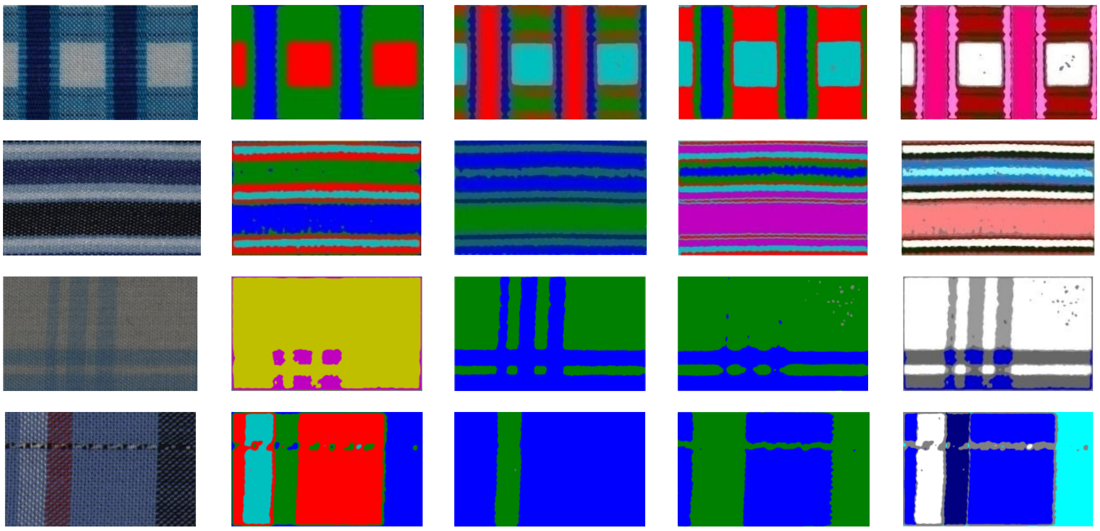

(a) (b) (c) (d) (e)

Figure 4.8 Experimental results using the telephoto lens: (a) source images; (b-d) segmentation results in the L*, a* and b* channels; (e) final segmentation results of dominant colour regions.

4.3.3. Computational Complexity Analysis

Figure 4.9 shows the time complexity of the proposed algorithm using the macro and telephoto lenses. As shown in Fig. 9, the initial times for processing one image using lenses with 25 and 100 mm focal lengths are approximately 0.5 and 0.6 s respectively. For yarn dyed fabric images captured by the 25 and 100 mm focal length lenses, the processing time per dominant colour region is approximately 0.045 and 0.075 s respectively.

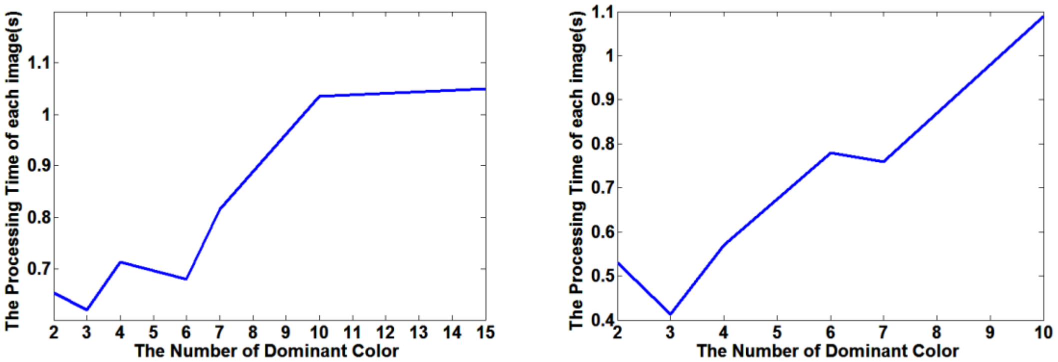

(a) (b)

Figure 4.9 The processing time per image using lenses with 25 and 100 mm focal lengths: (a) the processing time per image using the 25mm lens; (b) the processing time per image using the 100mm lens.

4.3.4. Comparison Experiments

The proposed method was also compared with the seeded region growing [92] and quadtree segmentation [94] methods. In the seeded region growing method, seeds were chosen manually and randomly in each dominant colour region. In the quadtree segmentation method, the test image was first cropped to 512*512 pixels, as this method is appropriate primarily for square-sized images whose dimensions are a power of 2. Then, the image is split into regions by thresholds 0.13, 0.18, and 0.09 in the L*, a*, and b* channels. These thresholds were tuned manually to produce best segmentation in each colour channel. After that, the mean values were calculated. Finally, the segmentation results were obtained by applying the same thresholds in the splitting procedure. Figure 4.10 shows the segmentation results of dominant colour regions using these methods.

As shown in Figure 4.10f-h, oversegmentation occurs in the seeded region growing method. This is considered as a result of colour changes at yarn intersections and interstices between weft and warp yarns. Because of the colour changes, the seeded region growing method rejects the inclusion of the corresponding pixels to a dominant colour region. The major problem of the seeded region growing method is how to select seeds. The final number of segmented regions must also be known a priori in this method. As shown in Figure 4.10j-l, over segmentation and under segmentation occur when the quadtree method is applied. It is difficult to find a global threshold to split the image in the quadtree segmentation method.

A quantitative comparison of the proposed method, the seeded region growing method, and the quadtree segmentation method was also conducted. As shown in Figure 4.11a, dominant colour regions were manually labeled as ground truth. The overlap areas between the ground truth and segmentation regions by these three methods were viewed as successful segmentation. The degree of overlap was defined as:

$$D = \frac{\sum_{i=1}^{n} A_i}{\sum_{i=1}^{n} W_i * H_i} \tag{4.11}$$

where A_i denotes the number of pixels in the i-th rectangle of the overlap areas, and W_i and H_i represent the width and length of the i-th dominant colour region in the ground truth.

Figure 4.11b shows the quantitative comparison results. It is concluded that the proposed method performs better in detecting dominant colour regions than the other two methods.

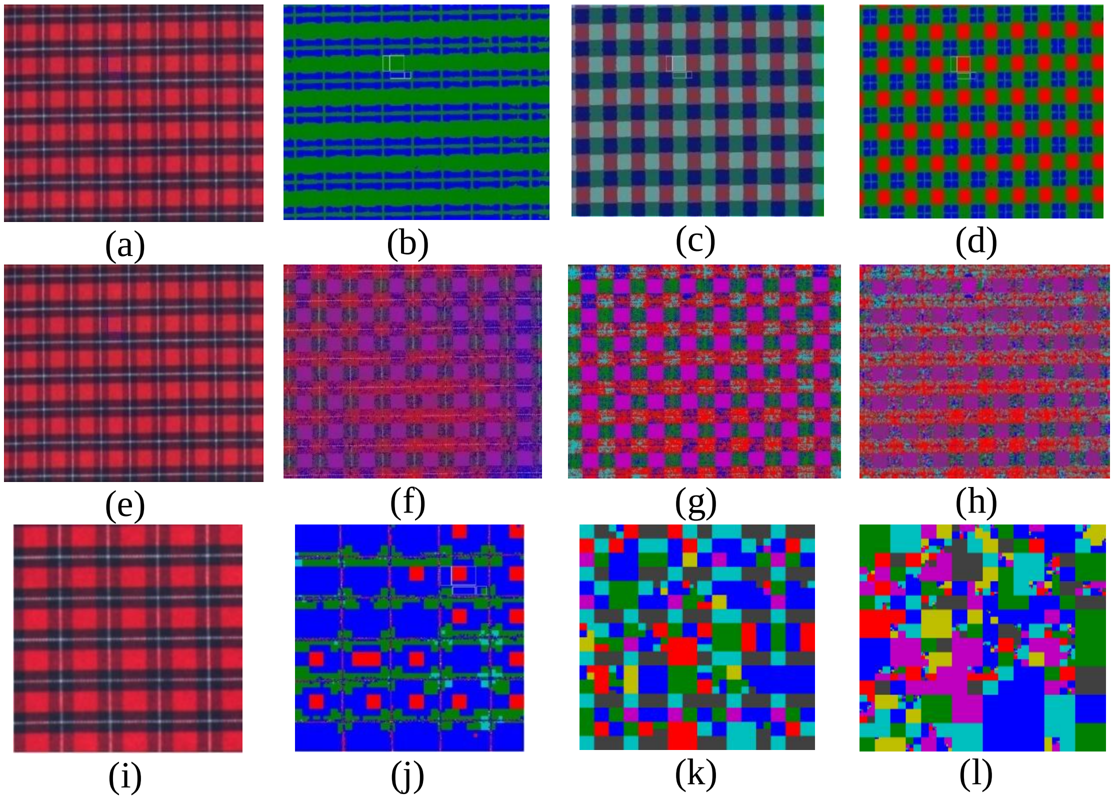

Figure 4.10 Comparative experiments using the proposed method, region growing method, and quadtree decomposition method: (a), (e), and (i) source images; (b-d) segmentation results in the L*, a* and b* channels by the proposed method; (f-h) segmentation results in the L*, a* and b* channels by the region growing method; (j-l) segmentation results in the L*, a* and b* channels by the quadtree decomposition method.

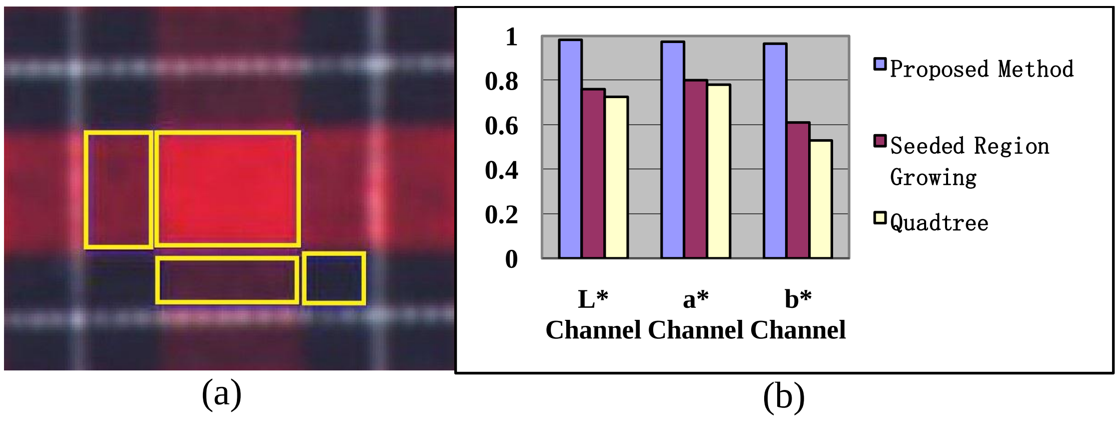

Figure 4.11 The dominant colour regions chosen in the quantitative experiment and the comparison result: (a) the chosen four dominant colour regions are shown in yellow rectangles; (b) the quantitative result of the proposed method, region growing method and quadtree method.

4.4. Conclusion

An unsupervised method of dominant colour region segmentation in yarn dyed fabric images is developed in this chapter. This method is based on a probabilistic model and includes three steps. Firstly, the colour histograms of a dominant colour region are estimated from those of yarns in a yarn dyed fabric image. Secondly, dominant colour region segmentation is performed in three colour channels independently. Finally, a hierarchical segmentation structure is devised to obtain dominant colour regions by combining segmentation results in three colour channels. Experiments show that the proposed approach achieves excellent dominant colour region segmentation performance for yarn dyed fabric images captured by both macro and telephoto lenses. The time for processing one dominant colour region of images captured by the macro and telephoto lenses is approximately 0.045s and 0.075s respectively, which demonstrates this approach is suitable for industrial applications.

Chapter 5 Solid-colour and Multi-colour Region Detection

The approach introduced in Chapter 4 achieves dominant colour region segmentation in yarn dyed fabric images. However, a dominant colour region can be either solid-colour (weft and warp yarns with the same colour) or multi-colour (weft and warp yarns with different colours). In this chapter, an efficient approach to detect solid-colour and multi-colour regions in real yarn dyed fabric images is presented. Based on the reflection model introduced in Chapter 3, solid-colour and multi-colour regions can be distinguished in the CIExyY space.

5.1. Background

A yarn dyed fabric is cross-woven by weft and warp yarns. When the colour of weft and warp yarns is identical, the region interlaced by these yarns is so-called solid-colour. In contrast, multi-colour regions are intertwined by weft and warp yarns with different colours. Traditionally, colour measurements of solid-colour regions are achieved by spectrophotometers. However, a spectrophotometer cannot be directly used to measure colours of multi-colour regions because this type of instrument can only measure the average colour of a sample [151]. With the development of digital imaging technology, multispectral imaging (MSI) systems [48,50] are adopted to extract colour information of a fabric sample. A MSI system can provide not only the spectral information but also the spatial information of a sample. The spatial information can help understand important knowledge about a yarn dyed fabric, such as the location distributions of weft and warp yarns and their structures. When a MSI system is applied to measure the colour of a solid-colour yarn-dyed fabric, colours of weft wand warp yarns can be exacted without weft and warp yarn segmentation as they have same colours. In contrast, a MSI system is obliged to segment weft and warp yarns of a multi-colour region before calculating their colours. Thus, it is necessary to initially detect solid-colour and multi-colour regions in yarn-dyed fabric images before analyzing their colours.

In this chapter, an efficient approach to segment solid-colour and multi-colour regions in real yarn-dyed fabric images is introduced. Based on the reflection model introduced in Chapter 3, solid-colour and multi-colour regions in yarn-dyed fabric images can be distinguished in the CIExyY space. The CIExyY histograms of a solid-colour region accord with one Gaussian distribution but those of a multi-colour region agree with a combination of two Gaussian distributions.

5.2. Solid-colour and Multi-colour Region Detection

5.2.1. Spectral Response of a MSI system

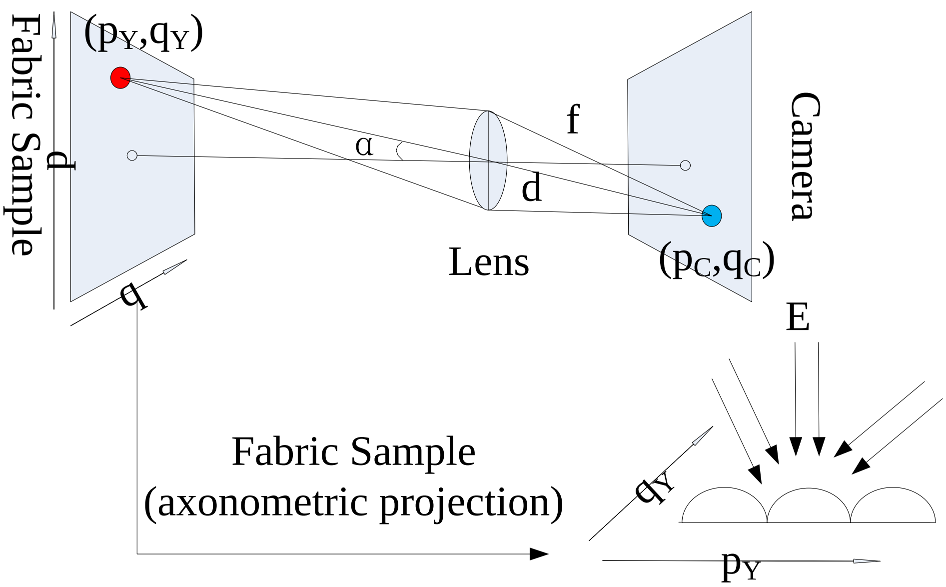

d: radius of lens f: distance from lens to image plane
α : angle of the sample with respect to view

Figure 5.1 The basic optics within a MSI system

Figure 5.1 shows the basic optics within a multispectral imaging system. Given lens radius d, distance from lens to image plane f, and angle of the yarn dyed fabric with respect to the view α, the irradiance at pixel (p_C, q_C) of the image plane, $E(\lambda, p_C, q_C)$ is given [134,135]:

$$E(\lambda, p_C, q_C) = L(\lambda, p_Y, q_Y)\frac{\pi}{4}(\frac{d}{f})^2 \cos^4 \alpha \tag{5. 1}$$

where $L(\lambda, p_Y, q_Y)$ denotes the radiance at the yarn dyed fabric surface (p_Y, q_Y), (p_Y, q_Y) represents the position on the yarn dyed fabric corresponding to (p_C, q_C), λ expresses the wavelength.

Based on the reflection model proposed in Chapter 3, the light reflected by a yarn dyed fabric can be modeled as:

$$\begin{aligned} L(\lambda, p_Y, q_Y) = {} & m_b(p_Y, q_Y)H(p_Y, q_Y)E(\lambda)R_1(\lambda) \\ & + m_b(p_Y, q_Y)A(p_Y, q_Y)E(\lambda)R_1(\lambda)R_2(\lambda) \end{aligned} \tag{5. 2}$$

where $E(\lambda)$ denotes the illuminant spectrum, $m_b(p_Y, q_Y)$, $H(p_Y, q_Y)$ and $A(p_Y, q_Y)$ express the influences of fabric surface, illuminant of the MSI system and inter-reflection between neighbouring yarns, $R_1(\lambda)$ and $R_2(\lambda)$ represent the nominal reflectance of the measured yarn and its neighbouring yarn. In a solid-colour region, $R_1(\lambda)$ is equal to $R_2(\lambda)$. In contrast, $R_1(\lambda)$ and $R_2(\lambda)$ are different in a multi-colour region.

Substituting Eqn (5.2) into Eqn (5.1), we have:

$$E(\lambda, p_C, q_C) = m_b(p_Y, q_Y)H(p_Y, q_Y)E(\lambda)R_1(\lambda)\frac{\pi}{4}(\frac{d}{f})^2 \cos^4 \alpha$$
$$+ m_b(p_Y, q_Y)A(p_Y, q_Y)E(\lambda)R_1(\lambda)R_2(\lambda)\frac{\pi}{4}(\frac{d}{f})^2 \cos^4 \alpha \quad (5.3)$$

When the NIST White Tiles is used to calibrate the MSI system, the irradiance at pixel (p_C, q_C) is:

$$E_S(\lambda, p_C, q_C) = E(\lambda)\frac{\pi}{4}(\frac{d}{f})^2 \cos^4 \alpha \quad (5.4)$$

Combining Eqn (5.3) and Eqn (5.4), the spectral response of the MSI system to a yarn dyed fabric can be modeled as:

$$\begin{aligned} R_b(\lambda, p_C, q_C) &= \frac{E(\lambda, p_C, q_C)}{E_S(\lambda, p_C, q_C)} \\ &= m_b(p_Y, q_Y)H(p_Y, q_Y)R_1(\lambda) \\ &\quad + m_b(p_Y, q_Y)A(p_Y, q_Y)R_1(\lambda)R_2(\lambda) \end{aligned} \quad (5.5)$$

5.2.2. Colour in the CIEXYZ and CIELAB Spaces

Given the CIE colour matching functions $\bar{x}(\lambda)$, $\bar{y}(\lambda)$, $\bar{z}(\lambda)$, the tristimulus of the pixel (p_C, q_C) can be specified as [125]:

$$\begin{cases} X(p_C,q_C) = k\int_\lambda R_b(\lambda,p_C,q_C)E(\lambda)\bar{x}(\lambda)d\lambda \\ \qquad = km_b(p_Y,q_Y)[H(p_Y,q_Y)\int_\lambda E(\lambda)R_1(\lambda)\bar{x}(\lambda)d\lambda + A(p_Y,q_Y)\int_\lambda E(\lambda)R_1(\lambda)R_2(\lambda)\bar{x}(\lambda)d\lambda] \\ Y(p_C,q_C) = k\int_\lambda R_b(\lambda,p_C,q_C)E(\lambda)\bar{y}(\lambda)d\lambda \\ \qquad = km_b(p_Y,q_Y)[H(p_Y,q_Y)\int_\lambda E(\lambda)R_1(\lambda)\bar{y}(\lambda)d\lambda + A(p_Y,q_Y)\int_\lambda E(\lambda)R_1(\lambda)R_2(\lambda)\bar{y}(\lambda)d\lambda] \\ Z(p_C,q_C) = k\int_\lambda R_b(\lambda,p_C,q_C)E(\lambda)\bar{z}(\lambda)d\lambda \\ \qquad = km_b(p_Y,q_Y)[H(p_Y,q_Y)\int_\lambda E(\lambda)R_1(\lambda)\bar{z}(\lambda)d\lambda + A(p_Y,q_Y)\int_\lambda E(\lambda)R_1(\lambda)R_2(\lambda)\bar{z}(\lambda)d\lambda] \end{cases} \tag{5. 6}$$

where k is a normalising factor given by $k = 100/\int_\lambda E(\lambda)\bar{y}(\lambda)d\lambda$.

The CIELAB colour of pixel (p_C,q_C) can be specified as [125]:

$$\begin{cases} L^*(p_C,q_C) = 116f(Y(p_C,q_C)/Y_n) - 16 \\ a^*(p_C,q_C) = 500[f(X(p_C,q_C)/X_n) - f(Y(p_C,q_C)/Y_n)] \\ b^*(p_C,q_C) = 200[f(Y(p_C,q_C)/Y_n) - f(Z(p_C,q_C)/Z_n)] \end{cases} \tag{5.7}$$

where

$$f(t) = \begin{cases} t^{1/3} & t > (\frac{6}{29})^3 \\ \frac{1}{3}(\frac{29}{6})^2 t + \frac{4}{29} & \text{otherwise} \end{cases} \tag{5.8}$$

$[X_n,Y_n,Z_n]$ denotes the tristimulus values for the reference white point. $[X_n,Y_n,Z_n]$ represents the influence of illuminant on colour, i.e., $[X_n,Y_n,Z_n]$ changes with illuminants or CIELAB colours calculated by different $[X_n,Y_n,Z_n]$ values imply a sample is viewed under different illuminants.

$$\begin{cases} \dfrac{X(p_C,q_C)}{X_n} = \dfrac{k[H(p_Y,q_Y)\int_\lambda E(\lambda)R_1(\lambda)\bar{x}(\lambda)d\lambda + A(p_Y,q_Y)\int_\lambda E(\lambda)R_1(\lambda)R_2(\lambda)\bar{x}(\lambda)d\lambda]}{X_n/m_b(p_Y,q_Y)} \\ \dfrac{Y(p_C,q_C)}{Y_n} = \dfrac{k[H(p_Y,q_Y)\int_\lambda E(\lambda)R_1(\lambda)\bar{y}(\lambda)d\lambda + A(p_Y,q_Y)\int_\lambda E(\lambda)R_1(\lambda)R_2(\lambda)\bar{y}(\lambda)d\lambda]}{Y_n/m_b(p_Y,q_Y)} \\ \dfrac{Z(p_C,q_C)}{Z_n} = \dfrac{k[H(p_Y,q_Y)\int_\lambda E(\lambda)R_1(\lambda)\bar{z}(\lambda)(\lambda)d\lambda + A(p_Y,q_Y)\int_\lambda E(\lambda)R_1(\lambda)R_2(\lambda)\bar{z}(\lambda)(\lambda)d\lambda]}{Z_n/m_b(p_Y,q_Y)} \end{cases} \quad (5.9)$$

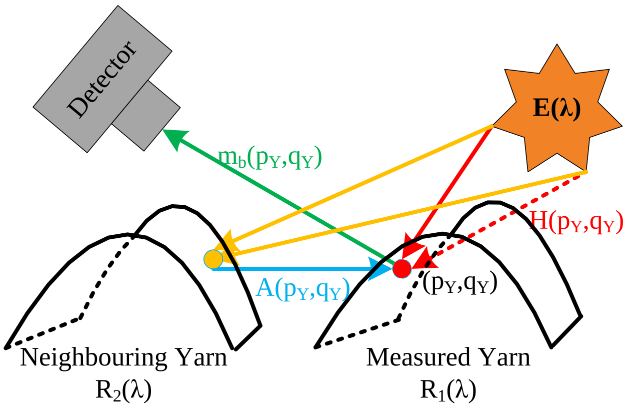

Figure 5.2 Influences of coefficients $m_b(p_Y,q_Y)$, $H(p_Y,q_Y)$, and $A(p_Y,q_Y)$ on measured colour. The yarn-dyed fabric is viewed in axonometric projection.

As shown in Figure 5.2, it is trivial to understand that $H(p_Y,q_Y)$ and $A(p_Y,q_Y)$ represent the influences of the MSI system and neighbouring yarns on measured colour. $H(p_Y,q_Y)$ expresses the percentage of beams shining on the surface position (p_Y,q_Y) from the illuminant of the MSI system. $A(p_Y,q_Y)$ implies the intensity of light reflected by neighbouring yarns. However, it is much more difficult to understand the impact of $m_b(p_Y,q_Y)$ on measured colour, especially

CIELAB colour. In the reflectance and CIEXYZ spaces, Eqn (5.5) and Eqn (5.6) express reflectance and tristimulus values are scaled by $m_b(p_Y, q_Y)$. In the CIELAB space, the influence of $m_b(p_Y, q_Y)$ can be interpreted that pixel (p_Y, q_Y) is viewed under the illuminant which tristimulus values is $[X_n/m_b(p_Y,q_Y), Y_n/m_b(p_Y,q_Y), Z_n/m_b(p_Y,q_Y)]$ rather than $[X_n, Y_n, Z_n]$, as shown by Eqn (5.9).

According to the Oren–Nayar reflectance model [113], the geometric variable can be specified as $m_b(p_Y, q_Y) = \cos(\theta)$, where θ is the incident angle at (p_Y, q_Y). In the peak areas of a yarn dyed fabric surface, the incident angle approximates to zero and thus the geometric term approaches one. In contrast, the geometric term comes up to zero in valley areas because of large incident angle. In the transition areas between parks and valleys, the geometric term changes from zero to one. Therefore, pixel colours change with surface positions for both solid-colour and multi-colour regions in terms of tristimulus values and CIELAB colours. It should be noted that subtraction operation to calculate CIELAB colours from tristimulus values in Eqn (5.7) would reduce but cannot eliminate the influence of geometric term. As a consequence, $m_b(p_Y, q_Y)$ has a great impact on CIEXYZ and CIELAB colours for both solid-colour and multi-colour yarn-dyed fabric regions. The geometric term hampers determining thresholds of CIEXYZ or CIELAB colour histograms to distinguish solid-colour and multi-colour regions.

5.2.3. Chromaticity Coordinates

The chromaticity coordinates of a yarn-dyed fabric is directly calculated from tristimulus values [125]:

$$\begin{cases} x(p_C,q_C)=\dfrac{X(p_C,q_C)}{X(p_C,q_C)+Y(p_C,q_C)+Z(p_C,q_C)} \\ \quad =\dfrac{H(p_Y,q_Y)\int_\lambda E(\lambda)R_1(\lambda)\bar{x}(\lambda)d\lambda+A(p_Y,q_Y)\int_\lambda E(\lambda)R_1(\lambda)R_2(\lambda)\bar{x}(\lambda)d\lambda}{H(p_Y,q_Y)\int_\lambda E(\lambda)R_1(\lambda)(\bar{x}(\lambda)+\bar{y}(\lambda)+\bar{z}(\lambda))d\lambda+A(p_Y,q_Y)\int_\lambda E(\lambda)R_1(\lambda)R_2(\lambda)(\bar{x}(\lambda)+\bar{y}(\lambda)+\bar{z}(\lambda))d\lambda} \\ y(p_C,q_C)=\dfrac{Y(p_C,q_C)}{X(p_C,q_C)+Y(p_C,q_C)+Z(p_C,q_C)} \\ \quad =\dfrac{H(p_Y,q_Y)\int_\lambda E(\lambda)R_1(\lambda)\bar{y}(\lambda)d\lambda+A(p_Y,q_Y)\int_\lambda E(\lambda)R_1(\lambda)R_2(\lambda)\bar{y}(\lambda)d\lambda}{H(p_Y,q_Y)\int_\lambda E(\lambda)R_1(\lambda)(\bar{x}(\lambda)+\bar{y}(\lambda)+\bar{z}(\lambda))d\lambda+A(p_Y,q_Y)\int_\lambda E(\lambda)R_1(\lambda)R_2(\lambda)(\bar{x}(\lambda)+\bar{y}(\lambda)+\bar{z}(\lambda))d\lambda} \end{cases} \tag{5. 10}$$

Eq.(5.10) expresses chromaticity coordinates of a yarn dyed fabric are not affected by the geometric term $m_b(p_Y,q_Y)$ but the occlusion coefficient $H(p_Y,q_Y)$ and the ambient coefficient $A(p_Y,q_Y)$.

5.2.4. Solid-colour and Multi-colour Region Segmentation

Instead of the CIEXYZ and CIELAB colours, the CIExyY colour is used to distinguish solid-colour and multi-colour regions in yarn dyed fabric images. By dividing the numerators and denominators by the occlusion coefficient $H(p_Y, q_Y)$ in Eqn (5.10), the CIExyY colour of the yarn-dyed fabric can be expressed as:

$$
\begin{cases}
x(p_C, q_C) = \dfrac{\int_\lambda E(\lambda)R_1(\lambda)\bar{x}(\lambda)d\lambda + \dfrac{A(p_Y, q_Y)}{H(p_Y, q_Y)}\int_\lambda E(\lambda)R_1(\lambda)R_2(\lambda)\bar{x}(\lambda)d\lambda}{\int_\lambda E(\lambda)R_1(\lambda)(\bar{x}(\lambda)+\bar{y}(\lambda)+\bar{z}(\lambda))d\lambda + \dfrac{A(p_Y, q_Y)}{H(p_Y, q_Y)}\int_\lambda E(\lambda)R_1(\lambda)R_2(\lambda)(\bar{x}(\lambda)+\bar{y}(\lambda)+\bar{z}(\lambda))d\lambda} \\
y(p_C, q_C) = \dfrac{\int_\lambda E(\lambda)R_1(\lambda)\bar{y}(\lambda)d\lambda + \dfrac{A(p_Y, q_Y)}{H(p_Y, q_Y)}\int_\lambda E(\lambda)R_1(\lambda)R_2(\lambda)\bar{y}(\lambda)d\lambda}{\int_\lambda E(\lambda)R_1(\lambda)(\bar{x}(\lambda)+\bar{y}(\lambda)+\bar{z}(\lambda))d\lambda + \dfrac{A(p_Y, q_Y)}{H(p_Y, q_Y)}\int_\lambda E(\lambda)R_1(\lambda)R_2(\lambda)(\bar{x}(\lambda)+\bar{y}(\lambda)+\bar{z}(\lambda))d\lambda} \\
Y(p_C, q_C) = km_b(p_Y, q_Y)[H(p_Y, q_Y)\int_\lambda E(\lambda)R_1(\lambda)\bar{y}(\lambda)d\lambda + A(p_Y, q_Y)\int_\lambda E(\lambda)R_1(\lambda)R_2(\lambda)\bar{y}(\lambda)d\lambda
\end{cases}
\tag{5. 11}
$$

In the peak areas of a yarn dyed fabric surface, the contribution of system illuminant is dominant ($H(p_Y, q_Y) >> A(p_Y, q_Y)$) as the occlusion coefficient approximates 1 but the ambient coefficient is close to 0. As a consequence, the ratio of $A(p_Y, q_Y)$ to $H(p_Y, q_Y)$ approaches to 0. In the transition areas between peak and valley areas, both the system and ambient illuminants contribute to chromaticity coordinates. The contribution of the system illuminant becomes less with positions more approaching valley areas. In the valley areas of a surface, the contribution of ambient illuminant is dominant.

While the surface of a yarn dyed fabric can be divided into peak, valley and transition areas, the possibility of pixels locating in the peak areas is much larger than valley and transition areas because the real yarn cross-sectional shape of yarn dyed fabrics approximates race-track [121], lens [122] or shoulder squareness [123] rather than ideal circle, as shown in Figure 3.4. In addition, the surface shape of a yarn dyed fabric would be influenced by many factors such as fiber strength, yarn count, yarn twist factor, cover factor, and thread density. According to the central limit theorem (CLT) [131], almost any measured quantity which depends on several underlying factors has a Gaussian probability density distribution. Thus, the chromaticity and luminance histograms have a Gaussian distribution for both weft and warp yarns.

For a solid-colour region, the colour of weft and warp yarns is identical, i.e., $R_1(\lambda) = R_2(\lambda)$ in Eqn (5.11). As a consequence, the chromaticity and luminance histograms accord with one Gaussian distribution respectively.

For a multi-colour region, three situations are included according to the CIExyY colours of weft and warp yarns: different chromaticity coordinates, similar chromaticity coordinates but distinctly different luminance, and same chromaticity coordinates and similar luminance. Firstly, when weft and warp yarns have different chromaticity coordinates, the chromaticity histograms of the region agree with a combination of two Gaussian distributions. Secondly, when weft and warp yarns have similar chromaticity coordinates but distinctly different luminance values, both of chromaticity and luminance histograms can be used to determine if the region is multi-colour. The chromaticity histograms may accord with a combination of two Gaussian distributions because influences of the above mentioned factors (fiber strength, yarn count, yarn twist factor, cover factor, and thread density) on weft and warp yarns may be different. In addition, the luminance histogram accords with a combination of two Gaussian distributions since the luminance values of weft and warp yarns are different. For solid-colour regions, however, luminance histograms accord with one Gaussian distribution. Finally, weft and warp yarns with similar chromaticity and similar luminance are ignored because this is quite uncommon in real industrial applications.

5.3. Results and Discussion

Simulation and real experiments were conducted to evaluate the proposed approach to distinguish solid-colour and multi-colour yarn dyed fabric regions. Tristimulus values of a region were transformed from its reflectance by Eqn (5.6). The CIExyY and CIELAB colours were transformed from the CIEXYZ colour by Eqn (5.11) and Eqn (5.7). The CIEXYZ, CIELAB, and CIExyY histograms were normalized to eliminate the influence of region size. Colour histograms were distributed among 256 bins to fully show their shapes.

5.3.1. Simulation Experiment

The first experiment checked the influences of the occlusion and ambient coefficients on the chromaticity histograms of a solid-colour yarn dyed fabric region. Given the reflectance of yarns and the illuminant of the MSI system, the chromaticity coordinates of a solid-colour region yarn dyed fabric is determined by the ratio $A(p_Y,q_Y)/H(p_Y,q_Y)$, as shown by Eqn (5.11). We can find the relationship between $A(p_Y,q_Y)/H(p_Y,q_Y)$ and luminance $Y(p_C,q_C)$ from Eqn (5.11) as:

$$\frac{A(p_Y,q_Y)}{H(p_Y,q_Y)}=\frac{1}{km_b(p_Y,q_Y)H(p_Y,q_Y)\int_\lambda E(\lambda)R_1(\lambda)R_2(\lambda)\bar{y}(\lambda)d\lambda}Y(p_C,q_C) \\ -\frac{\int_\lambda E(\lambda)R_1(\lambda)\bar{y}(\lambda)d\lambda}{\int_\lambda E(\lambda)R_1(\lambda)R_2(\lambda)\bar{y}(\lambda)d\lambda} \tag{5. 12}$$

Eqn (5.12) expresses that $A(p_Y,q_Y)/H(p_Y,q_Y)$ is linearly decreased with less $Y(p_C,q_C)$. As mentioned in Section 5.2.2, $H(p_Y,q_Y)$ and $A(p_Y,q_Y)$ represent the influences of the system and ambient illuminants on measured chromaticity coordinates. $H(p_Y,q_Y)$ is large in peak areas but in reverse in valley areas. In the transition areas between peak and valley areas, $H(p_Y,q_Y)$ becomes larger with pixels more approaching peaks. However, $A(p_Y,q_Y)$ changes reversely with $H(p_Y,q_Y)$. Thus, we can use the following equation to estimate the contributions of occlusion coefficient $H(p_Y,q_Y)$ and the ambient coefficient $A(p_Y,q_Y)$ to chromaticity coordinates:

$$\frac{A}{H}=\begin{cases}0 & P_Y \geq b \\ -\frac{a}{b}P_Y + a & P_Y < b\end{cases} \tag{5. 13}$$

where P_Y denotes the percentile of the luminance histogram, a and b express the thresholds of $A(p_C, q_C)/H(p_C, q_C)$ and luminance. When $P_Y \geq b$, the contribution of system illuminant to chromaticity values is dominant and ambient illuminant is assumed to be negligible. When $P_Y < b$, the contribution of the system illuminant becomes less with more close to valleys linearly. At the valley of the surface, the contribution of ambient illuminant is a times than system illuminant.

Given the luminance of a solid-colour region and the reflectance of weft and warp yarns, Figure 5.3 shows the simulation results of the influences of $H(p_Y, q_Y)$ and $A(p_Y, q_Y)$ on the chromaticity histograms. Figure 5.3a and b show the luminance image of the solid-colour region and the reflectance of yarns. The parameters a and b are set to the range of [10, 50] with an interval of 10 and the range of [0.7, 1.0] with an interval of 0.1. Figure 5.3c plots the ratio A/H with respect to P_Y. Figure 5.3d shows the simulated chromaticity histograms. It can be observed that chromaticity histograms are more leptokurtosis [136] with larger b. This implies that the threshold b would influence shapes of chromaticity histograms. However, the thresholds a have less impact on the chromaticity histograms than b. While shapes of chromaticity histograms depend on the thresholds a and b, all the chromaticity histograms accord with one Gaussian distribution except for those simulated by $b = 0.7$. It can be concluded that the thresholds of b should not less than 0.7. Figure 5.3e shows the real chromaticity histograms of the solid-colour region.

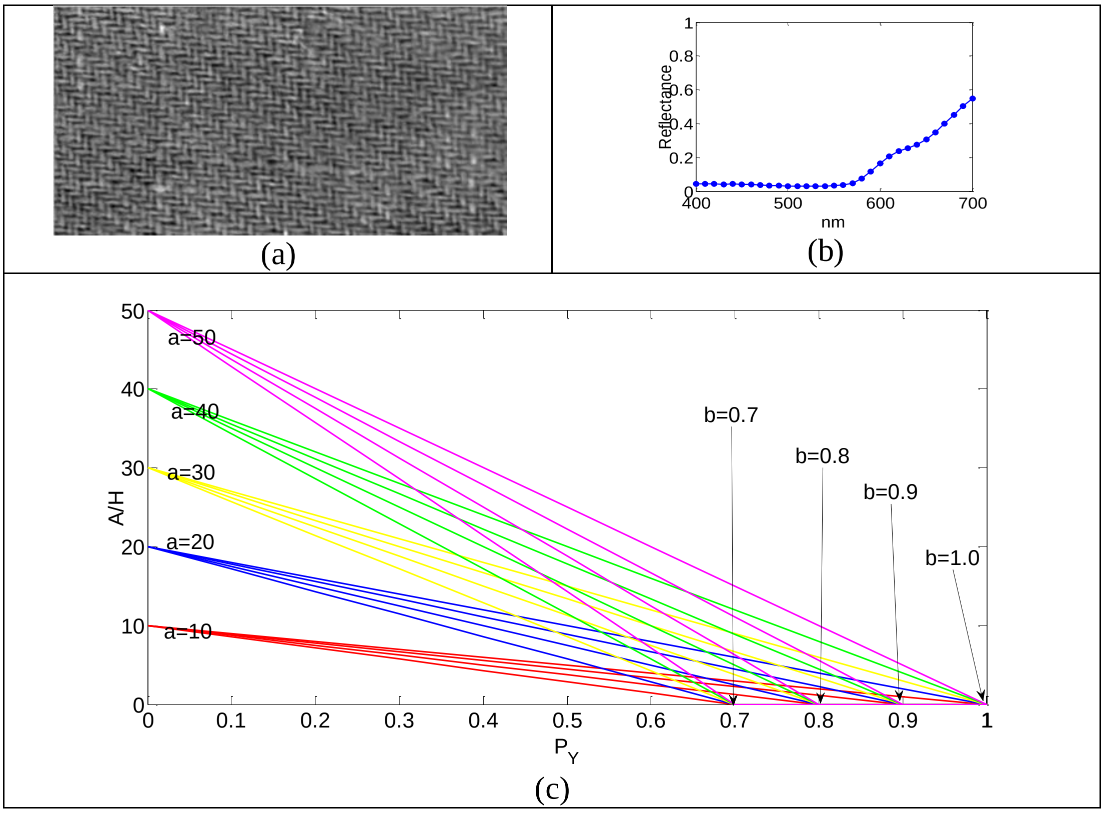

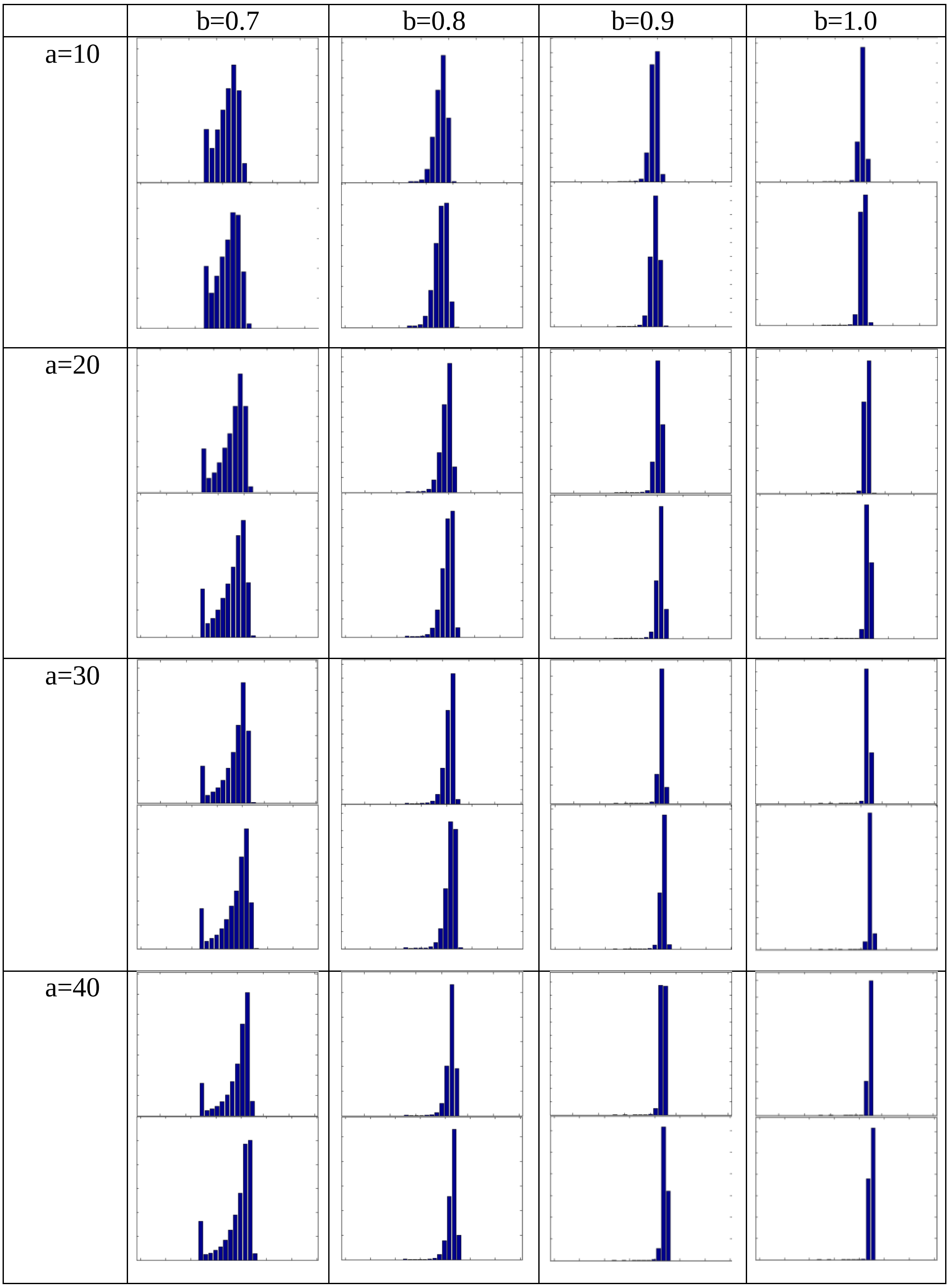
b=0.7
b=0.8
b=0.9
b=1.0
a=10
a=20
a=30
a=40

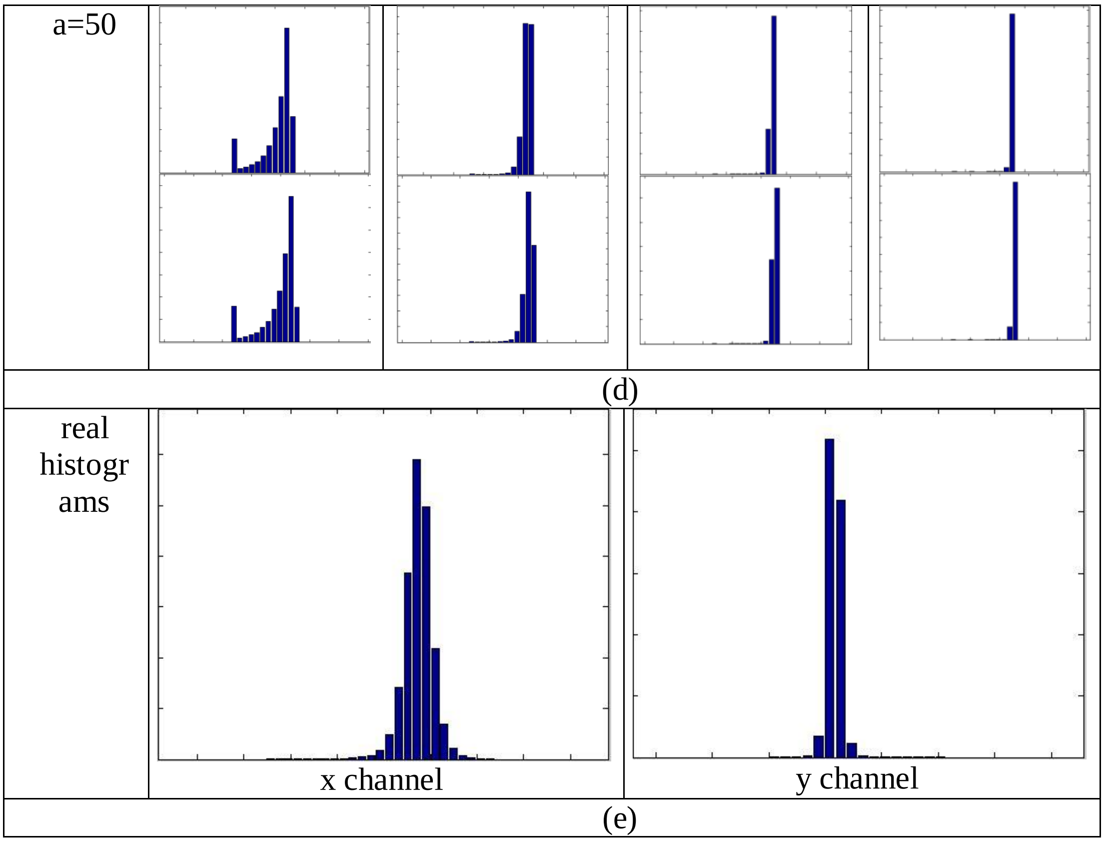

Figure 5.3 The simulation of chromaticity histograms of a solid-colour yarn dyed fabric region: (a) the luminance image; (b) the reflectance of weft and warp yarns; (c) the ratio A/H with respect to P_Y; (d) the simulation results; (e) the real chromaticity histograms. In (d), the top and bottom rows show the x and y histograms, respectively.

5.3.2. Yarns with Different Chromaticity Coordinates

A real yarn dyed fabric sample cross-woven by red and blue yarns was used to analyze CIEXYZ, CIELAB, and CIExyY histograms of solid-colour and multi-colour regions. The linear density of the fabric was 30 Ne for the weft and warp yarns. Thread count of the fabric was 80*60 TPI (thread per inch) in warp and weft directions. The material of yarns was cotton. As shown in Figure 5.4a, the solid-colour region was intertwined by red yarns, whereas the multi-colour region was interlaced by red yarns (weft direction) and blue yarns (warp direction). Coefficient of determination (R^2) [137] was used to test the hypothesis that a histogram accords with one Gaussian distribution or a combination of two Gaussian distributions. Parameters of Gaussian distributions were estimated by the maximum likelihood method [138]. In general, larger R^2 between 0 and 1 indicates a better Gaussian fitting. However, a hypothesis is not correct if R^2 is smaller than 0 or larger than 1. For example, one Gaussian distribution fitting is conducted to a histogram which actually accords with a combination of two Gaussian distributions.

As shown in Figure 5.4b, tristimulus histograms of the solid-colour region highly fit one Gaussian distribution, i.e., R^2 is 0.94, 0.96 and 0.99 in the X, Y, and Z channels. However, the multi-colour region has unstable R^2 when one Gaussian distribution fitting is applied to its tristimulus histograms, i.e., 0.29, 0.87 and 0.09 in the X, Y, and Z channels. This can be considered as a result that the geometric term has different impacts on the weft and warp yarns. The X, Y, or Z histogram of a multi-colour region would fit one Gaussian distribution when the corresponding tristimulus value of weft and warp yarns is similar.

For colour specified in the CIELAB space, the lightness histograms have large R^2 for both the solid-colour and multi-colour regions (0.92 and 0.90) when one Gaussian distribution fitting is carried out. This indicates that the lightness histograms highly accord with one Gaussian distribution for both the solid-colour and multi-colour regions. However, the a* and b* histograms have different R^2 for the solid-colour (0.93 and 0.98) and the multi-colour regions (-0.70 and 1.14). This implies that the a* and b* histograms highly agree with one Gaussian distribution for the solid-colour region but do not for the multi-colour region. As shown in Figure 5.4b, it is apparent that the a* and b* histograms of the multi-colour region fit a combination of two Gaussian distributions better than one Gaussian distribution. Coefficient of determination is 0.28 and 0.58 when a combination of two Gaussian distributions is used to fit the a* and b* histograms. The small and mediate R^2 values imply that the a* and b* histograms of multi-colour regions do not highly agree with a combination of two Gaussian distributions. This can be considered as a result of the influence of the geometric term on a* and b* colours. We can conclude that it is difficult to determine thresholds to distinguish solid-colour regions from multi-colour regions in term of tristimulus and CIELAB histograms. As expressed in Eqn (5.6) and Eqn (5.7), this stems from tristimulus values and CIELAB colours are affected by the geometric term for both solid-colour and multi-colour regions.

As shown in Figure 5.4b, chromaticity histograms have large R^2 (0.96 and 0.99) for the solid-colour region but do not for the multi-colour region (0.43 and 0.57) when one Gaussian distribution fitting is conducted. Chromaticity histograms of the multi-colour region are composed by two Gaussian distributions, which correspond to the chromaticity histograms of the weft and warp yarns. R^2 is 0.79 and 0.92 when the chromaticity histograms are regressed by a combination of two Gaussian functions. The large R^2 implies that chromaticity histograms of the multi-colour region accord with a combination of two Gaussian functions. As a conclusion, chromaticity histograms of a solid-colour yarn dyed fabric region highly accord with one Gaussian distribution and those of a multi-colour region greatly agree with a combination of two Gaussian distributions.

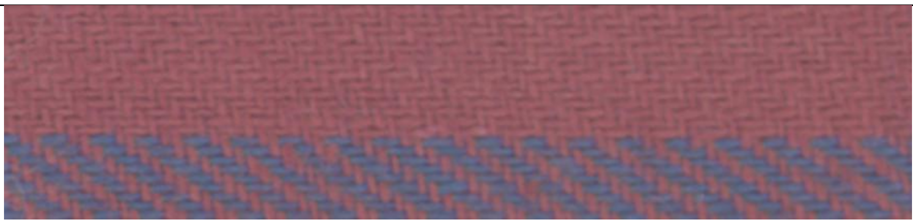
(a)

	solid-colour region	multi-colour region
X	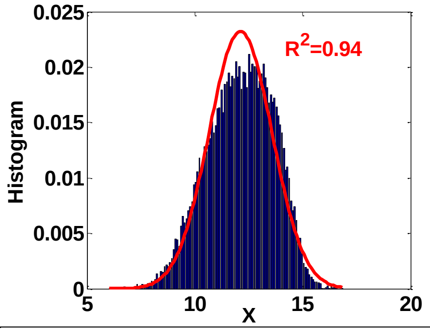	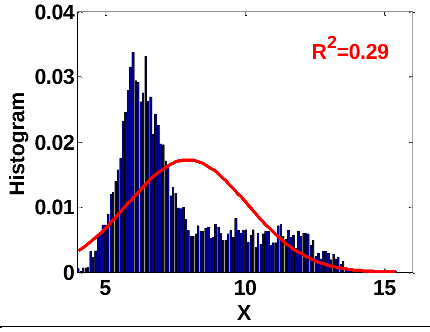
Y	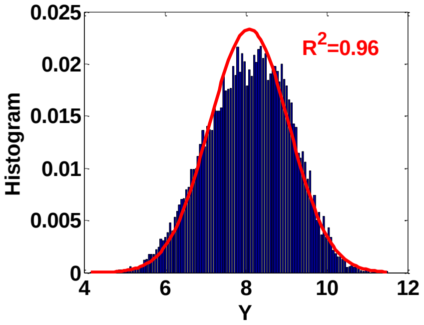	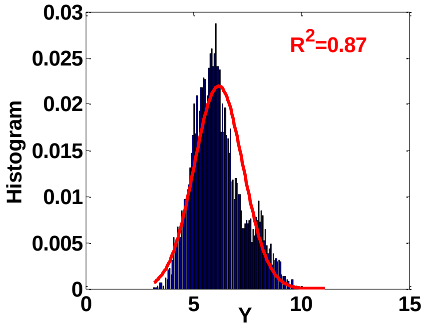
Z	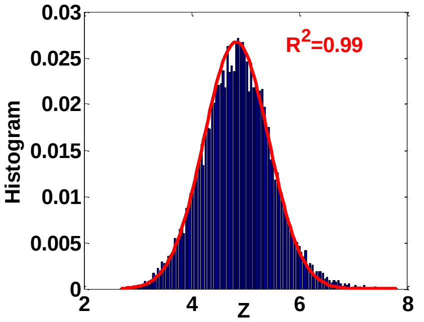	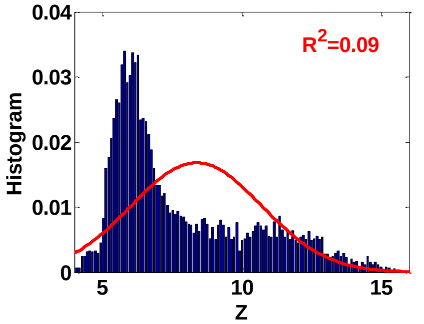
L*	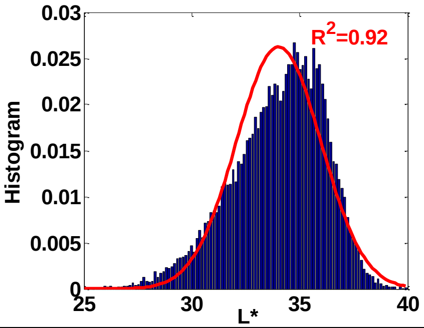	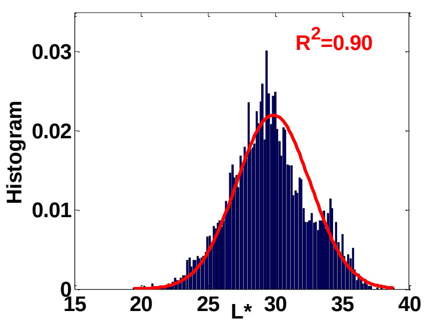

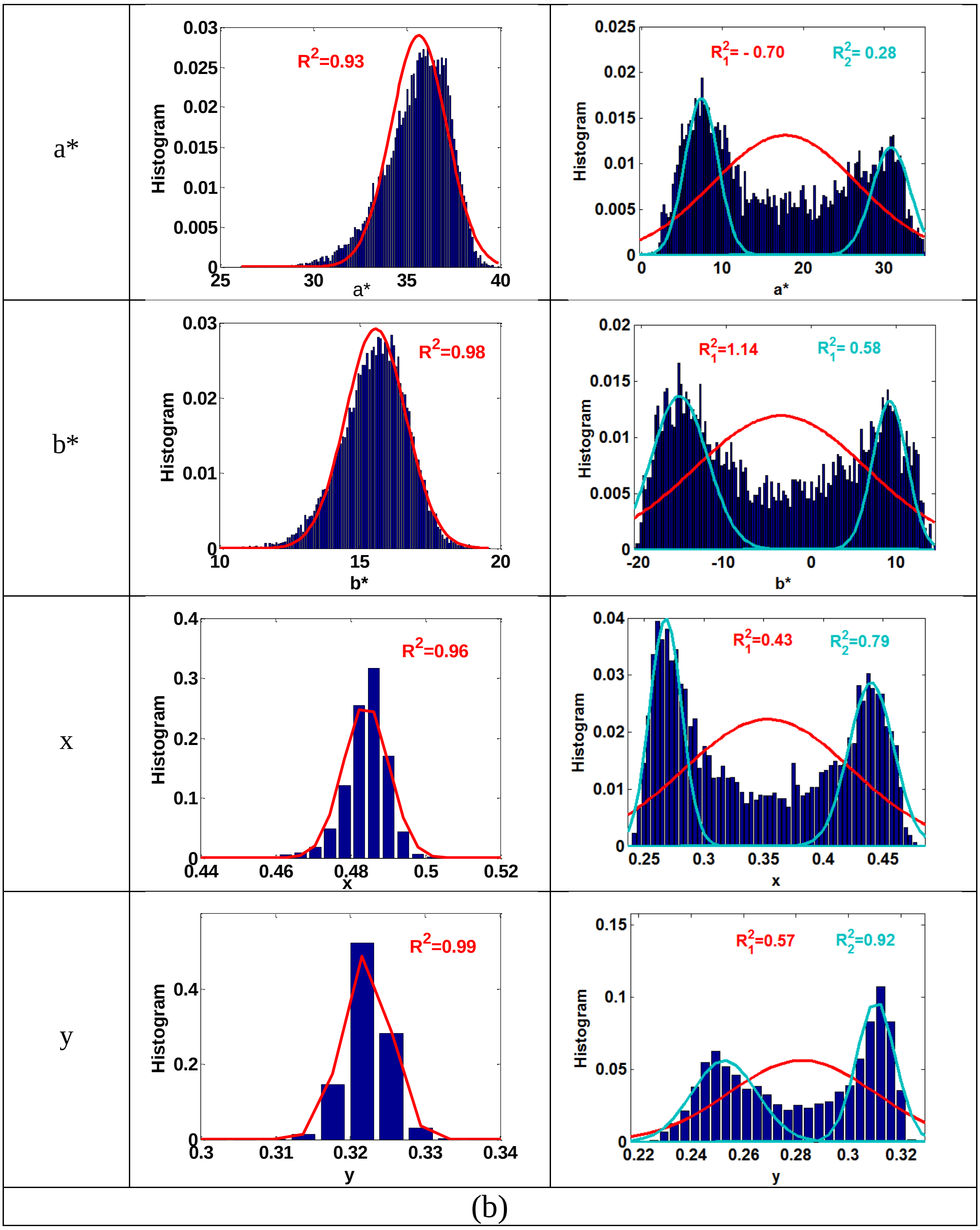

Figure 5.4 The tristimulus, CIELAB and chromaticity histograms of solid-colour and multi-colour regions: (a) the solid-colour region (top) and multi-colour region (bottom); (b) the tristimulus, CIELAB, and chromaticity histograms of the solid-colour and multi-colour regions. The blue bars show the histograms. The red and dark turquoise curves depict the regressed lines by one Gaussian distribution and a combination of two Gaussian distributions fittings.

5.3.3. Yarns with Similar Chromaticity Coordinates

A real yarn dyed fabric cross-woven by white and black yarns was used to analyze CIExyY histograms of solid-colour and multi-colour regions with similar chromaticity coordinates but distinct luminance values. The linear density of the fabric was 40 Ne for weft and warp yarns. Thread count of the fabric was 100*100 TPI in warp and weft directions. The material of yarns was cotton. As shown in Figure 5.5a, the solid-colour yarn dyed fabric region was cross-woven by the white yarns, whereas the multi-colour region was interlaced by white yarns (weft direction) and black yarns (warp direction). As shown in Figure 5.5b, the coefficient of determination is 0.62 and -0.52 for luminance histograms of solid-colour and multi-colour regions when one Gaussian distribution fitting is conducted. The luminance histogram of the multi-colour region has a R^2 of 0.25 when a combination of two Gaussian distribution fitting is carried out. For the chromaticity histograms, R^2 of one Gaussian distribution fitting is [0.82, 0.82] and [0.69 0.59] for solid-colour and multi-colour regions. When a combination of two Gaussian distribution fitting is carried out to the y histogram of the multi-colour region, R^2 is 0.93. As a consequence, the solid-colour and multi-colour regions can be distinguished in terms of chromaticity histograms. R^2 is 0.82 and 0.59 when one Gaussian distribution fitting is conducted to the y histograms of the solid-colour and multi-colour regions. However, R^2 is 0.93 when a combination of two Gaussian distribution fitting is carried out to the y histogram of the multi-colour region. In addition, the luminance histograms can convince of the solid-colour and multi-colour region detection, i.e., R^2 is -0.52 and 0.25 when one Gaussian distribution and two Gaussian distribution fittings are carried out to the luminance histogram of the multi-colour region.

(a)

	solid-colour region	multi-colour region
Y	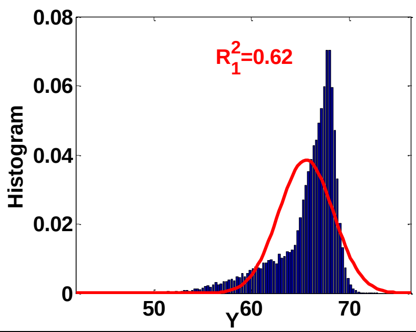	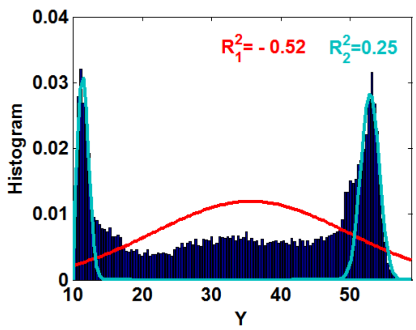

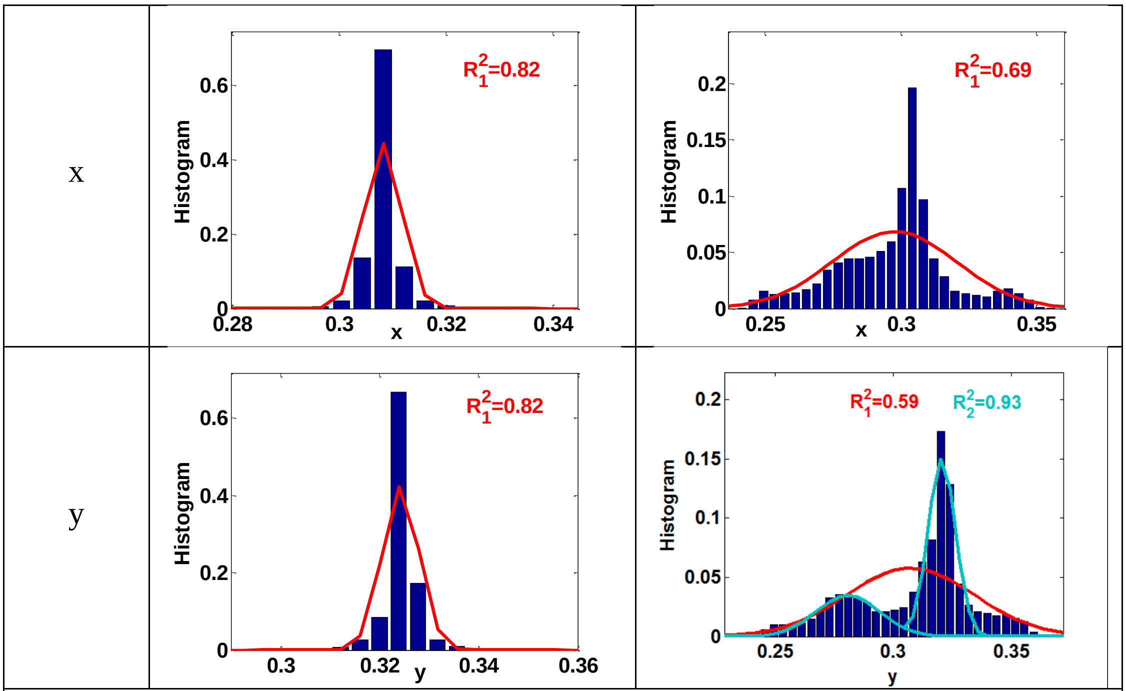

(b)

Figure 5.5 The luminance and chromaticity histograms of solid-colour and multi-colour regions with similar chromaticity coordinates but distinct luminance values: (a) the yarn-dyed fabric with solid-colour multi-colour regions; (b) the chromaticity and luminance histograms of the solid-colour and multi-colour regions. The red and dark turquoise curves depict the regressed lines by one Gaussian distribution and a combination of two Gaussian distributions fittings.

5.3.4. Fabrics with Large Fabric Density

In general, a yarn dyed fabric with large fabric density would hamper the effectiveness of solid-colour and multi-colour region detection since weft and warp yarns are tightly woven together. The fabric density of a yarn dyed fabric can be measured by thread count or threads per inch (TPI) [139]. As shown in Figure 5.6, 16 yarn dyed fabrics with large TPI were used to evaluate the proposed approach to solid-colour and multi-colour yarn dyed fabric detection. These fabrics were cross-woven by four coloured yarns: blue, green, red and white. The linear density of these fabrics was 50 Ne for weft and warp yarns. The fabric density was 160*100 TPI in warp and weft directions. The material of yarns was cotton. A yarn dyed fabric was labeled as BG when it was cross-woven by blue yarns (weft direction) and green yarns (warp direction). The similar nomenclature was applied to the other fabrics, as shown in Figure 5.6. Figure 5.7 shows the coefficient of determination (R^2) of Gaussian fittings (one Gaussian function fitting and two Gaussian function fitting) to the chromaticity histograms of these 16 fabrics. For the solid-colour regions (BB, GG, RR and WW samples in Figure 5.6), R^2 of one Gaussian distribution fitting is large, i.e., the red points in Figure 5.7a which approach the point (1,1). In contrast, the chromaticity histograms of multi-colour regions have small R^2 for one Gaussian distribution fitting. For the 12 multi-colour regions, two Gaussian fitting has larger R^2 than one Gaussian fitting, as shown in Figure 5.7b. This implies that the chromaticity histograms of multi-colour fabrics accord with a combination of two Gaussian distributions better than one Gaussian distribution. Figure 5.7 demonstrates that the proposed approach can distinguish solid-colour and multi-colour regions for the yarn dyed fabrics with large fabric density.

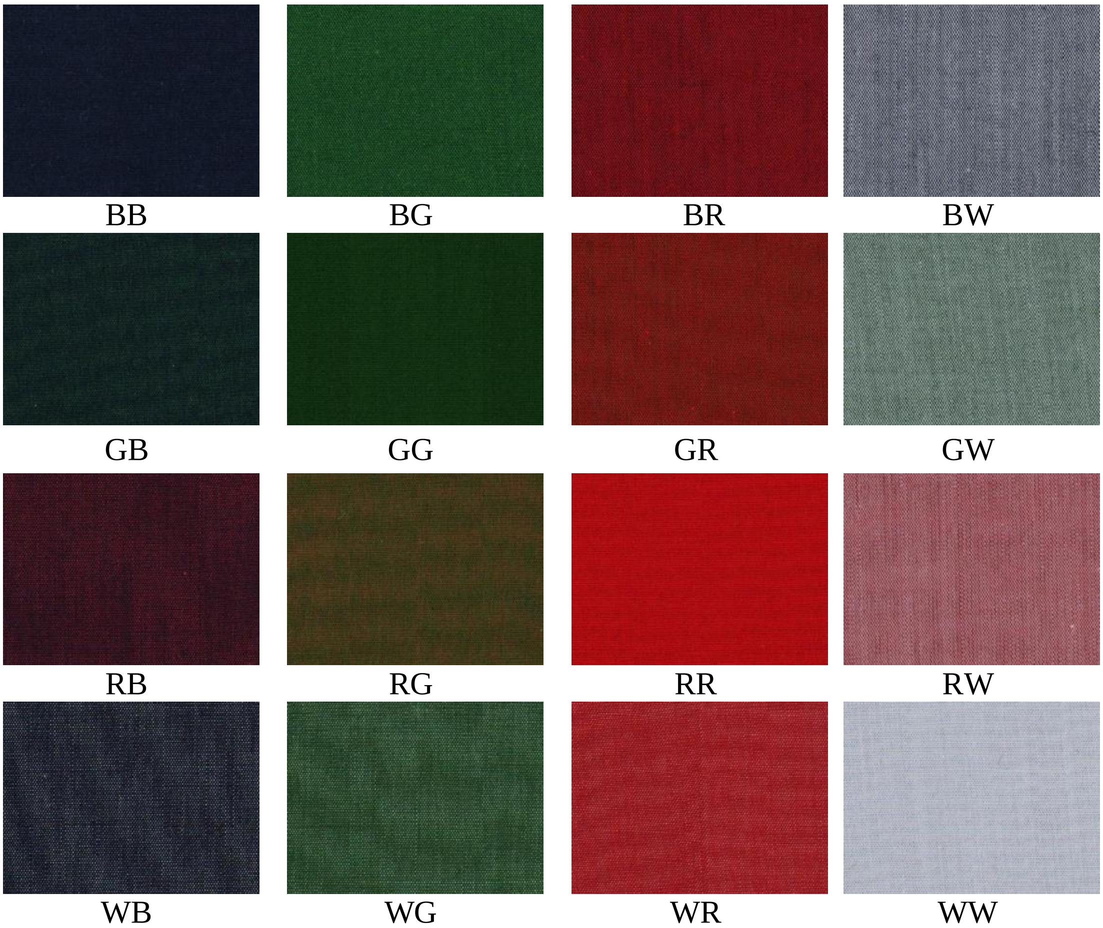

Figure 5.6 16 yarn dyed fabrics with 50 Ne yarn count and 160*100 TPI. A fabric is labeled as BG when it is cross-woven by blue yarns (weft) and green yarns (warp).

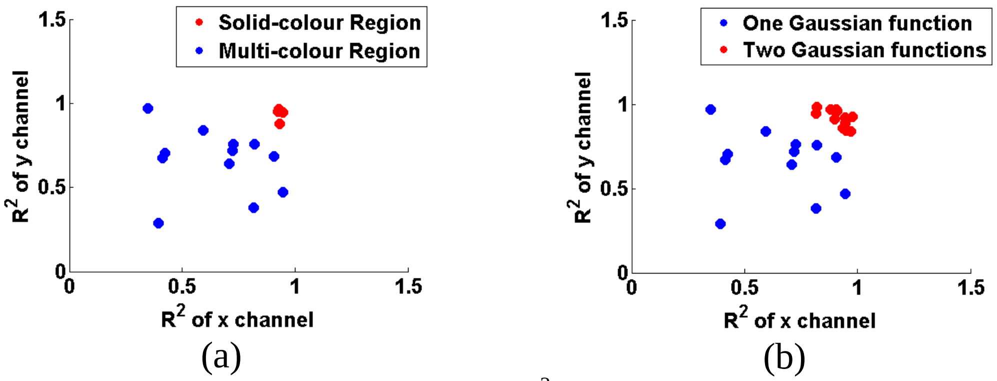

Figure 5.7 Coefficient of determination (R^2) of Gaussian fitting to chromaticity coordinates of the yarn-dyed fabrics shown in Figure 5.6: (a) R^2 of one Gaussian function fitting to the chromaticity histograms of solid-colour and multi-colour regions; (b) R^2 of one Gaussian function and two Gaussian function fittings to the chromaticity histograms of multi-colour regions.

5.4. Conclusion

This chapter introduces an efficient method segmenting solid-colour and multi-colour regions in real yarn dyed fabric images. The spectral response of a multispectral imaging system to yarn dyed fabrics is first derived from the reflection model proposed in Chapter 3. It is then concluded that solid-colour and multi-colour regions cannot be distinguished in terms of reflectance, tristimulus or CIELAB colours, but CIExyY colours owing to a geometric term. The geometric term brings about difficulty in determining thresholds of tristimulus and lightness histograms to segment solid-colour and multi-colour regions. However, chromaticity coordinates are impervious to the geometric term. In addition, chromaticity histograms of a solid-colour region accord with one Gaussian function but those of a multi-colour region agree with a combination of two Gaussian distributions. The simulation results show that chromaticity histograms of a solid-colour region accord with one Gaussian distribution. The experiment on a real yarn dyed fabric sample demonstrates that solid-colour and multi-colour region segmentation can be achieved in terms of CIExyY histograms but not in terms of CIEXYZ and CIELAB histograms. The proposed approach was also evaluated by

16 yarn dyed fabric samples with large fabric density. Experimental results show that the proposed approach can successfully distinguish solid-colour regions from multi-colour regions in yarn dyed fabrics with large fabric density.

Chapter 6 Weft and Warp Yarn Segmentation

An efficient approach detecting solid-colour and multi-colour regions in yarn dyed fabric images is introduced in Chapter 5. A multi-colour region is interlaced by weft and warp yarns with different colours. In order to analyze the colours of a multi-colour yarn dyed fabric, its weft and warp yarns need to be separated before measuring their colours. This chapter introduces an effective method to segment weft and warp yarns of a multi-colour yarn dyed fabric.

6.1. Background

A yarn dyed fabric is composed of solid-colour regions and multi-colour regions. A solid-colour region is cross-woven by same coloured weft and warp yarns whereas a multi-colour region is interlaced by yarns with different colours. The colour of a solid-colour yarn dyed fabric can be measured by spectrophotometers, the most widely used instruments in textile and garment. However, a spectrophotometer cannot directly measure the colour of a multi-colour yarn dyed fabric. However, a multispectral imaging (MSI) system [48,50] has the potential to measure the color of a multi-colour region. Compared with spectrophotometers, MSI systems can provide not only the spectral information but also the spatial information of a yarn dyed fabric. The spectral information can be used in predicting illuminant metamerism [12] and obtain illuminant-independent colour. The spatial information can help understand important knowledge about a yarn dyed fabric, such as the location distributions of weft and warp yarns and their structures. When a MSI system is applied to measure the colour of a multi-colour region, one needs to segment its weft and warp yarns before analyzing their colours.

Based on the physical model introduced in Chapter 5, a modified K-means clustering approach is utilized to separate weft and warp yarns in a multi-colour yarn dyed fabric image. The number of clusters is fixed to two. The metric to measure the distance between a pixel and the mean of a cluster is not the traditional Euclidean distance but the CIELAB colour difference. The initial means of clusters are determined by the expected values of the two fitted Gaussian distributions to the CIExyY colour histograms rather than the traditional random methods.

6.2. Weft and Warp Yarn Segmentation

6.2.1. Response of a MSI System

According to the reflection model introduced in Chapter 3 and Chapter 5, the measured reflectance $R_b(\lambda, p_C, q_C)$ at pixel (p_C, q_C) can be modeled as:

$$\begin{aligned} R_b(\lambda, p_C, q_C) = & m_b(p_Y, q_Y)H(p_Y, q_Y)R_1(\lambda) \\ & + m_b(p_Y, q_Y)A(p_Y, q_Y)R_1(\lambda)R_2(\lambda) \end{aligned} \tag{6. 1}$$

where (p_Y, q_Y) is the position on the yarn dyed fabric which corresponds to (p_C, q_C), $R_1(\lambda)$ and $R_2(\lambda)$ represent the nominal reflectance of the measured yarn and its neighbouring yarn, $m_b(p_Y, q_Y)$, $H(p_Y, q_Y)$ and $A(p_Y, q_Y)$ express the influence of the fabric surface, system illuminant and inter-reflection between yarns.

When the CIExyY space is used to specify the colour of a multi-colour yarn dyed fabric, $m_b(p_Y, q_Y)$ only affects luminance rather than chromaticity coordinates:

$$\begin{cases} Y(p_C,q_C)=km_b(p_Y,q_Y)[H(p_Y,q_Y)\int_\lambda E(\lambda)R_1(\lambda)\bar{y}(\lambda)d\lambda+A(p_Y,q_Y)\int_\lambda E(\lambda)R_1(\lambda)R_2(\lambda)\bar{y}(\lambda)d\lambda] \\ x(p_C,q_C)=\dfrac{\int_\lambda E(\lambda)R_1(\lambda)\bar{x}(\lambda)d\lambda+\dfrac{A(p_Y,q_Y)}{H(p_Y,q_Y)}\int_\lambda E(\lambda)R_1(\lambda)R_2(\lambda)\bar{x}(\lambda)d\lambda}{\int_\lambda E(\lambda)R_1(\lambda)(\bar{x}(\lambda)+\bar{y}(\lambda)+\bar{z}(\lambda))d\lambda+\dfrac{A(p_Y,q_Y)}{H(p_Y,q_Y)}\int_\lambda E(\lambda)R_1(\lambda)R_2(\lambda)(\bar{x}(\lambda)+\bar{y}(\lambda)+\bar{z}(\lambda))d\lambda} \\ y(p_C,q_C)=\dfrac{\int_\lambda E(\lambda)R_1(\lambda)\bar{y}(\lambda)d\lambda+\dfrac{A(p_Y,q_Y)}{H(p_Y,q_Y)}\int_\lambda E(\lambda)R_1(\lambda)R_2(\lambda)\bar{y}(\lambda)d\lambda}{\int_\lambda E(\lambda)R_1(\lambda)(\bar{x}(\lambda)+\bar{y}(\lambda)+\bar{z}(\lambda))d\lambda+\dfrac{A(p_Y,q_Y)}{H(p_Y,q_Y)}\int_\lambda E(\lambda)R_1(\lambda)R_2(\lambda)(\bar{x}(\lambda)+\bar{y}(\lambda)+\bar{z}(\lambda))d\lambda} \end{cases} \tag{6.2}$$

where $\bar{x}(\lambda)$, $\bar{y}(\lambda)$ and $\bar{z}(\lambda)$ denote the CIE colour matching functions, k is a normalising factor given by $k=100/\int_\lambda E(\lambda)\bar{y}(\lambda)d\lambda$.

6.2.2. Interstice Detection

As shown in Figure 6.1a, interstices exist between weft and warp yarns in multi-colour region images, especially for fabrics with large yarn count and low areal density. Interstices influence the segmentation accuracy of weft and warp yarns since they cause false segmentation, i.e., background pixels are detected as pixels on weft or warp yarns. Eqn (6.1) expresses that pixels on interstices would have zero reflectance when a yarn dyed fabric is placed on a black platform. However, the measured reflectance values of some interstice pixels are larger than zero owing to noises on the platform. Instead of detecting pixels with zero reflectance, interstice detection is achieved by the image difference method, i.e., CIELAB colour difference between a yarn dyed fabric image and the background image. A pixel (p_C, q_C) is labeled as interstice if the CIELAB colour difference between the yarn dyed fabric image $\mathrm{F}(p_C, q_C)$ and the background image $\mathrm{B}(p_C, q_C)$ is smaller than a threshold T, and *vice versa*:

$$I(p_C, q_C) = \begin{cases} 1 & \Delta\mathrm{E}(\mathrm{F}(p_C, q_C), \mathrm{B}(p_C, q_C)) \le \mathrm{T} \\ 0 & \Delta\mathrm{E}(\mathrm{F}(p_C, q_C), \mathrm{B}(p_C, q_C)) > \mathrm{T} \end{cases} \tag{6. 3}$$

where $I(p_C, q_C)$, $\mathrm{F}(p_C, q_C)$ and $\mathrm{B}(p_C, q_C)$ denote interstice detection results, the yarn dyed fabric image, and the background image, $\Delta\mathrm{E}(\cdot,\cdot)$ expresses the CIELAB colour difference.

Figure 6.1b shows the interstice detection results of Figure 6.1a with $\mathrm{T} = 5$, where the white pixels represent detected interstices.

6.2.3. Modified K-means Clustering

It can be concluded from Eqn (6.2) that the CIExyY histograms of a multi-colour region accord with a combination of two Gaussian distributions. Consequently, pixels on weft and warp yarns consist of two dominant clumps in the CIExyY space. One cluster is formed by colours of the weft yarns and the other by those of the warp yarns. A modified K-means clustering method is proposed to segment weft and warp yarns in a multi-colour yarn-dyed fabric image.

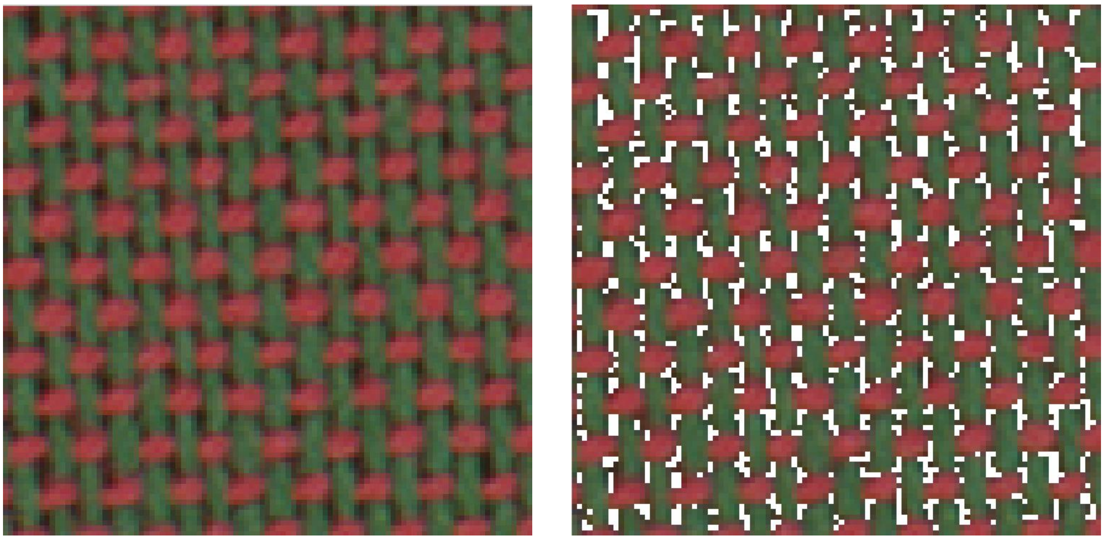

(a) (b)

Figure 6.1 Example of interstice detection in a multi-colour region. The yarn dyed fabric is cross-woven by weft and warp yarns with 30*30 Ne yarn count and 60*80 density: (a) the multi-colour region image; (b) interstice detection results. The white pixels imply the detected interstices.

Given pixels of an image $(x_1, x_2, ..., x_n)$, K-means clustering method partitions the pixels into k sets $S = \{s_1, s_2, ..., s_k\} (k \le n)$ so that the within-cluster distance (WCD) is minimized [140]:

$$\arg\min_S \sum_{i=1}^{k} \sum_{x_j \in s_i} D(x_j - \mu_i) \tag{6. 4}$$

where μ_i denotes the mean of pixels in the set s_i, $D(x_j - \mu_i)$ represents the distance between x_j and μ_i.

With an initial set of means, K-means clustering algorithm proceeds by alternating between an assignment step and an update step [140]. The assignment step assigns each pixel to the cluster whose mean yields the least WCD. The update step computes the means of the new clusters. The K-means clustering algorithm converges when the assignments of pixels no longer change. Given an initial set of k means $(m_1^{(1)}, m_2^{(1)}, ..., m_k^{(1)})$, the K-means clustering algorithm can be summarized as:

- **Assignment step:**

$$S_i^{(t)} = \{x_p : D(x_p - m_i^{(t)}) \leq D(x_p - m_j^{(t)}), \forall 1 \leq j \leq k\} \tag{6. 5}$$

- **Update step:**

$$m_i^{(t+1)} = \frac{1}{\left|S_i^{(t)}\right|} \sum_{x_j \in S_i^{(t)}} x_j \tag{6. 6}$$

The performance of K-means clustering depends on three factors: the initialization method, the metric to calculate the distance between a pixel and the mean of a cluster, and the number of clusters. The initial means are commonly determined by the Forgy and Random Partition methods [141]. The Forgy method randomly chooses k pixels from an image as the initial means. The Random Partition method randomly assigns a cluster to each pixel and then calculates the centroid of each cluster as its initial mean. The distance between a pixel and the mean of a cluster can be measured by different metrics. The common used metrics include Euclidean distance (2-norm distance), Manhattan distance (1-norm), maximum norm distance, and inner product space [142,143]. The number of clusters k is another important parameter to influence the performance of K-means clustering because an inappropriate choice of k can yield poor results. Several algorithms have been proposed to determine the number of clusters in a data set, such as the information theoretic approach [144], the silhouette method [145], and the kernel matrix method [146].

While there are no standard criteria to determine the initial means, the metric to calculate distance, and the number of clusters, a modified K-mean clustering algorithm is proposed to segment weft and warp yarns in multi-colour yarn dyed fabric images. Firstly, the number of clusters is fixed to two, i.e., $k = 2$. As shown in Figure 6.1b, pixels locate on either the green warp yarns or the red weft yarns after interstice detection. Thus, pixels should be clustered into two groups: weft yarns or warp yarns. Secondly, the distance between a pixel and the mean of a cluster is measured by the CIELAB colour difference rather than the Euclidean distance. The CIELAB space is more perceptually uniform than the CIExyY space. In addition, it is very effective to compute the CIELAB colour difference. Finally, the initial means can be determined by a much more effective method rather than the random methods. As concluded from Chapter 5, the CIExyY histogram of a multi-colour yarn dyed fabric accords with a combination of two Gaussian distributions. The expected values of these two Gaussian distributions are good initial estimates to colours of the weft and warp yarns.

Figure 6.2 illustrates the weft and warp yarn segmentation in the multi-colour yarn dyed fabric region shown in Figure 6.1b. Figure 6.2a shows the CIExyY histogram of the multi-colour region. The red and green points in Figure 6.2a represent the initial means which are determined by the expected values of the two fitted Gaussian functions by the method introduced in Chapter 5. Figure 6.2b depicts the clustering results in the CIExyY space. Figure 6.2c and Figure 6.2d show the segmentation results of the weft and warp yarns.

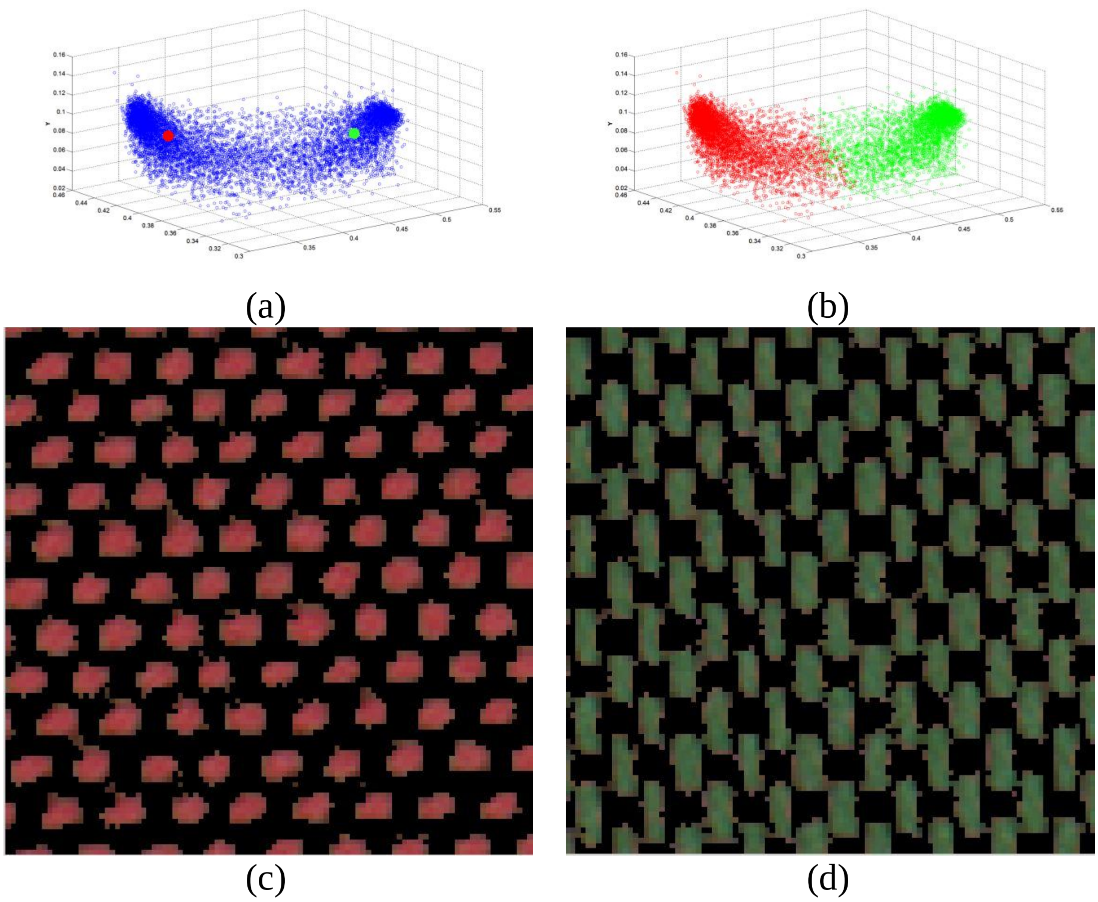

Figure 6.2 Weft and warp yarn segmentation of the multi-colour region shown in Figure 6.1b: (a) the CIExyY histogram and the initial means; (b) the K-means clustering results in the CIExyY space; (c) the segmentation results of weft yarns; (d) the segmentation results of warp yarns. The red and green points in (a) denote the assigned initial means.

6.3. Results and Discussion

Multi-colour yarn dyed fabric samples with different areal density (threads per inch, abbreviated as TPI) and linear density (Ne) were utilized to assess the performance of the proposed method. As shown in Figure 6.3, a 5.5*7.5 cm fabric can be captured by ICM and the image is composed of 1040*1392 pixels. In order to clearly illustrate the experimental results, only the central part with 200*200 pixels (the red rectangle in Figure 6.3) was selected to show in the following experiments.

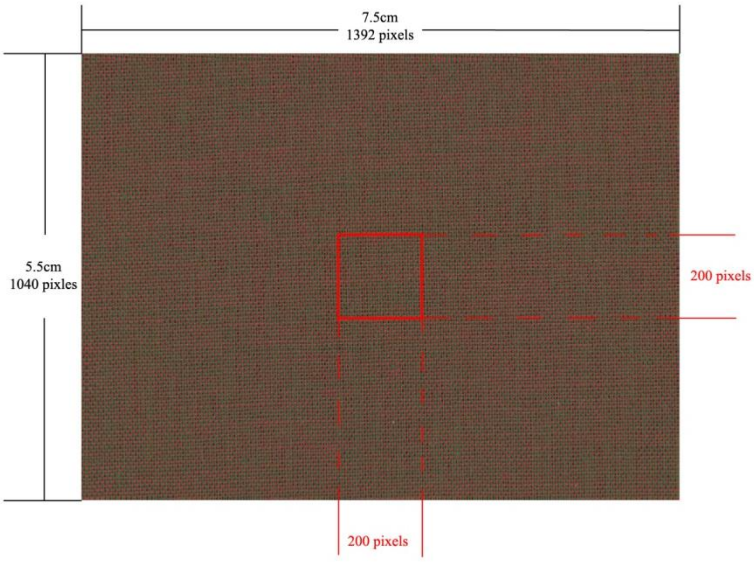

Figure 6.3 The specification of multi-colour yarn dyed fabrics used in the experiment. The red rectangle represents the area selected to show the results.

6.3.1. Experiments on Fabrics with Different Linear and Areal Densities

Figure 6.4 and Figure 6.5 show the weft and warp yarn segmentation results of yarn dyed fabrics with different linear density (40*40 Ne and

50*50 Ne) and areal density (80*100 and 100*160 TPI in the weft and warp directions). Figure 6.4b and Figure 6.5b show the interstice detection results, where the white pixels represent the detection results. It can be observed that all the white pixels in Figure 6.4b locate at the black background compared with Figure 6.4a. This implies that the interstice detection results accord with the perceptual detection results. The same interstice detection results can be found in Figure 6.5b.

Figure 6.4c-d and Figure 6.5c-d show the weft and warp yarn segmentation results of Figure 6.4b and Figure 6.5b. It can be observed that the warp yarns shown in Figure 6.5d are much denser than weft yarns in Figure 6.5c. This can be considered as a result of the different areal density in the warp direction (160) and the weft direction (100). The same areal density difference in the weft and warp directions can be found in Figure 6.4c-d. It can be concluded from Figure 6.1, Figure 6.2, Figure 6.4, and Figure 6.5 that weft and warp yarn segmentation in multi-colour regions can be achieved for yarn dyed fabrics with different linear density and areal density.

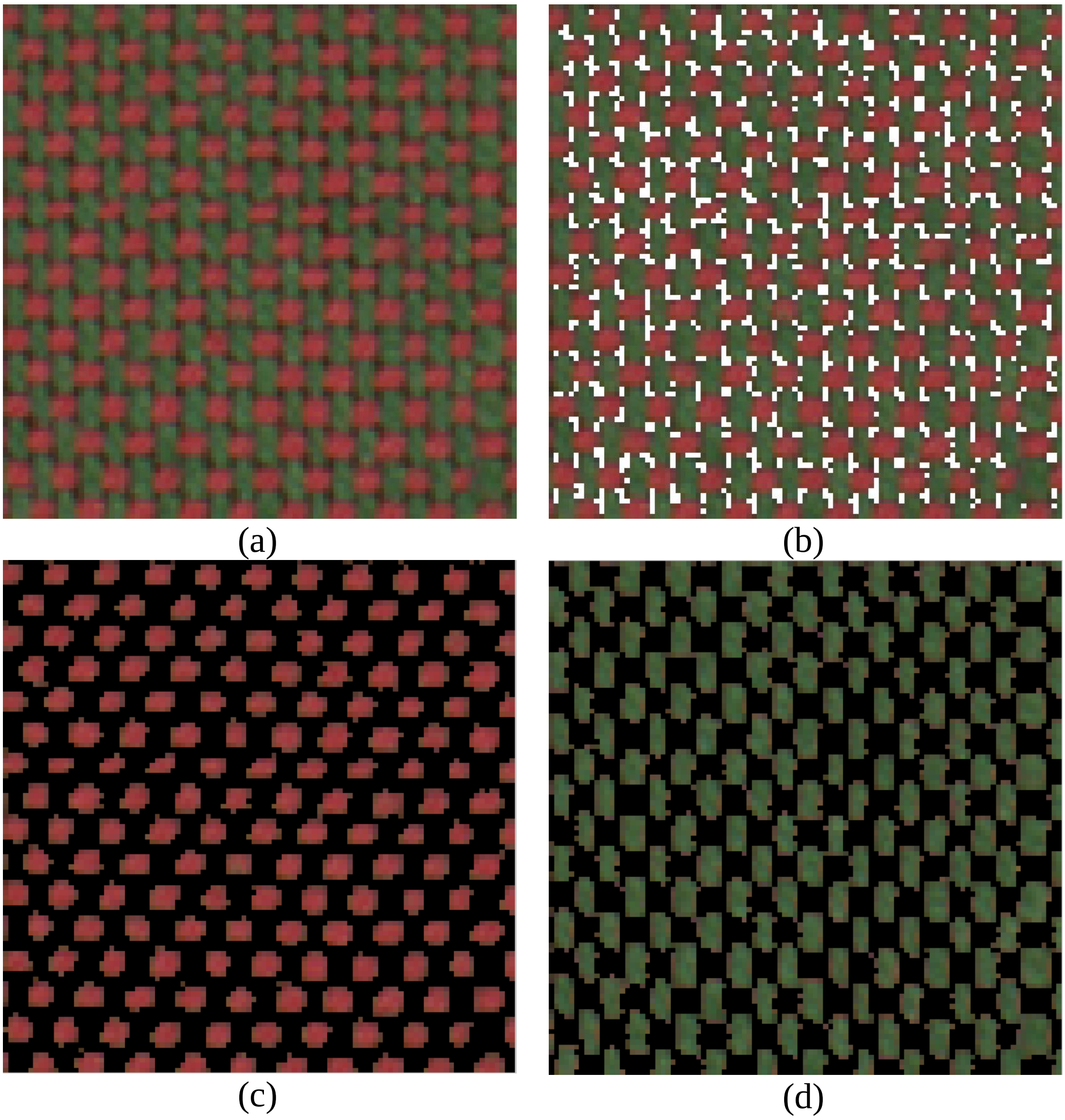
(a) (b) (c) (d)

Figure 6.4 Weft and warp yarn segmentation of a multi-colour yarn dyed fabric with 40*40 Ne yarn count and 80*100 TPI: (a) the image of the fabric; (b) the interstice detection results, where the white pixels represent the interstices; (c) the segmentation results of weft yarns. (d) the segmentation results of warp yarns.

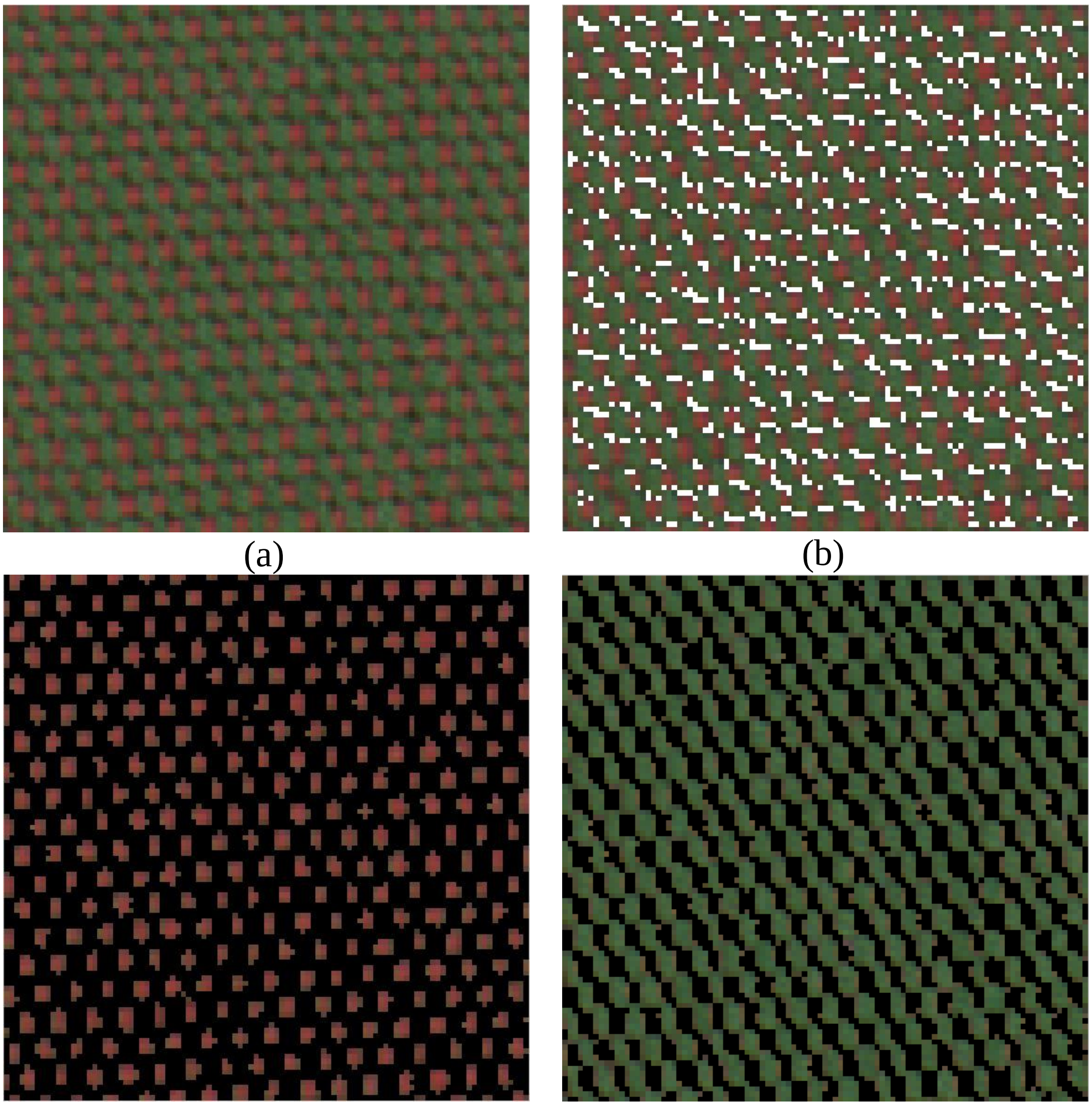
(a) (b) (c) (d)

Figure 6.5 Weft and warp yarn segmentation of a multi-colour yarn dyed fabric with 50*50 Ne yarn count and 100*160 TPI: (a) the captured image of the fabric; (b) the interstice detection results, where the white pixels represent the interstices; (c) the segmentation results of weft yarns. (d) the segmentation results of warp yarns.

6.3.2. Comparative Experiments

The proposed approach was also compared with original K-means clustering algorithms applied in the CIEXYZ and CIELAB spaces. The number of clusters and metric to calculate WCD were set to two and the

CIELAB colour difference. However, the initial means were determined by the Forgy method [141] in the CIEXYZ and CIELAB spaces. Figure 6.6 and Figure 6.7 show the weft and warp yarn segmentation results of the fabric shown in Figure 6.5b. As seen in Figure 6.6, false segmentation exists in the results of the original K-means clustering applied in the CIEXYZ space. Only the edges between the weft and warp yarns are detected as weft yarns. As mentioned in Chapter 5, the poor segmentation can be considered as a result of the influence of the geometric term. The geometric term causes the distinct discrimination between weft and warp yarns in the CIExyY space is not valid in the CIEXYZ space. As seen in Figure 6.7, the segmentation results of K-means clustering in the CIELAB space is better than those in the CIEXYZ space. However, holes and spines exist in the segmentation results. In contrast, the segmentation results by the proposed method (Figure 6.5c-d) show better integrity.

In addition to the segmentation accuracy, the iteration time of these three methods were also compared. As given in Table 6.1, K-means clustering in the CIEXYZ and CIELAB spaces need sixteen and twelve iterations to converge, while the proposed method just needs one iteration. These results clearly indicate that the proposed method can dramatically reduce the iteration time.

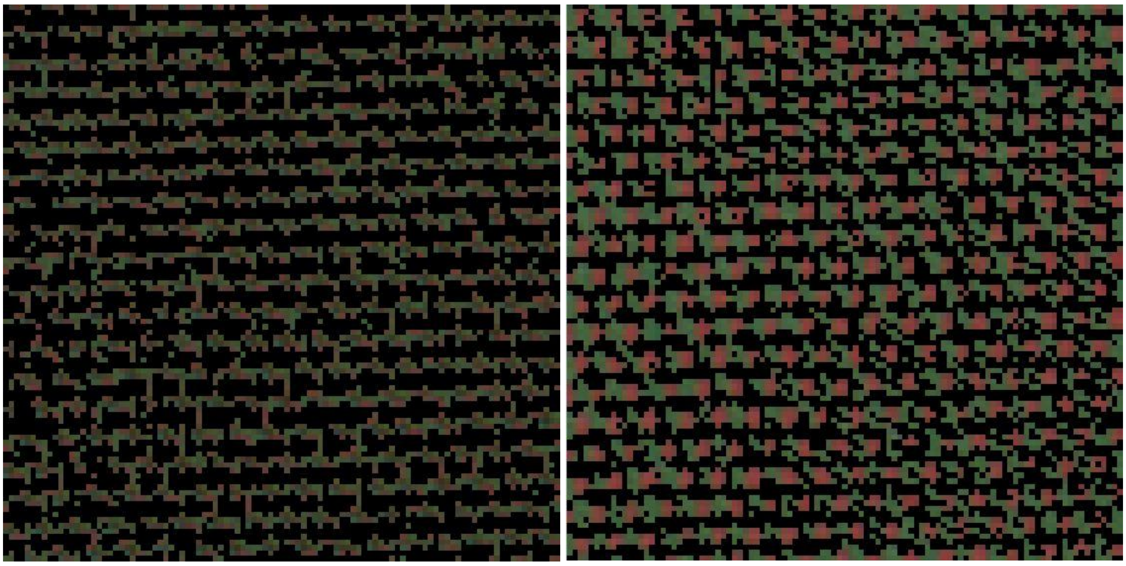

(a) (b)

Figure 6.6 Weft and warp yarn segmentation results by K-means clustering in the CIEXYZ space: (a) the segmentation results of weft yarns; (b) the segmentation results of warp yarns.

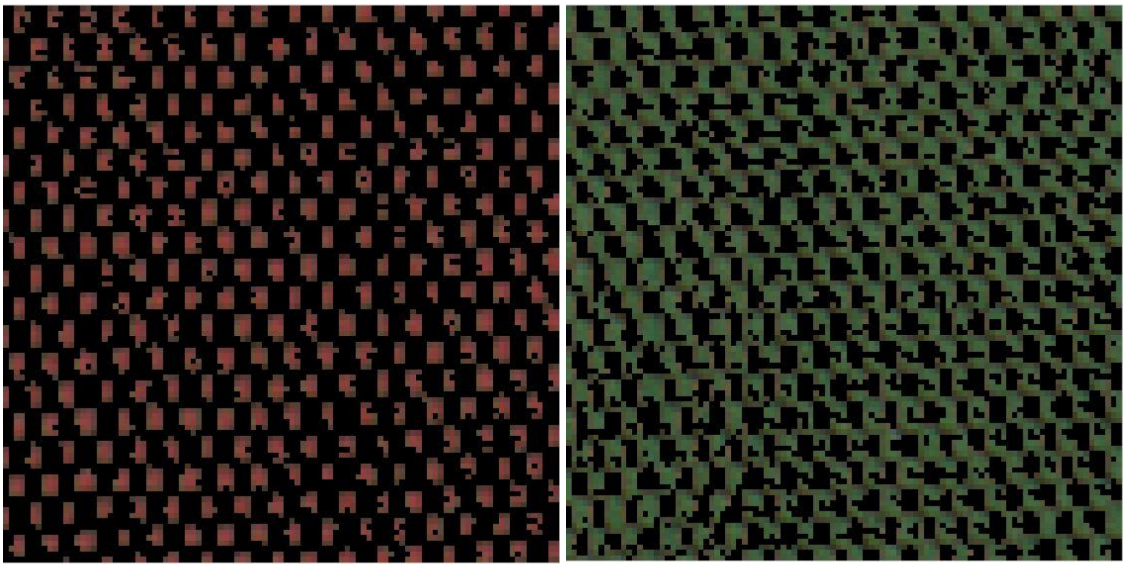

(a) (b)

Figure 6.7 Weft yarn and warp yarn segmentation results by K-means clustering in the CIELAB space: (a) the segmentation results of weft yarns; (b) the segmentation results of warp yarns.

Table 6.1 Iteration time of the three methods

Method	Iteration Times
CIEXYZ+ Forgy method	16
CIELAB+ Forgy method	12
The Proposed method	1

6.4. Conclusion

This chapter introduces an effective method to segment weft and warp yarns in a multi-colour yarn dyed fabric image. Interstices between weft and warp yarns are first detected by the image difference method. A modified K-means clustering approach is then proposed to separate weft and warp yarns. The number of clusters is fixed to two. The metric to measure the distance between a pixel and the mean of a cluster is not the traditional Euclidean distance but the CIELAB colour difference. The initial means are determined by the expected values of the fitted Gaussian distributions to the CIExyY colour histogram rather than the traditional random methods. Experimental results indicate that the proposed method can segment weft and warp yarns of yarn dyed fabrics, with both high segmentation accuracy and fast processing speed.

Chapter 7 Colour Measurement of Single Yarns

Colour measurement of yarn dyed fabrics can be achieved by the algorithms introduced in Chapter 4, Chapter 5, and Chapter 6. However, the colour of a yarn dyed fabric is dramatically influenced by woven structure and linear density. In contrast, a single yarn has a much simpler structure than a yarn dyed fabric. A novel multispectral imaging approach to accurate colour measurements of single yarns is developed in this chapter.

7.1. Background

Generally, the colour of a yarn dyed fabric is dramatically influenced by woven structure and linear density [147,148,149,150]. According to the reflection model introduced in Chapter 3, the light reflected by a yarn dyed fabric is determined by three factors [151]: the surface texture of a fabric, inter-reflection between yarns, and occlusion of system illuminant. The influence of surface texture on instrumental colour is formulated by a geometric term. This term would cause the measured luminance changing with surface position because it is determined by the angle between the incident light and the normal of the surface. Inter-reflection between neighbouring yarns would yield a second illumination. Inter-reflection would cause colour shift when a weft or warp yarn is cross-woven by different coloured yarns. Occlusion of system illuminant is modeled by an occlusion parameter which represents the fraction of light from the system illumination reaching the fabric surface. All of these three factors can be influenced by the woven structure and thread density of a yarn dyed fabric. In contrast, a single yarn has a much simpler structure than a yarn dyed fabric. Inter-reflection does not exist in a single yarn.

Traditionally, colours of yarn dyed fabric samples are measured by spectrophotometers which are the most widely used instruments in textile and garment industries. A spectrophotometer can provide accurate and precise spectral information of a sample. The spectral information is independent of the characteristics of acquisition systems and illuminants. As a consequence, reflectance measured by a spectrophotometer can be transformed to any colour spaces and can be interpreted for any illuminants. However, spectrophotometers cannot be directly used to measure colours of single yarns. As described in Chapter 3, this problem is caused by the inherent characteristic of a spectrophotometer: only the average colour of a sample can be measured [151]. In other words, a spectrophotometer cannot measure the colour of a sample with size smaller than the aperture. Therefore, a spectrophotometer cannot be used to conduct colour measurement of a single yarn. With the development of digital imaging technology, multispectral imaging (MSI) systems [48,50] are being adopted to measure the colour of a sample. A MSI system can provide not only the spectral information but also the spatial information of a sample. The spatial information alleviates the limitation on the size of a sample because a camera with high resolution is used in MSI systems. Multispectral images with millions of pixels can be captured by a MSI system. With advanced image processing technologies, thus, a MSI system has the potential to directly measure the colour of a single yarn.

In this chapter, a novel multispectral imaging approach that accurately measures colours of single yarns is introduced. Firstly, a single yarn is fixed on a black flat platform to obtain its multispectral images. Secondly, the single yarn is segmented from background in multispectral images by image difference method. Finally, the reflectance of the single yarn is specified by the methods developed.

7.2. Colour Measurement of Single Yarns

7.2.1. Capture of Multispectral Images

In order to achieve accurate colour measure, single yarns should be completely straightened when they are captured by a multispectral imaging system. As shown in Figure 7.1, a device is designed to stretch single yarns on a black platform by screws. The multispectral images of single yarns are captured by the MSI system ICM.

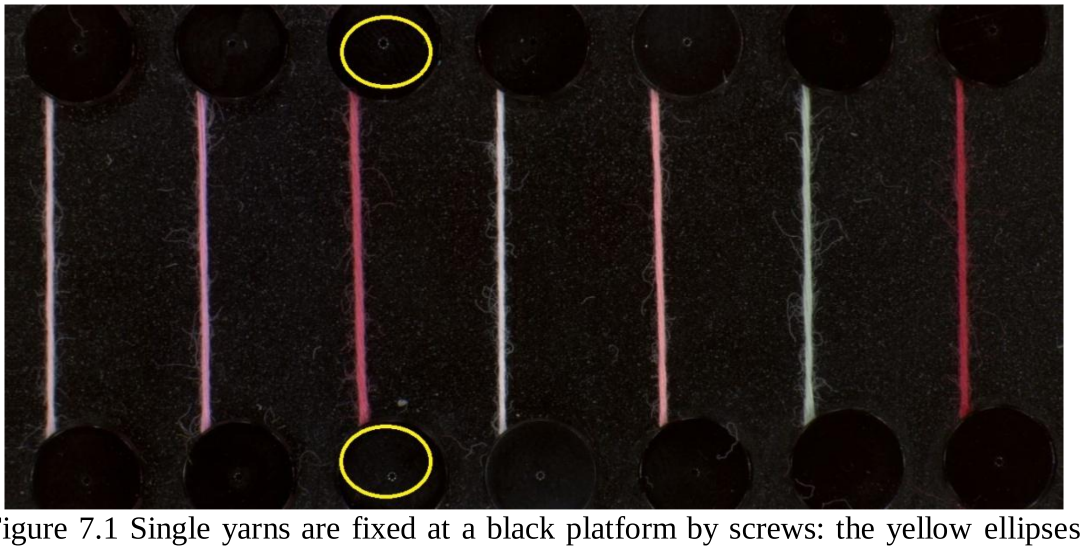

Figure 7.1 Single yarns are fixed at a black platform by screws: the yellow ellipses represent the two screws fixing the red yarn.

7.2.2. Segment Single Yarns

As shown in Figure 7.2a, one can select a single yarn to measure its colour. When a single yarn is fixed on a black platform, pixels on background should have zero reflectance. However, the measured reflectance values of some background pixels are larger than zero owing to noises, as shown in Figure 7.2b. Instead of detecting pixels with zero reflectance, single yarn segmentation is achieved in terms of image difference method, i.e., CIELAB colour difference between the yarn image and the background image. A pixel (p_C, q_C) is labeled as locating at the single yarn if the CIELAB colour difference between the single yarn image $\mathrm{F}(p_C, q_C)$ and the background image $\mathrm{B}(p_C, q_C)$ is larger than a threshold T, and *vice versa*:

$$I(p_C, q_C) = \begin{cases} 0 & \Delta\mathrm{E}(\mathrm{F}(p_C, q_C), \mathrm{B}(p_C, q_C)) \le \mathrm{T} \\ 1 & \Delta\mathrm{E}(\mathrm{F}(p_C, q_C), \mathrm{B}(p_C, q_C)) > \mathrm{T} \end{cases} \tag{7. 1}$$

where $I(p_C, q_C)$ denotes the yarn segmentation results, $\Delta\mathrm{E}(\cdot,\cdot)$ expresses the CIELAB colour difference. $I(p_C, q_C) = 1$ represents the pixel (p_C, q_C) locates at the single yarn, and *vice versa*.

Figure 7.2c shows the segmentation results of Figure 7.2b by the image difference method, where the segmentation threshold T is computed as the mean colour difference of all the pixels between the single yarn image and the background image.

7.2.3. Specify the Reflectance of Single Yarns

According to the reflection model introduced in Chapter 5, the measured reflectance $R_b(\lambda, p_C, q_C)$ at pixel (p_C, q_C) of a yarn dyed fabric image can be modeled as:

$$\begin{aligned} R_b(\lambda, p_C, q_C) = & m_b(p_Y, q_Y)H(p_Y, q_Y)R_1(\lambda) \\ & + m_b(p_Y, q_Y)A(p_Y, q_Y)R_1(\lambda)R_2(\lambda) \end{aligned} \qquad (7.\ 2)$$

where (p_Y, q_Y) is the position on the yarn dyed fabric which corresponds to (p_C, q_C), $R_1(\lambda)$ and $R_2(\lambda)$ represent the nominal reflectance of the measured yarn and its neighbouring yarn, $m_b(p_Y, q_Y)$, $H(p_Y, q_Y)$ and $A(p_Y, q_Y)$ express the influence of the fabric surface, the illuminant of the MSI system, and inter-reflection between neighbouring yarns on the measured reflectance.

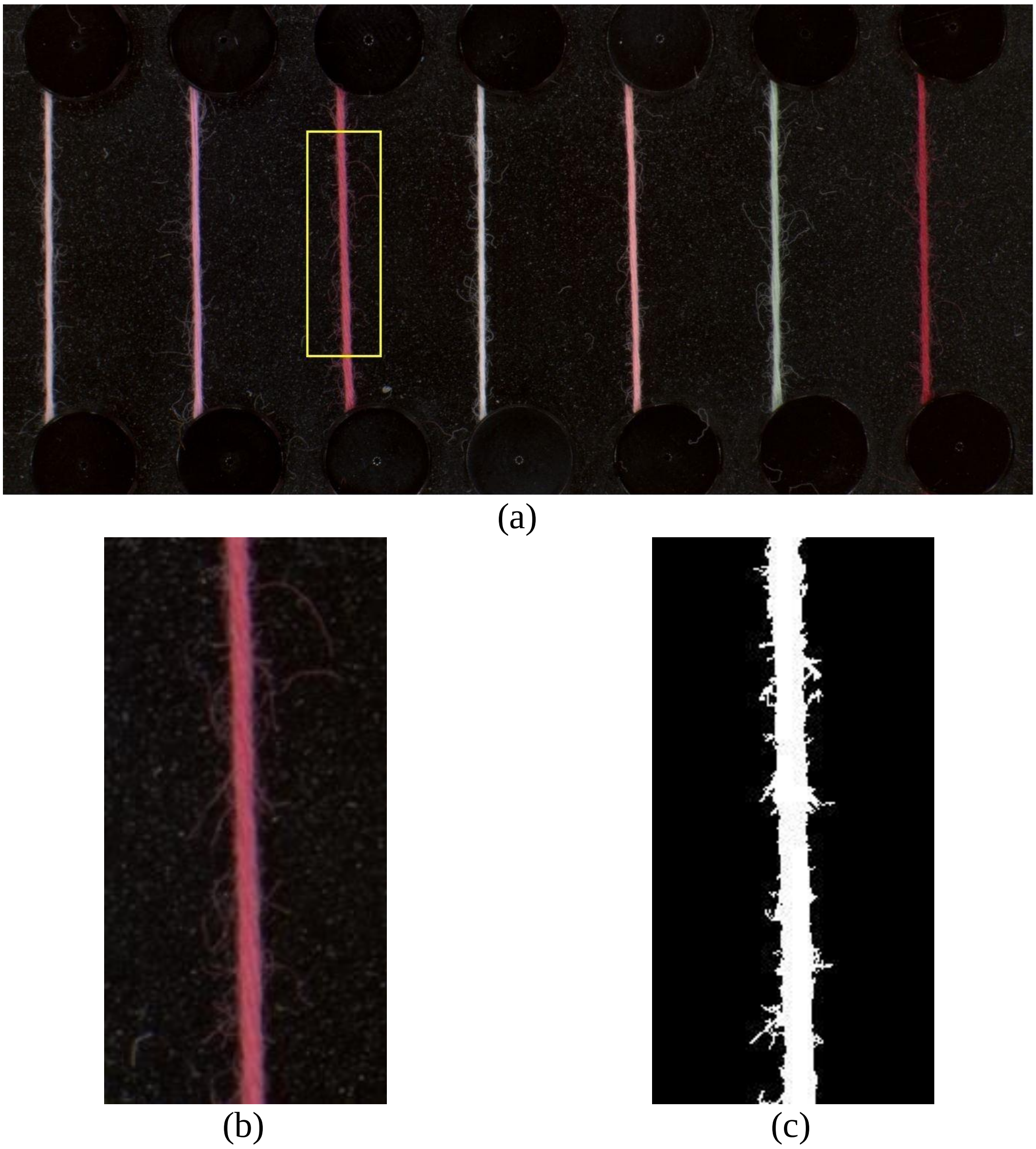

Figure 7.2 Example of single yarn segmentation: (a) a single yarn is selected to measure its colour (the yellow rectangle represents the selected segment of the single yarn); (b) the raw image of the selected single yarn; (c) the segmentation results, where the white pixels represent the single yarn;

For a single yarn fixed on a black platform, the reflection model can be simplified as:

$$\begin{aligned} R_b(\lambda, p_C, q_C) &= m_b(p_Y, q_Y)H(p_Y, q_Y)R_1(\lambda) \\ &= (m_b(p_Y, q_Y)H(p_Y, q_Y)\left|R_1(\lambda)\right|)\bar{R}_1(\lambda) \end{aligned} \tag{7. 3}$$

where $m_b(p_Y,q_Y)H(p_Y,q_Y)\left|R_1(\lambda)\right|$ is termed as the magnitude of the measured reflectance, $\bar{R}_1(\lambda)$ denotes the normalized nominal reflectance which defines the direction of the measured reflectance in the reflectance space.

Eqn (7.3) expresses that the spectral response of a multispectral imaging system to a single yarn defines a set of lines with identical direction but different magnitudes in the reflectance space. The direction of these lines is determined by the normalized nominal reflectance of the single yarn $\left|R_1(\lambda)\right|$. Their magnitudes depend on the geometric term $m_b(p_Y,q_Y)$, the occlusion coefficient $H(p_Y,q_Y)$, and the magnitude of the nominal reflectance $\left|R_1(\lambda)\right|$.

Colour specification of a single yarn is to estimate its reflectance from the measured reflectance of all the pixels on the single yarn. We can formulate this problem as:

$$\arg\min\Big(\sum_{p_C,q_C} W(p_C,q_C)\times(R(\lambda)-R_b(\lambda,p_C,q_C))^2\Big) \qquad (7.4)$$

where $R(\lambda)$ denotes the specified reflectance of the single yarn, $W(p_C,q_C)$ expresses the weight of pixel (p_C,q_C) to calculate $R(\lambda)$. When $W(p_C,q_C)$ is known, $R(\lambda)$ can be found by the least square method [129].

Method 1: Average of all pixels (AA)

A plausible assumption is that all the pixels have the same contribution to the specified reflectance, i.e., $W(p_C,q_C)=1/N_{p_C,q_C}$, where N_{p_C,q_C} denotes the total number of pixels on the single yarn. The specified reflectance of the single yarn is solved:

$$R(\lambda)=\frac{\sum_{p_C,q_C} R_b(\lambda,p_C,q_C)}{N_{p_C,q_C}} \tag{7. 5}$$

Eqn (7.5) expresses that the reflectance of a single yarn measured by a multispectral imaging system can be specified as the average reflectance of all the pixels on the single yarn. This is similar to the measurement result by a spectrophotometer as described in Chapter 3, i.e., the reflectance measured by a spectrophotometer is an average estimate to the nominal reflectance of a sample [151].

Method 2: Average of pixels in the central area (AC)

According to the Oren–Nayar reflectance model [113], the geometric term in Eqn (7.3) is defined as $m_b(p_Y, q_Y) = \cos(\theta)$, where θ is the incident angle at the surface position (p_Y, q_Y). In the edge area of a single yarn, the geometric term approaches zero due to large incident angle. As a consequence, the radiance of pixels in the edge area is low. These pixels have much smaller signal-to-noise ratio (SNR) [152] than pixels in central area. Thus, it is plausible to ignore pixels in the edge when specifying the colour of a single yarn because a signal with small SNR is sensitive to noises:

$$W(p_C, q_C) = \begin{cases} \dfrac{1}{N^{\Omega}_{p_C, q_C}} & \text{pixels in the central area} \\ 0 & \text{otherwise} \end{cases} \tag{7.6}$$

where Ω and $N^{\Omega}_{p_C, q_C}$ denote the central area and the number of pixels in the central area. The reflectance of a single yarn, $R(\lambda)$, is specified as:

$$R(\lambda) = \frac{\sum_{\Omega} R_b(\lambda, p_C, q_C)}{N^{\Omega}_{p_C, q_C}} \tag{7.7}$$

Method 3: Maxima of all pixels (MA)

As mentioned in Chapter 5, the occlusion coefficient $H(p_Y, q_Y)$ represents the fraction of light from the system illumination reaching the surface position (p_Y, q_Y). In the peak area of a single yarn, both of the occlusion coefficient and the geometric term approximate one. As a consequence, the radiance of pixels in the peak area is maximum and the measured reflectance is equal to the nominal reflectance of the single yarn. Thus, a reasonable estimate of the specified reflectance is the measured reflectance of pixel with maximum reflectance:

$$W(p_C, q_C) = \begin{cases} 1 & \text{pixel with maximum reflectance} \\ 0 & \text{otherwise} \end{cases} \tag{7. 8}$$

$$R(\lambda) = \max(R_b(\lambda, p_C, q_C)) \tag{7. 9}$$

Method 4: Lightness weighting (LW)

While the AC method can reduce the influence of noises on colour specification, the dilemma is how to define the central area of a single yarn. When the MA method is employed to specify the colour of a single yarn, the problem is that only the pixel with the maximum reflectance is considered. The colour information of other pixels is ignored. In order to combine both of the advantages of these two methods, a lightness weighting method is proposed:

$$W(p_C, q_C) = L^*(p_C, q_C) \tag{7. 10}$$

$$R(\lambda) = \frac{\sum_{p_C, q_C} L^*(p_C, q_C) R_b(\lambda, p_C, q_C)}{\sum_{p_C, q_C} L^*(p_C, q_C)} \tag{7. 11}$$

where $L^*(p_C, q_C)$ denotes the lightness of pixel (p_C, q_C).

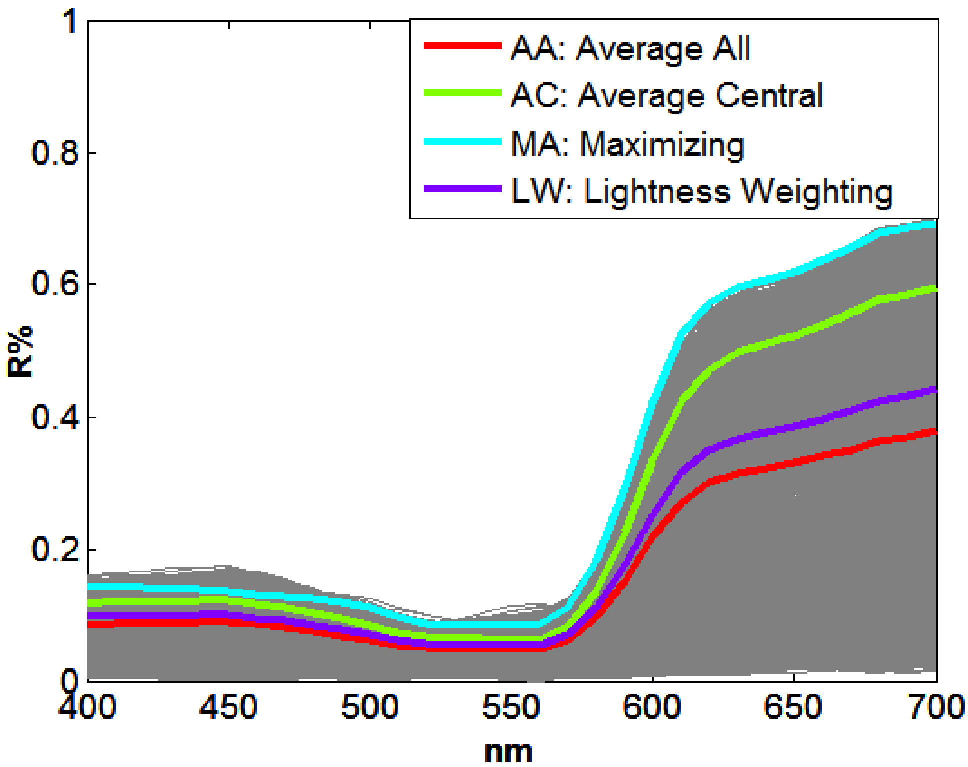

Figure 7.3 The reflectance curves of all the pixels on the single yarn showed in Figure 7.2d and the reflectance specified by the AA, AC, MA, and LW methods.

Figure 7.3 illustrates the reflectance of the single yarn showed in Figure 7.2d specified by the four proposed methods.

7.3. Results and Discussion

7.3.1. Comparison of Colour Specification Methods for Single Yarns

Colour distribution of pixels on a single yarn

The first experiment checked the colour distribution of pixels on the single yarn shown in Figure 7.2b. As shown in Figure 7.4a, the lightness of pixels in the edge area of the single yarn is small whereas the lightness of pixels in the central area is large. This can be considered as a result that the geometric term and occlusion coefficient of pixels in the edge area are small.

Figure 7.4b shows pixels on the single yarn are divided into three groups: pixels in edge area (red), pixels in central area (blue), and pixels in edge-central transition area (green). Figure 7.4c-d show the normalized reflectance of pixels in the three groups. The normalized reflectance of pixels in the edge area has a large range, [0, 0.4206].

However, the normalized reflectance of pixels in the central area has a small range, [0.0140, 0.3566]. The range of normalized reflectance of pixels in the edge-central transition area is [0.0167, 0.3677]. We can conclude that pixels in the edge area have a larger range of normalized reflectance than pixels in the central and edge-central transition areas. This can be considered as a result that pixels in the edge area are much more sensitive to noises owing to their low lightness.

In order to compare the normalized reflectance of pixels in the three areas, Eqn (3.18) was employed to calculate the angle between the normalized reflectance and their mean normalized reflectance. Figure 7.4f-h show the angles of pixels in the edge, edge-central transition, and central areas. The mean angles are 20.4791°, 8.6320°, and 3.2506° for pixels in the edge, edge-central transition, and central areas, respectively. Pixels in the central area have the smallest angles which coincides the results as shown in Figure 7.4c-d.

Figure 7.4i shows the chromaticity diagram of pixels in the three areas, where the size of a dot represents the luminance of the corresponding pixel. It can be observed that pixels in the edge area have lowest luminance but pixels in the central area have the highest luminance. In addition, chromaticity coordinates of pixels in the central area are much less scattered than pixels in the edge and edge-central transition areas.

Comparison of different colour specification methods

Figure 7.5 shows the comparison results of the four methods to specify the colour of the single yarn shown in Figure 7.2b. As shown in Figure 7.5a, the normalized reflectance specified by the four methods is approximately identical. The angle between the four normalized reflectance and their mean normalized reflectance was computed by Eqn (3.18). As shown in Figure 7.5b, the mean angles are 1.5336°, 1.6045°, 1.6625°, and 1.2336° for the normalized reflectance specified by the AA, AC, MA, and LW methods. The reflectance specified by the MA and LW methods has the largest and smallest angles. This can be considered as a result that the MA method just considers the pixel with the maximum reflectance whereas the LW method takes all the pixels on the single yarn into account. The magnitudes of the reflectance specified by the four methods were also analyzed by Eqn (3.18). As shown in Figure 7.5c, the magnitudes of the reflectance specified by the AA, AC, MA, and LW methods are 1.1372, 1.7790, 2.1211, and 1.3231, respectively. It can be concluded that the reflectance specified by the AA and MA methods yield the smallest and largest magnitudes.

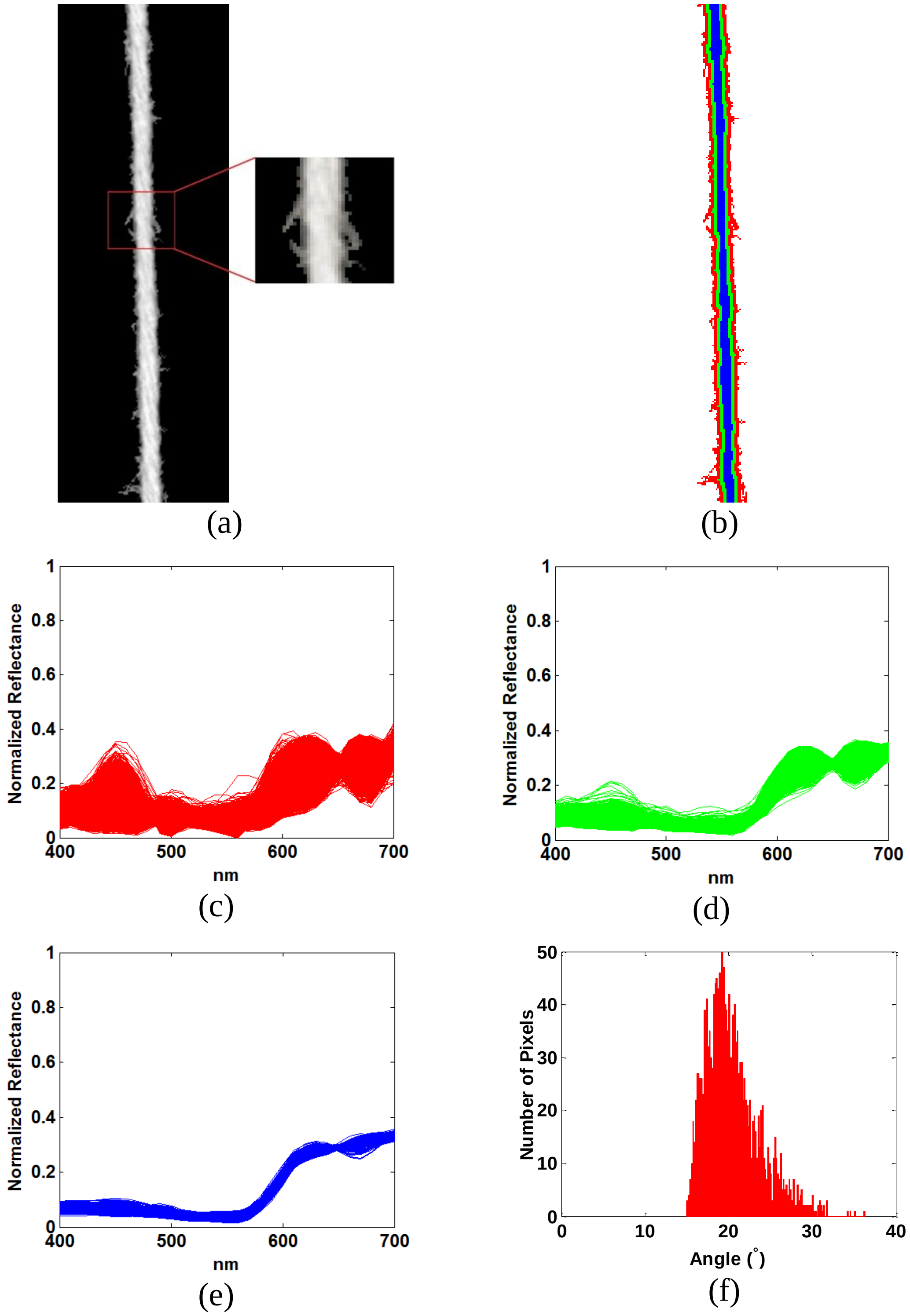

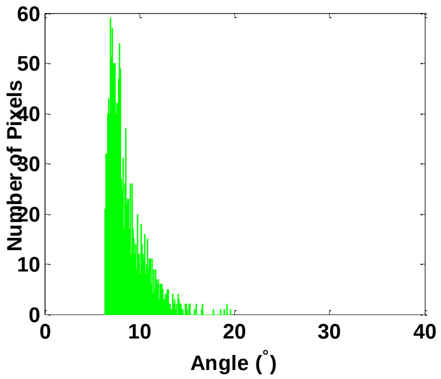

(g)

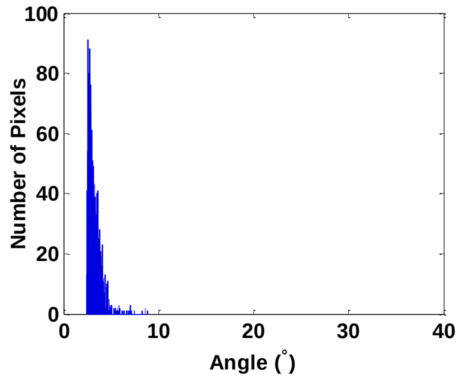

(h)

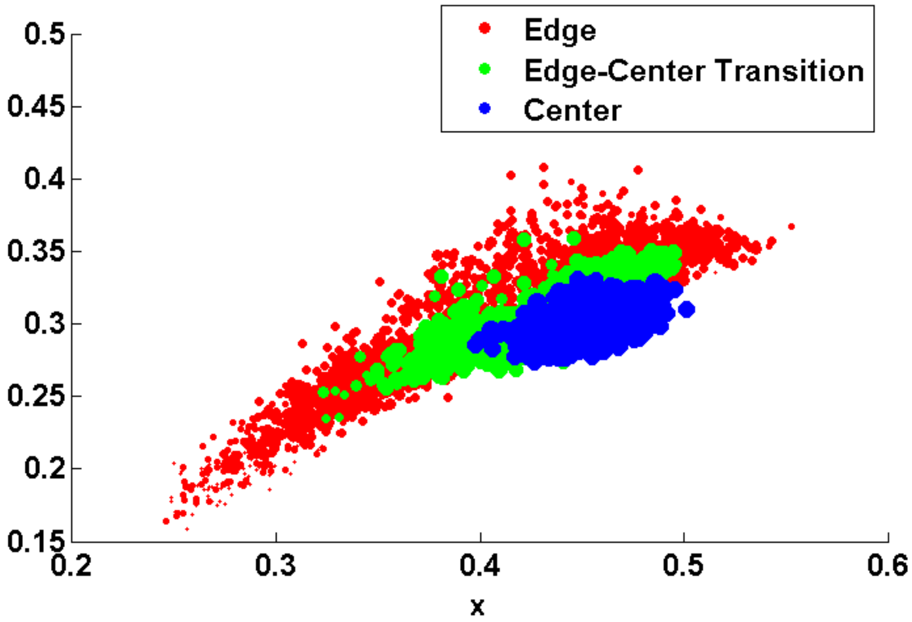

(i)

Figure 7.4 The colour distribution of pixels on the single yarn shown in Figure 7.2b: (a) the lightness of the single yarn; (b) pixels on the single yarn are labeled to 3 groups: pixels in edge area (red), pixels in central area (blue), and pixels in edge-central transition area (green); (c)-(e) the normalized reflectance of pixels in the edge, edge-central transition, and central areas; (f)-(h) the angles of pixels in the edge, edge-central transition, and central areas; (i) the chromaticity diagram of pixels in the edge, edge-central transition, and central areas. In (c)-(d), ranges is fixed to [0 1] to compare the variation of normalized reflectance of pixels in different areas. In (f)-(h), ranges are fixed to [0 ° 40 °] to compare the angles of pixels in different areas. In (i), the size of a dot represents the luminance of the corresponding pixel.

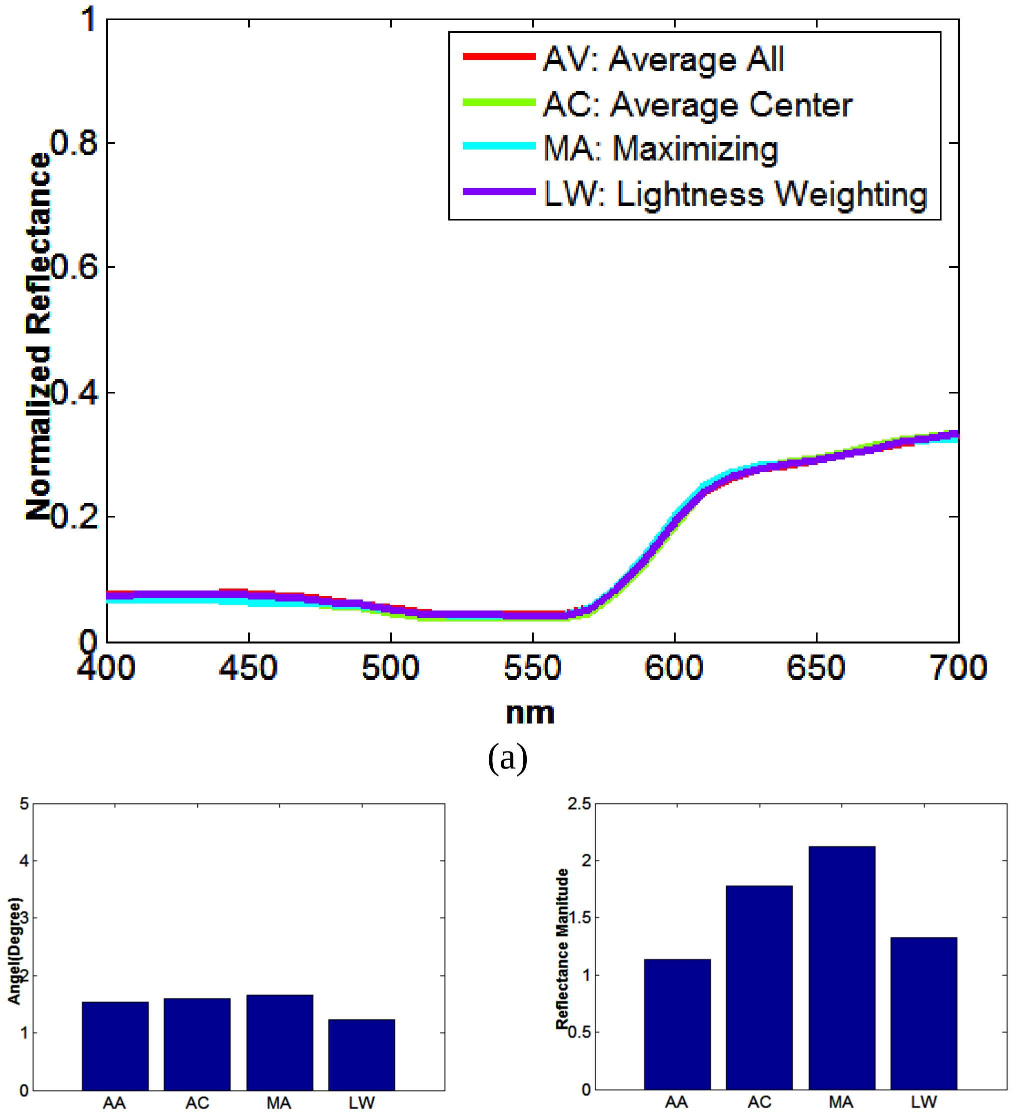

(a)

(b) (c)

Figure 7.5 Comparison of the four proposed methods to specify the reflectance of the single yarn shown in Figure 7.2b: (a) the normalized reflectance curves specified by the proposed methods; (b) the angel difference between the four normalized reflectance and their mean normalized reflectance; (c) the magnitudes of the reflectance specified by the proposed methods.

While the AA method is used by spectrophotometers to specify the reflectance of a sample, this method considers the contributions of all the pixels on the sample are identical. Although the AC method can reduce the influence of noises on colour specification as shown in Figure 7.4e and Figure 7.4h, the dilemma is how to define the central area of a single yarn. The drawback of the MA method is this method just considers the pixel with the maximum reflectance and ignores the information of other pixels. In contrast, the LW method combines both of the advantages of the AC and MA methods. Thus, it can be concluded that the best method to specify the colour of a single yarn is the LW method among the four methods.

7.3.2. Repeatability and Reproducibility

The first experiment checked the repeatability and reproducibility of ICM in colour measurement of single yarns. Repeatability is the ability of a colour measurement instrument repeats its measures of colour of a sample under the same conditions, such as the same operator and the same measurement procedures [153]. Repeatability is quantified as the mean colour difference between each measurement and the mean of all measurements ($MeanCDM$) [12]:

$$MCDM = \frac{\sum_{i=1}^{N} \Delta E_i}{N} \tag{7. 12}$$

where ΔE_i denotes the colour difference between the *i*-th measurement and the mean of all measurements, N is the number of measurements.

The maximum and minimum colour difference between each measurement and the mean of measurements ($MaxCDM$ and $MinCDM$) are defined as:

$$\begin{cases} MaxCDM = Max(\Delta E_1, \Delta E_2, \cdots \Delta E_N) \\ MinCDM = Min(\Delta E_1, \Delta E_2, \cdots \Delta E_N) \end{cases} \tag{7. 13}$$

Reproducibility is similar to repeatability except that some aspects of the measurement conditions have changed. For example, the same measurement procedures are used but the operator or the laboratory is changed [153]. The spatial reproducibility is one of most important concepts when a multispectral imaging system is used to measure the colour of a sample. The spatial reproducibility is a measure of how close the measurements of a sample are when the same measurement procedures are used but the sample is placed at different positions. Spatial reproducibility is also qualified as $MeanCDM$, $MaxCDM$ and $MinCDM$.

(a)

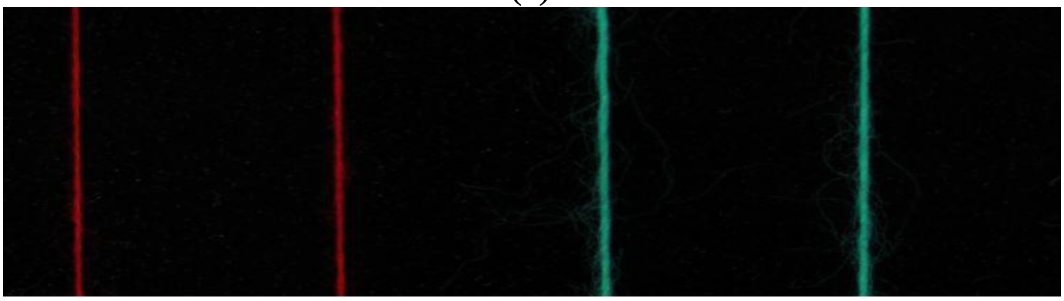

(b)

Figure 7.6 Single yarn samples used to conduct repeatability and reproducibility experiments: (a) the colour centres of these single yarns; (b) the arrangement of these single yarns. In (b), the single yarns from left to right are labeled Red 1, Red 2, Green 1, and Green 2.

As shown in Figure 7.6a, sixteen single yarns in eight colour centres were used to assess the repeatability and spatial reproducibility of the proposed approach in measuring single yarn colour. The material of these single yarns was cotton. The yarn count of these single yarns was 20 Ne. As shown in Figure 7.6b, two single yarn segments from the same cone were placed adjacently to assess the spatial reproducibility of ICM. The left and right single yarn segments in a colour centre C were labeled as C1 and C2. For example, the two red single yarns in Figure 7.6b were named Red 1 (left) and Red 2 (right). These single yarns were measured by the MSI system ICM in every thirty minutes for a period of eight hundred and ten minutes. The LW Method was employed to specify the reflectance of a single yarn. The colour difference between each measurement and the mean of all measurements was calculated by the CMC(2:1) formula.

Table 7. 1 Repeatability and spatial reproducibility of ICM in measuring the sixteen single yarns shown in Figure 7.6.

	Repeatability			Spatial Reproducibility		
Single Yarns	MeanCDM	MaxCDM	MinCDM	MeanCDM	MaxCDM	MinCDM
Green 1	0.1150	0.3889	0.0232	0.2756	0.3111	0.2514
Green 2	0.1276	0.3889	0.0232	0.2756	0.3111	0.2514
Purple 1	0.0906	0.3010	0.0225	0.3163	0.5006	0.1570
Purple 2	0.0906	0.3010	0.0225	0.3163	0.5005	0.1570
Brown 1	0.1090	0.2032	0.0191	0.2724	0.5642	0.0868
Brown 2	0.1090	0.2032	0.0191	0.2721	0.5634	0.0868
Red 1	0.1591	0.4338	0.0267	0.2817	0.3924	0.1710
Red 2	0.1591	0.4338	0.0267	0.2818	0.3924	0.1712
Light Grey 1	0.1376	0.3684	0.0260	0.3170	0.4310	0.2200
Light Grey 2	0.1376	0.3684	0.0260	0.3164	0.4302	0.2193
Dark Grey 1	0.1166	0.3461	0.0293	0.3396	0.3842	0.2552
Dark Grey 2	0.1166	0.3461	0.0293	0.3385	0.3829	0.2541
Blue 1	0.1137	0.3826	0.0064	0.2801	0.4203	0.1478
Blue 2	0.1137	0.3826	0.0064	0.2801	0.4203	0.1478
Orange 1	0.0999	0.2586	0.0278	0.1798	0.2320	0.1260
Orange 2	0.0999	0.2586	0.0278	0.1798	0.2320	0.1260
average	0.1185	0.3353	0.0226	0.2827	0.4043	0.1768

The repeatability and spatial reproducibility of ICM in measuring the colours of single yarns are shown in Table 7. 1. For the sixteen single yarns, the average *MeanCDM* of repeatability is 0.1185 CMC(2:1) units. The average *MaxCDM* and *MinCDM* of repeatability are 0.3353 and 0.0026 CMC(2:1) units. ICM has the best repeatability performance in measuring the purple single yarns (Purple 1 and Purple 2), i.e., 0.0906 and 0.0906 CMC(2:1) units. The repeatability of ICM in measuring the red single yarns (Red 1 and Red 2) is worst, 0.1591 and 0.1591 CMC(2:1) units, which are relatively larger than the measurement results of purple single yarns. This implies that the repeatability of ICM in measuring colours of purple single yarns is better than red single yarns. The spatial reproducibility of ICM in measuring colours of these sixteen single yarns is 0.2827 CMC(2:1) units within the range of 0.1768 and 0.4043 CMC(2:1) units. ICM has the best spatial reproducibility performance in measuring the orange single yarns (Orange 1 and Orange 2), i.e., 0.1798 and 0.1798 CMC(2:1) units. Table 7. 1 shows that the multispectral imaging system ICM has good repeatability and spatial reproducibility in measuring single yarn colour.

7.3.3. Colour Matching

The second experiment compared the colour matching abilities of single yarns measured by ICM and solid-colour yarn dyed fabrics measure by spectrophotometers. Colour matching is a vital process in ensuring continuity of colour from a master standard to a subsequent batch [154]. Colour matching between standard and batch fabrics can be conducted by two methods: instrumental evaluation and visual assessment. The instrumental method employs a colour measurement instrument to measure the colours of the standard and the batch samples. Colour matching is achieved by comparing the colour difference between the standard and batch samples with a tolerance beforehand determined by users. If the colour difference is smaller than the tolerance, the colour matching result is 'pass', i.e., the colour of the batch sample matches that of the standard sample, and *vice versa*. The instrumental method is more accurate than the visual method as the latter is a subjective process. Inconsistent colour matching results may exist among different inspectors. Spectrophotometers are the most widely used instruments to conduct colour matching of fabrics. However, a spectrophotometer can only carry out colour matching of solid-colour fabrics and yarn cards.

Based on the proposed method, colour matching between standard and batch single yarns can be achieved.

Twenty-four solid-colour yarn dyed fabrics and corresponding single yarns were used to conduct the colour matching comparison experiment between single yarns and solid-colour fabrics. A desktop spectrophotometer Datacolor 650 (D650) was used to provide the dye formulas to reproduce these twenty-four solid-colour standard yarn dyed fabrics. Based on these formulas, twenty-four solid-colour batch yarn dyed fabrics were dyed. The corresponding single yarns of these dyed yarn dyed fabrics were used as batch single yarns. The colours of these twenty-four pairs of standard and batch single yarns were measured by the multispectral imaging system ICM. The colours of the twenty-four pairs of standard and batch yarn dyed fabrics were measured by the D650 system. The specular component excluded (SCE) and UV excluded modes were applied to eliminate the influence of specular light and UV on samples. The colour difference between standard and batch samples (solid-colour yarn dyed fabrics and corresponding single yarns, respectively) was calculated by the CMC(2:1) formula under standard illuminant D65. The tolerance to determine colour matching results ('pass' or 'fail') in this experiment was set to 1.0 CMC(2:1) units. The reflectance values of the standard yarn dyed fabrics and corresponding single yarns are shown in Figure 7.7.

The colour matching results are shown in Figure 7.8. The horizontal and vertical axes denote the colour matching results conducted by single yarns (measured by ICM) and solid-colour yarn dyed fabrics (measured by D650). The black line represents same colour matching results are achieved by single yarns and corresponding solid-colour yarn dyed fabrics. When a dot more approaches to the black line, the colour matching result by single yarns is closer to that by yarn dyed fabrics. Dots above the black line imply that the colour difference between yarn dyed fabrics is larger than the colour difference between corresponding single yarns, and *vice versa*. As shown in Figure 7.8, five blue dots are above the black line but approaching it, implying the colour difference of these five pairs of yarn dyed fabrics is slightly larger than that of the corresponding five pairs of single yarns. Sixteen blue dots are below the black line, indicating that the colour difference of these sixteen pairs of yarn dyed fabrics is smaller than that of the corresponding pairs of single yarns. In addition, the colour difference of these sixteen pairs of single yarns is smaller than 1.0 CMC(2:1) units. For the twenty-one pairs of yarn dyed fabrics and single yarns shown as blue dots in Figure 7.8, the same colour matching results are achieved when the tolerance is set as 1.0 CMC(2:1) units, i.e., twenty pairs of yarn dyed fabrics and corresponding single yarns obtain the 'pass' result, and one pair of fabric and corresponding single yarn samples have the result of 'fail'.

However, three pairs of yarn dyed fabrics and single yarns yield different colour matching results, as shown as the three red dots in Figure 7.8. The colour difference of the three pairs of single yarns measured by MSI is 0.34, 0.35, 0.70 CMC(2:1) units, which is smaller than the colour matching tolerance of 1.0 CMC(2:1) unit. In contrast, the colour difference of the three corresponding pairs of yarn dyed fabrics measured by D650 is 1.27, 1.90, and 1.38 CMC(2:1) units, which is larger than the tolerance of 1.0 CMC(2:1) unit. As a consequence, the colour matching results from single yarns are 'pass' but 'fail' from corresponding solid-colour yarn dyed fabrics. This can be considered as a result of the influence of woven structure on colour. The fabric structure of a yarn dyed fabric, such as areal density and yarn direction, can affect the spectrophotometric colour of the fabric. Therefore, it is possible that the colour difference of two fabrics is larger 1.0 CMC(2:1) units but that of the corresponding single yarns is smaller than 1.0 CMC(2:1) units. We can conclude from Figure 7.8 that single yarns measured by multispectral imaging systems can achieve the similar colour matching results as yarn dyed fabrics measured by spectrophotometers when the influences of areal density and yarn direction are negligible.

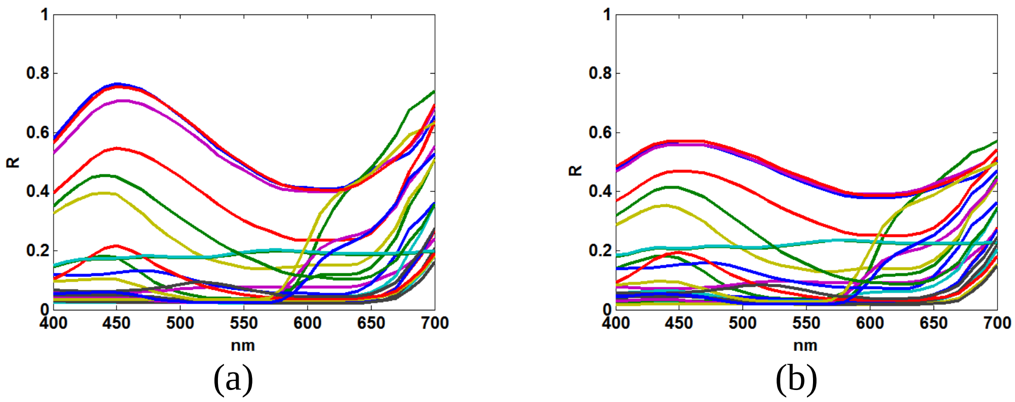

Figure 7.7 The reflectance of the twenty-four standard yarn dyed fabrics and corresponding single yarns: (a) the reflectance of the twenty-four standard yarn dyed fabrics; (b) the reflectance of the corresponding standard single yarns.

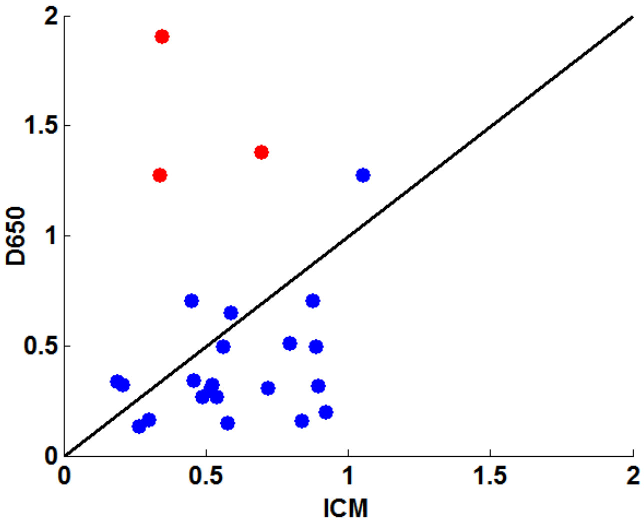

Figure 7.8 The colour matching comparison results between single yarns measured by ICM and solid-colour yarn dyed fabrics measured by a Datacolor 650 spectrophotometer (D650): the black line denotes the same colour match results are achieved by ICM and D650.

7.4. Conclusion

This chapter introduces a novel multispectral imaging method that accurately measures colours of single yarns. Firstly, a single yarn is fixed on a black flat platform to obtain its multispectral images. Secondly, the single yarn is segmented from background by the image difference method. Finally, the reflectance of the single yarn is specified by four methods. In the experiments, the colour distribution of pixels on a single yarn was first analyzed. It is concluded that pixels in the central area have much less scattered chromaticity coordinates than those in the edge area. Then, the four colour specification methods were compared. It is concluded that the best method to specify the colour of a single yarn is the Lightness Weighting method. The repeatability and spatial reproducibility to measure single yarn colour were assessed by sixteen single yarns in every thirty minutes for a period of eight hundred and ten minutes. Experimental results show that the repeatability and spatial reproducibility are 0.1185 and 0.2827 CMC(2:1) units. The colour matching experiment based on the MSI system ICM and a spectrophotometer Datacolor 650 was conducted using forty-eight solid-colour yarn dyed fabrics and their corresponding single yarns. Experimental results show single yarns measured by ICM can achieve the similar colour matching results as solid-colour yarn dyed fabrics measured by the spectrophotometer Datacolor 650.

Chapter 8 Colour Mapping between Single Yarns and Yarn Cards

A multispectral imaging method that accurately measures colours of single yarns is introduced in Chapter 7. While the proposed method can achieve single yarn colour measurement and colour matching, colour reproduction is not available because the existing method to predict the dye recipe of a yarn dyed fabric is based on the colorant formulation system inside a spectrophotometer. However, spectrophotometers can only predict the recipe of a solid-colour region, such as a yarn card. In order to achieve colour reproduction of yarn dyed fabrics based on colour measurement of single yarns and colorant formulation system inside a spectrophotometer, the colour of a single yarn measured by a multispectral imaging system must be mapped to the colour of the corresponding yarn card measured by a spectrophotometer. This chapter proposes a novel method to map colours between a single yarn and its corresponding yarn card.

8.1. Background

While the colorant formulation system inside a spectrophotometer can yield satisfied dye recipe prediction for colour reproduction of yarn dyed fabrics, this method has three limitations. Firstly, only solid-colour yarn dyed fabrics with relatively large area, larger than the aperture size of a spectrophotometer, can be reproduced. In order to estimate the recipes for multi-colour yarn dyed fabrics, weft and warp yarns must be manually separated, and then winded on yarn cards. Secondly, the recipe for a solid-colour yarn dyed fabric changes with fabric areal density because this parameter has a great impact on spectrophotometric colour. Finally, yarns may not be sufficient to prepare a yarn card when just a small standard yarn dyed fabric sample is provided. While spectrophotometers have these drawbacks in colour reproduction of yarn dyed fabrics, it is not trivial to establish a new colorant formulation system based on multispectral imaging systems. Instead, it is more practicable to map the colour of a single yarn measured by a multispectral imaging system to that of the corresponding yarn card measured by a spectrophotometer, and then utilize the colorant formulation system inside the spectrophotometer to achieve colour reproduction.

8.2. Colour Mapping between Single Yarns and Yarn Cards

8.2.1. Colours of Yarn Cards

As introduced in Chapter 3, the light reaching the position (p_Y, q_Y) on a yarn dyed fabric surface is composed of two components: light from the system illuminant and light reflected by neighbouring yarns. The light from the system illuminant is affected by fabric surface texture and occlusion of system illuminant. The light reflected by neighbouring yarns is influenced by fabric surface texture and inter-reflection between neighbouring yarns. A geometric term, $m_b(p_Y, q_Y)$, is used to formulate the influence of fabric surface texture, which is determined by the incident angle at the position (p_Y, q_Y). $m_b(p_Y, q_Y)$ would influence the measured reflectance magnitude of a fabric. Occlusion of system illuminant is modeled as a block parameter, $H(p_Y, q_Y)$, which represents the fraction of the light from the system illumination reaching the surface.

$H(p_Y, q_Y) = 0$ implies that the system illuminant is completely blocked, and *vice versa*. Inter-reflection between neighbouring yarns would cause a second illumination and is represented by a term $A(p_Y, q_Y)$. According to Eqn (3.7), the radiance at the position (p_Y, q_Y) of a yarn dyed fabric, $L_{yarn}(\lambda, p_Y, q_Y)$, can be modeled as:

$$\begin{aligned} L_{yarn}(\lambda, p_Y, q_Y) = & \, m_b(p_Y, q_Y) H(p_Y, q_Y) E(\lambda) R_1(\lambda) \\ & + m_b(p_Y, q_Y) A(p_Y, q_Y) E(\lambda) R_1(\lambda) R_2(\lambda) \end{aligned} \tag{8. 1}$$

where $E(\lambda)$, $R_1(\lambda)$ and $R_2(\lambda)$ represent the spectrum of the system illuminant, the nominal reflectance of the measured yarn and neighbouring yarn.

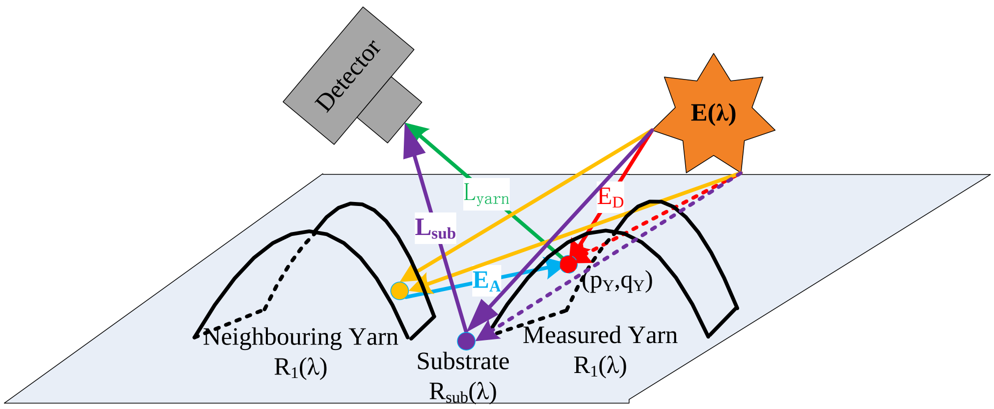

Figure 8.1 The reflection schematic in a yarn card.

Analogous to the reflection model of yarn dyed fabrics, surface roughness, system illuminant occlusion and inter-reflection between neighbouring yarns would influence the radiance of a yarn card, as showing in Figure 8.1. In addition, the light reflected by the substrate of the yarn card (the purple line in Figure 8.1) would also contribute the flux at the detector of a spectrophotometer. Consequently, the light reach the detector of a spectrophotometer, $L_{YC}(\lambda, p_Y, q_Y)$, can be modeled as:

$$\begin{aligned} L_{YC}(\lambda, p_Y, q_Y) &= L_{sub}(\lambda, p_Y, q_Y) + L_{yarn}(\lambda, p_Y, q_Y) \\ &= W_{sub}(p_Y, q_Y)E(\lambda)R_{sub}(\lambda) \\ &\quad + m_b(p_Y, q_Y)H(p_Y, q_Y)E(\lambda)R_1(\lambda) \\ &\quad + m_b(p_Y, q_Y)A(p_Y, q_Y)E(\lambda)R_1(\lambda)^2 \end{aligned} \tag{8. 2}$$

where $L_{sub}(\lambda, p_Y, q_Y)$ represents the light reflected by the substrate, $W_{sub}(p_Y, q_Y)$ and $R_{sub}(\lambda)$ denote the fraction of the light reflected by the substrate and the nominal reflectance of the substrate.

Combining Eqn (3.8), Eqn (3.11), and Eqn (8.2), the reflectance of a yarn card measured by a spectrophotometer, $R_{YC}(\lambda)$, can be modeled as:

$$\begin{aligned} R_{YC}(\lambda) = &\frac{\iint_{p_Y, q_Y} W_{sub}(p_Y, q_Y)dp_Y dq_Y}{A_r} R_{sub}(\lambda) + \frac{\iint_{p_Y, q_Y} m_b(p_Y, q_Y)H(p_Y, q_Y)dp_Y dq_Y}{A_r} R_1(\lambda) \\ &+ \frac{\iint_{p_Y, q_Y} m_b(p_Y, q_Y)A(p_Y, q_Y)dp_Y dq_Y}{A_r} R_1(\lambda)^2 \end{aligned} \tag{8. 3}$$

where A_r denotes the aperture area of the spectrophotometer.

8.2.2. Colours of Single Yarns

As introduced in Chapter 7, the reflectance $R_b(\lambda, p_C, q_C)$ of pixel (p_C, q_C) at a single yarn measured by a multispectral imaging system can be modeled as:

$$R_b(\lambda, p_C, q_C) = m_b(p_Y, q_Y) H(p_Y, q_Y) R_1(\lambda) \qquad (8.\ 4)$$

where $m_b(p_Y, q_Y)$ and $H(p_Y, q_Y)$ denote the influences of the yarn surface texture and the system illuminant on the measured reflectance, $R_1(\lambda)$ represents the nominal reflectance of the single yarn.

Four methods are investigated to specify the reflectance of a single yarn as showing by Eqn (7.5), Eqn (7.7), Eqn (7.9), and Eqn (7.11). These four methods can be summarized as:

$$R_{SY}(\lambda) = W_{SY} R_1(\lambda) \qquad (8.\ 5)$$

where $R_{SY}(\lambda)$ and W_{SY} denote the specified reflectance of a single yarn and the weight to calculate it.

$$W_{SY} = \begin{cases} \dfrac{\sum\limits_{p_C, q_C} m_b(p_Y, q_Y) H(p_Y, q_Y)}{N_{p_C, q_C}} & \text{average of all pixels} \\ \dfrac{\sum\limits_{\Omega} m_b(p_Y, q_Y) H(p_Y, q_Y)}{N^{\Omega}_{p_C, q_C}} & \text{average of all pixels in central area} \\ \max(m_b(p_Y, q_Y) H(p_Y, q_Y)) & \text{maxima of all pixels} \\ \dfrac{\sum\limits_{p_C, q_C} L^*(p_C, q_C) m_b(p_Y, q_Y) H(p_Y, q_Y)}{\sum\limits_{p_C, q_C} L^*(p_C, q_C)} & \text{lightness weighting method} \end{cases} \quad (8.6)$$

where (p_Y, q_Y) is the position on the single yarn corresponding to (p_C, q_C).

8.2.3. Colour Relationship between Yarn Cards and Single Yarns

Combining Eqn (8.3) and Eqn (8.5), we can model the relationship between the colours of a yarn card and its corresponding single yarn as:

$$R_{YC}(\lambda) = \frac{\iint\limits_{p_Y, q_Y} W_{sub}(p_Y, q_Y) dp_Y dq_Y}{A_r} R_{sub}(\lambda) + \frac{\iint\limits_{p_Y, q_Y} m_b(p_Y, q_Y) H(p_Y, q_Y) dp_Y dq_Y}{A_r W_{SY}} R_{SY}(\lambda) + \frac{\iint\limits_{p_Y, q_Y} m_b(p_Y, q_Y) A(p_Y, q_Y) dp_Y dq_Y}{A_r W_{SY}} R_{SY}(\lambda)^2 \quad (8.7)$$

Eqn (8.7) expresses that the reflectance of a yarn card measured by a spectrophotometer is a linear combination of three parts: the reflectance of the substrate, the reflectance of the corresponding single yarn measured by a multispectral imaging system, and the reflectance square of the single yarn. The square component represents the inter-reflection between yarns of the yarn card. The coefficients of these three components are determined by the weight to specify the reflectance of the single yarn W_{SY}, the aperture area of the spectrophotometer A_r, the fraction of the light reflected by the substrate W_{sub}, the geometric term $m_b(p_Y, q_Y)$, the occlusion parameter of system illumination $H(p_Y, q_Y)$, and the inter-reflection parameter between neighbouring yarns $A(p_Y, q_Y)$.

8.2.4. Coefficient Estimation

According to Eqn (8.7), the relationship between the colour of a single yarn measured by a multispectral imaging system and the colour of the corresponding yarn card measured by a spectrophotometer can be simplified as:

$$R_{YC}(\lambda) = c_0 R_{sub}(\lambda) + \sum_{i=1}^{2} c_i R_{SY}(\lambda)^i + c \tag{8. 8}$$

where

$$\begin{cases} c_0 = \iint\limits_{p_Y, q_Y} W_{sub}(p_Y, q_Y) dp_Y dq_Y / A_r \\ c_1 = \iint\limits_{p_Y, q_Y} m_b(p_Y, q_Y) H(p_Y, q_Y) dp_Y dq_Y / (A_r W_{SY}) \\ c_2 = \iint\limits_{p_Y, q_Y} m_b(p_Y, q_Y) A(p_Y, q_Y) dp_Y dq_Y / (A_r W_{SY}) \\ c = \text{the direct current component, such as the difference} \\ \quad \text{of dark current between ICM and spectrophotometer} \end{cases} \tag{8. 9}$$

The optimal coefficients $C^* = [c_0, c_1, c_2, c]^T$ can be defined as:

$$C^* = \arg\min \sum_{j=1}^{N} (CMC(Y_j, C^T X_j)) \qquad \text{subject to} \begin{cases} c_0 \geq 0 \\ c_1 \geq 0 \\ c_2 \geq 0 \end{cases} \tag{8. 10}$$

where $X_j = [R^j_{sub}(\lambda), R^j_{SY}(\lambda), R^j_{SY}(\lambda)^2]^T$ and $Y_j = R^j_{YC}(\lambda)$, N expresses the number of single yarns and corresponding yarn card pairs, $CMC(R_1, R_2)$ represents the CMC(2:1) colour difference between two reflectance curves $R_1(\lambda)$ and $R_2(\lambda)$.

As expressed in Eqn (8.10), it is difficult to analytically derive the gradient and second-order derivative information of the objective function since the calculation of CMC(2:1) colour difference from reflectance is complicated. Therefore, the least square method [129] cannot be employed to find the optimal solution of Eqn (8.10). Instead, the simplex method [155,156] is applied to solve the optimization problem. The simplex method is a popular algorithm for the optimization problem of linear programming [156,157,158]. Basically, the simplex method is composed by two phases [159]. In phase Ⅰ, an initial basic feasible solution is found and the problem is converted into a so-called canonical form. In phase Ⅱ, one basic feasible solution is moved to the next until no more improvement can be made. These two phases are carried out iteratively until the optimal solution is found.

8.3. Results and Discussion

100 pairs of yarn cards and corresponding single yarns were used to evaluate the proposed method. These samples were collected from a local textile company. The yarn count of these samples was 80 Ne. The colours of the yarn card samples were measured by a Datacolor 650 spectrophotometer and conducted under the 1964 CIE standard observer. The specular component excluded (SCE) and UV excluded modes were applied to eliminate the influence of specular light and UV on samples. The colours of the single yarn samples were measured by the MSI system ICM. The method introduced in Chapter 7 was used to specify

the colours of the single yarns, where the lightness weighting method was adopted.

Figure 8.2a and Figure 8.2b show the reflectance curves of the yarn cards and the corresponding single yarns. It can be observed that a yarn card has a higher reflectance than the corresponding single yarn. This accords with the colour relationship between a single yarn and its corresponding yarn card as shown in Eqn (8.7). The reflectance of a yarn card measured by a spectrophotometer is a linear combination of the reflectance of the substrate, the reflectance of the corresponding single yarn measured by a MIS system, and the reflectance square of the single yarn. Figure 8.2c shows the reflectance of the substrate measured by the Datacolor 650 spectrophotometer.

In order to analyze the reflectance relationship of a yarn card and its corresponding single yarn, their angle was calculated by Eqn (3.18). As shown in Figure 8.2d, the angles between normalized reflectance of single yarns and their corresponding yarn cards are in the range of [0.68°, 8.13°] except for one outlier with the angle of 14.18°. The large angles shown in Figure 8.2d demonstrates that the normalized reflectance of single yarns and yarn cards are different. Figure 8.2e shows the reflectance magnitudes of single yarns and yarn cards. We can see that the reflectance magnitudes of yarn cards is larger. This observation agrees with the results showing in Figure 8.2a and Figure 8.2b. As shown in Figure 8.2f, the 100 pairs of single yarn and yarn card samples were divided into training and testing datasets equally.

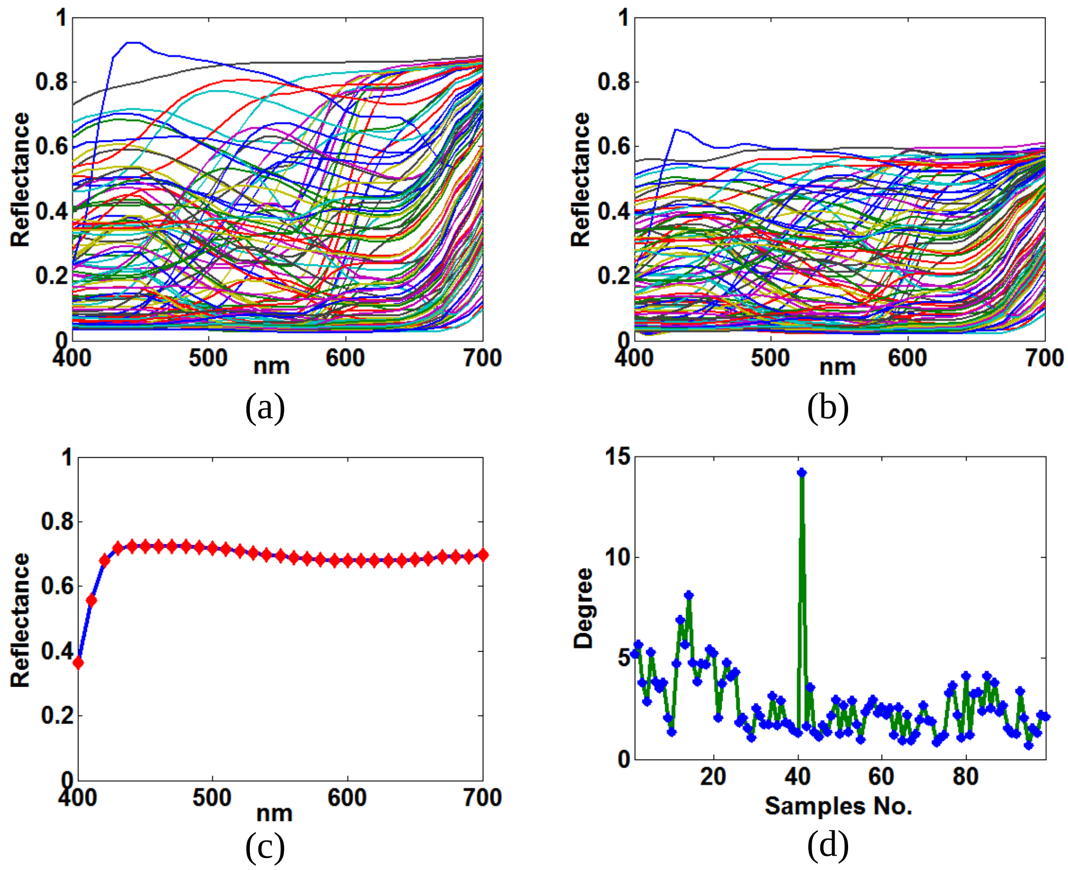

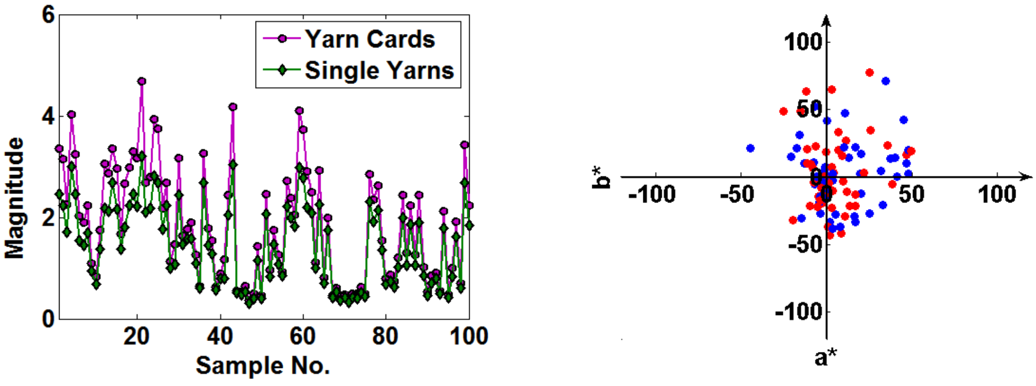

(e) (f)

Figure 8.2 The reflectance curves of single yarns, yarn cards, and the substrate: (a) the reflectance curves of yarn cards; (b) the reflectance curves of single yarns; (c) the reflectance of the substrate; (d) angel difference between reflectance of single yarns and yarn cards; (e) reflectance magnitudes of yarn cards and single yarns; (f) the distribution of training dataset (red) and testing dataset (blue) in the a*-b* plane.

The training and testing results are shown in Figure 8.3. As shown in Figure 8.3a, the real colour difference between single yarns and corresponding yarn cards in the training database is in the range of [0.90, 7.38] with the average of 2.97 CMC(2:1) units. After colour mapping, their colour difference reduces to the range of [0.40, 4.13] with the average of 1.20 CMC(2:1) units. As shown in Figure 8.3b, the real colour difference between single yarns and corresponding yarn cards in the testing database is in the range of [1.02, 8.77] with the average of 3.09 CMC(2:1) units. After colour mapping, their colour difference reduces to the range of [0.18, 5.09] with the average of 1.37 CMC(2:1) units.

The optimal coefficients for colour mapping between single yarns and yarn cards are $C^* = [0.005, 0.994, 0.469, 0.003]^T$, i.e., the relationship between the colours of a single yarn measured by ICM and its corresponding yarn card measured by a Datacolor 650 spectrophotometer can be modeled as:

$$R_{YC}(\lambda) = 0.005R_{sub}(\lambda) + 0.994R_{SY}(\lambda) + 0.469R_{SY}(\lambda)^2 + 0.003 \qquad (8.\ 11)$$

Eqn (8.11) expresses that the dominant component of the colour relationship between a single yarn and its corresponding yarn card is the reflectance of the single yarn, i.e., the coefficient is 0.994. The second dominant component is the reflectance square of the single yarn which represents the inter-reflection between yarns of the yarn card. The influence of inter-reflection is about half of the reflectance of the single yarn, i.e., the coefficient is 0.469 compared with 0.994. However, the influences of reflectance of substrate and dark current difference between systems are insignificant, i.e., the coefficients are 0.005 and 0.003. This can be considered as a result that samples are good prepared and systems are good calibrated.

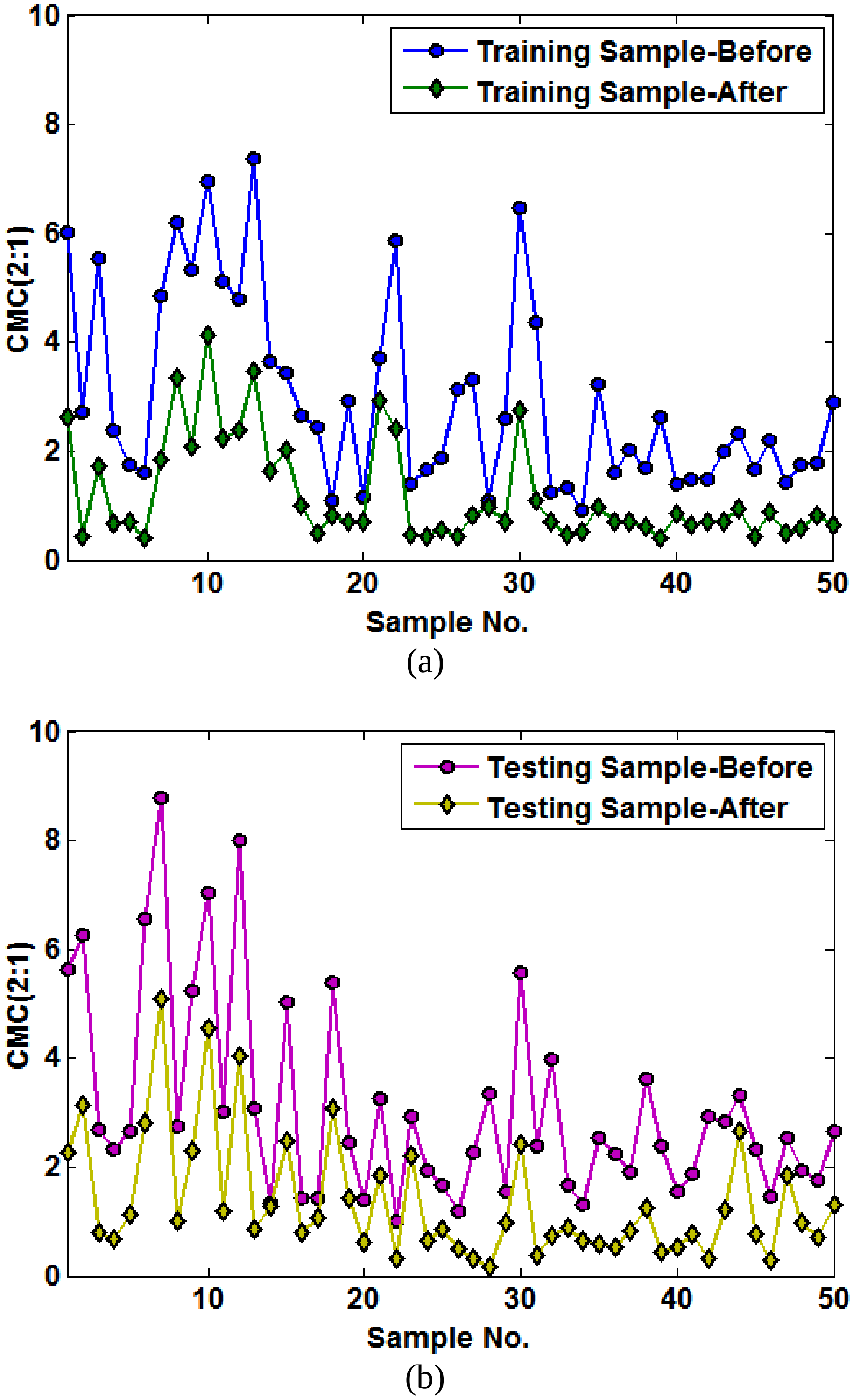

Figure 8.3 The colour difference between yarn cards and corresponding single yarns before and after colour mapping: (a) colour difference between samples in the training group; (b) colour difference between samples in the testing group.

8.4. Conclusion

This chapter introduces a novel colour mapping method between a single yarn measured by a multispectral imaging system and its corresponding yarn card measured by a spectrophotometer. Firstly, the relationship between the reflectance of a single yarn and its corresponding yarn card is modeled. The reflectance of a yarn card measured by a spectrophotometer is a linear combination of the reflectance of the substrate, the reflectance of the corresponding single yarn measured by a MIS system, and the reflectance square of the single yarn. Secondly, colour mapping between single yarns and yarn cards is transformed into an optimal problem. Finally, the simplex method is employed to find the optimal coefficients in the relationship model. 100 pairs of yarn cards and single yarns were used to evaluate the proposed method. Experimental results show that the colour difference between single yarns and yarn cards reduces from 2.97 to 1.20 CMC(2:1) units for 50 pairs of training samples and from 3.09 to 1.37 CMC(2:1) units for 50 pairs of testing samples.

Chapter 9 Conclusion and Suggestions for Future Research

This chapter concludes the thesis. A brief summary of the major ideas and proposed algorithms in the thesis is given firstly. The future work is then presented in the last section of this chapter.

9.1. Conclusion

- **Reflection model of yarn dyed fabrics**

  In Section 3.2, a reflection model is proposed to estimate interaction between light and a yarn dyed fabric. The model expresses that the light reflected by a yarn dyed fabric is composed by two parts: the occluded light from the system illuminant and the light reflected by neighbouring yarns. Texture, illuminant occlusion and inter-reflection between neighbouring yarns are taken into account in the model. The texture of a yarn dyed fabric has a major impact on the intensity of the reflected light and can be formulated by a geometric term. The occlusion of system illuminant would also affect the intensity of reflected light and is represented by a block parameter. The inter-reflection between neighbouring yarns would cause a second illumination on a sample and thus colour shift exists in the measured colour.

- **Reducing the influence of texture on colour**

In Section 3.3, the proposed reflection model of yarn dyed fabrics is utilized to estimate how the surface texture of a yarn dyed fabric influence its colour measured by a spectrophotometer. Based on proposed reflection model, the spectral response of a spectrophotometer to a yarn dyed fabric is estimated. In the reflectance space, fabrics with different textured surfaces define a set of lines with identical direction. The normalized reflectance curves of these fabrics are constant. In the CIEXYZ space, fabrics with different textured surfaces define a line and their chromaticity coordinates are identical. However, the linearity in the reflectance and CIEXYZ spaces is lost in the CIELAB space owing to the non-linear colour transformation from the CIEXYZ space to CIELAB space. A method is proposed to discount the influence of texture on colour. Experiments show that the influence of texture on colour for samples in four colour centres (green, gray, red and blue) can be reduced by 79%, 55%, 71% and 57% comparing to the real measured colour difference.

- **Dominant colour region segmentation in yarn dyed fabric images**

In Section 4.2, a novel unsupervised approach to detect dominant colour regions standing out conspicuously in yarn dyed fabric images is proposed. A probabilistic model is first proposed to associate colours of dominant colour regions with colours of their yarns. Based on this model, the colour histograms of a dominant colour region are then reconstructed from those of yarns. Finally, a hierarchical segmentation structure is devised to detect dominant colour regions in a yarn dyed fabric image. Experimental results show that the proposed approach achieves satisfactory performance for dominant colour region segmentation in yarn dyed fabric images, with high computational efficiency.

- **Solid-colour and multi-colour region detection in yarn dyed fabric images**

In Section 5.2, an efficient approach that detects solid-colour and multi-colour regions in a real yarn dyed fabric image is presented. A reflection model is first proposed to describe the spectral response of a MSI system to a yarn dyed fabric. The model explains solid-colour and multi-colour regions cannot be distinguished in terms of reflectance, tristimulus values or CIELAB colours owing to the influence of a geometric term. However, chromaticity coordinates are impervious to this term. In addition, chromaticity histograms of a solid-colour region accord with one Gaussian function but those of a multi-colour region agree with a combination of two Gaussian distributions. Simulation results show that chromaticity histograms of a solid-colour region accord with one Gaussian distribution. Experiments on real yarn dyed fabric samples demonstrate that solid-colour and multi-colour region segmentation can be achieved in terms of CIExyY histograms rather than CIEXYZ and CIELAB histograms.

- **Weft and warp yarn segmentation in multi-colour yarn dyed fabrics**

In Section 6.2, we propose an effective method to segment weft and warp yarns in multi-colour yarn dyed fabrics. Interstices between weft and warp yarns are first detected by the image difference method. A modified K-means clustering approach is then utilized to separate weft and warp yarns. Experimental results indicate that the proposed method can segment weft and warp yarns of yarn dyed fabrics with different areal and linear densities, with both high segmentation accuracy and fast running speed.

- **Colour measurement of single yarns**

In Section 7.2, a novel multispectral imaging method that accurately measures colours of single yarns is introduced. A single yarn is first fixed on a black flat platform to keep it stretched during capturing multispectral images. The single yarn is then segmented from background by image difference method. Finally, four methods are investigated to specify the reflectance of the single yarn. Experimental results show that the repeatability and spatial reproducibility of colour measurement of single yarns are 0.1185 and 0.2827 CMC(2:1) units. Experiment on forty-eight solid-colour yarn dyed fabrics and their corresponding single yarns shows that single yarns measured by a MSI system can achieve the same colour matching results as solid-colour yarn dyed fabrics measured by a spectrophotometer.

- **Colour mapping between single yarns and yarn cards**

In Section 8.2, a novel method is proposed to map colour from a single yarn measured by a multispectral imaging system to its corresponding yarn card measured by a spectrophotometer. The relationship between the reflectance of a single yarn and its corresponding yarn card is first modeled. The relationship model shows the reflectance of a yarn card measured by a spectrophotometer is a linear combination of three parts: the reflectance of substrate, the reflectance of the corresponding single yarn measured by a MSI system, and the reflectance square of the single yarn. The simplex method is then employed to find the optimal coefficients in the relationship model. Experiments on 100 pairs of yarn cards and corresponding single yarns show that the colour difference between single yarns and yarn cards reduces from 2.97 to 1.20 CMC(2:1) units for 50 pairs of training samples and from 3.09 to 1.37 CMC(2:1) units for 50 pairs of testing samples.

9.2. Areas of Further Research

- **Reflection model of yarn dyed fabrics**

For the proposed reflection model of yarn dyed fabric in Section 3.2, one assumption is that a yarn dyed fabric is placed on a platform with black colour, i.e., the background colour is black. However, this assumption may not be true for some applications, such as yarn dyed fabrics placed on a white paper. Thus, one of the future work should be the reflection model of yarn dyed fabrics taking background colour into account.

- **Colour region segmentation in yarn dyed fabric image**

While the segmentation method introduced in Chapter 4 can detect dominant colour regions in a yarn dyed fabric image, the proposed method cannot segment small colour regions. The proposed histogram-based segmentation method would yield undersegmentation for this type of images. Another problem of yarn dyed fabric image segmentation is how to accurately define the boundary of a region. Irregular three-dimensional shapes of yarns would cause the boundary of a colour region ambiguous. Segmentation of small colour regions and accurate boundary detection will be part of the future work.

- **Colour specification of single yarns**

While four colour specification methods are proposed in Section 7.2.3 and the lightness weighting method is chosen as the best one, results of this method are influenced by the yarn count of a single yarn. In the future, we will study the method to specify the colour of a single yarn invariant to its yarn count.

- **Colour matching of yarn dyed fabrics**

While Section 7.3.3 introduces the colour matching experiment of single yarns, colour matching of yarn dyed fabrics is not involved, especially colour matching of multi-colour yarn dyed fabrics. However, this kind of experiment needs a great number of standard and batch samples. In order to produce meaningful and comparable results, the ground truth of 'pass' and 'fail' of these samples should be beforehand determined by colour experts with rich colour matching experiences. In the future, colour matching of multi-colour yarn dyed fabric samples will be carried out with the widely use of ICM in textile and garment industries.

- **Coefficients in reflection model**

While a reflection model introduced in Section 3.2 expresses that the colour of a yarn dyed fabric is influenced by the surface texture, occlusion of system illumination, and inter-reflection between yarns, the question how these factors influence the instrumental colour of a yarn dyed fabric needs to be in-depth explored.

References

[1] J. H. Xin. *Total Colour Management in Textiles.* CRC Press, 2006.

[2] R. McDonald. *Colour Physics for Industry.* Society of Dyers and Colourists, 1997.

[3] R. W. G. Hunt. *Measuring Colour.* England: Fountain Press, 1998.

[4] VeriVide. http://www.verivide.com/

[5] Equiptex. http://www.equiptex.com/Lightcab.htm

[6] J. Schanda. *Colourimetry: Understanding the CIE System.* Wiley Interscience, 2007.

[7] CIE Publication 17.4. *International Lighting Vocabulary.* Commission Internationale de l'Eclairage, 1987.

[8] H. Fairman. New terminology for metamerism revisited. *Color Res. Appl. 11(1),* pp. 80-81. 1986.

[9] CIE Publication 15.2. *Colourimetry.* Vienna: Central Bureau of the CIE, 1986.

[10] G. Wyszecki and W. S. Stiles. *Color Science: Concepts and Methods, Quantitative Data and Formulae (Wiley Series in Pure and Applied Optics).* Wiley-Interscience, 2000.

[11] E. J. Giorgianni and T. E. Madden. *Digital Color Management: Encoding Solutions (Wiley-IS&T Series in Imaging Science and Technology).* Wiley, 2009.

[12] R. W. G. Hunt and M. R. Pointer. *Measuring Colour.* WILEY, 2011.

[13] W. Wu, J. Allebach and M. Analoui. Imaging colorimetry using a digital camera. *J. Imaging Sci. Technol. 44(4),* pp. 267-279. 2000.

[14] M. D. Fairchild, M. R. Rosen and G. M. Johnson. Spectral and metameric color imaging. Technical Report, *RIT-MCSL*, 2001.

[15] R. S. Berns, R. J. Motta and M. E. Gorzynski. CRT colorimetry. part I: Theory and practice. *Color Res. Appl. 18(5),* pp. 299-314. 1993.

[16] R. S. Berns, M. E. Gorzynski and R. J. Motta. CRT colorimetry. part II: Metrology. *Color Res. Appl. 18(5),* pp. 315-325. 1993.

[17] J. Mullikin, L. Vanvliet, H. Netten, F. Boddeke, G. Vanderfeltz and I. Young. Methods for CCD Camera Characterization, *Proc. SPIE*, vol.2173, pp.73-84. 1994

[18] M. Pointer, G. Attridge and R. Jacobson. Practical camera characterization for colour measurement. *Imaging Sci. J. 49(2),* pp. 63-80. 2001.

[19] G. Hong, M. Luo and P. Rhodes. A study of digital camera colorimetric characterization based on polynomial modeling. *Color Res. Appl. 26(1),* pp. 76-84. 2001.

[20] K. Barnard and B. Funt. Camera characterization for color research. *Color Res. Appl. 27(3),* pp. 152-163. 2002.

[21] P. Green. "Overview of characterization methods," in *Color Engineering*, P. Green and L. MacDonald, New York: John Wiley & Sons, 2002, .

[22] F. Martinez-Verdu, J. Pujol and P. Capilla. Characterization of a digital camera as an absolute tristimulus colorimeter. *J. Imaging Sci. Technol. 47(4),* pp. 279-295. 2003.

[23] V. Cheung, S. Westland, C. Li, J. Hardeberg and D. Connab. Characterization of trichromatic color cameras by using a new multispectral imaging technique. *J. Opt. Soc. Am. A 22(7),* pp. 1231-1240. 2005.

[24] W. Ji and P. A. Rhodes. Spectral color characterization of digital cameras: A review. *Photonics and Optoelectronics Meetings (Poem) 2011: Optoelectronic Sensing and Imaging.* 2012.

[25] H. L. Shen, C. Weng, H. Wan and J. H. Xin. Correcting cross-media instrument metamerism for reflectance estimation in multispectral imaging. *J. Opt. Soc. Am. A 28(4),* pp. 511-516. 2011.

[26] M. Guenay. Determination of dyeing levelness using surface irregularity function. *Color Res. Appl. 34(4),* pp. 285-290. 2009.

[27] G. Cui, M. Luo, P. Rhodes, B. Rigg and J. Dakin. Grading textile fastness. part 1: Using a digital camera system. *Color. Technol. 119(4),* pp. 212-218. 2003.

[28] G. Cui, M. Luo, P. Rhodes, B. Rigg and J. Dakin. Grading textile fastness. part 2: Development of a new staining fastness formula. *Color. Technol. 119(4),* pp. 219-224. 2003.

[29] G. Cui, M. Luo, B. Rigg, M. Butterworth and J. Dakin. Grading textile fastness. part 3: Development of a new fastness formula for assessing change in colour. *Color. Technol. 120(5),* pp. 226-230. 2004.

[30] G. Cui, M. Luo, B. Rigg, M. Butterworth, N. Maplesden and J. Dakin. Grading textile fastness. part 4: An inter-laboratory trial using DigiEye systems. *Color. Technol. 120(5),* pp. 231-235. 2004.

[31] M. R. Luo, G. H. Cui and C. Li. Apparatus and method for measuring colour (DigiEye system). British patent 0124683.4, 2001.

[32] Lovibond. http://www.lovibond.com

[33] Datacolor. http://www.datacolor.com

[34] J. Y. Hardeberg, F. Schmitt and H. Brettel. Multispectral image capture using a tunable filter. *Proceedings of SPIE, Colour Imaging, Device-Independent Colour, Colour Hardcopy, and Graphic Arts*, 2000.

[35] J. Hardeberg, F. Schmitt and H. Brettel. Multispectral color image capture using a liquid crystal tunable filter. *Opt. Eng. 41(10),* pp. 2532-2548. 2002.

[36] A. Ibrahim, S. Tominaga and T. Horiuchi. Material classification for printed circuit boards by spectral imaging system. *Computational Color Imaging* pp. 216-225. 2009.

[37] A. Ibrahim, S. Tominaga and T. Horiuchi. Spectral imaging method for material classification and inspection of printed circuit boards. *Opt. Eng. 49(5)*, pp. 057201. 2010.

[38] Y. Murakami, M. Yamaguchi and N. Ohyama. Hybrid-resolution multispectral imaging using color filter array. *Opt. Express 20(7),* pp. 7173-7183. 2012.

[39] A. N. Rencz and R. A. Ryerson. *Manual of Remote Sensing Vol. 3, Remote Sensing for the Earth Sciences.* New York: Wiley & Sons, 1999.

[40] S. Hamilton, A. Lowell and R. Lodder. Hyperspectral techniques in analysis of oral dosage forms. *J. Biomed. Opt. 7(4),* pp. 561-570. 2002.

[41] K. Thorp and L. Tian. A review on remote sensing of weeds in agriculture. *Precis. Agric. 5(5),* pp. 477-508. 2004.

[42] A. Ribes, F. Schmitt, R. Pillay and C. Lahanier. Calibration and spectral reconstruction for CRISATEL: An art painting multispectral acquisition system. *J. Imaging Sci. Technol. 49(6),* pp. 563-573. 2005.

[43] D. Nakao, N. Tsumura and Y. Miyake. Real-time multi-spectral image processing for mapping pigmentation in human skin. *Proceedings of Color and Imaging Conference*. 2001.

[44] Y. Murakami, T. Obi, M. Yamaguchi, N. Ohyama and Y. Komiya. Spectral reflectance estimation from multi-band image using color chart. *Opt. Commun. 188(1-4),* pp. 47-54. 2001.

[45] Y. Murakami, T. Obi, M. Yamaguchi and N. Ohyama. Nonlinear estimation of spectral reflectance based on Gaussian mixture distribution for color image reproduction. *Appl. Opt. 41(23),* pp. 4840-4847. 2002.

[46] N. Shimano. Optimization of spectral sensitivities with Gaussian distribution functions for a color image acquisition device in the presence of noise. *Opti. Eng. 45(1),* pp. 13201. 2006.

[47] N. Shimano. Recovery of spectral reflectances of objects being imaged without prior knowledge. *IEEE Trans. Image Process. 15(7),* pp. 1848-1856. 2006.

[48] H. L. Shen, P. Cai, S. Shao and J. H. Xin. Reflectance reconstruction for multispectral imaging by adaptive wiener estimation. *Opt. Express 15(23),* pp. 15545-15554. 2007.

[49] H. L. Shen and J. Xin. Spectral characterization of a color scanner based on optimized adaptive estimation. *J. Opt. Soc. Am. A 23(7),* pp. 1566-1569. 2006.

[50] H. L. Shen, J. H. Xin and S. Shao. Improved reflectance reconstruction for multispectral imaging by combining different techniques. *Opt. Express 15(9),* pp. 5531-5536. 2007.

[51] P. Geladi, J. Burger and T. Lestander. Hyperspectral imaging: Calibration problems and solutions. *Chemometrics Intellig. Lab. Syst. 72(2),* pp. 209-217. 2004.

[52] Caddon printing & imaging GmbH. http://caddon.com/

[53] H. L. Shen, Z. Zheng, W. Wang, X. Du, S. Shao and J. H. Xin. Autofocus for multispectral camera using focus symmetry. *Appl. Opt. 51(14),* pp. 2616-2623. 2012.

[54] S. Shafer. Using color to separate reflection components. *Color Res. Appl.* 10(4), pp.210–218. 1985.

[55] A. Artusi, F. Banterle and D. Chetverikov. A survey of specularity removal methods. *Comput. Graphics Forum 30(8),* pp. 2208-2230. 2011.

[56] S. Mallick, T. Zickler, P. Belhumeur and D. Kriegman. Specularity removal in images and videos: A PDE approach. *Computer Vision - Eccv 2006 , Pt 1, Proceedings 3951* pp. 550-563. 2006.

[57] H. L. Shen and Q. Cai. Simple and efficient method for specularity removal in an image. *Appl. Opt. 48(14),* pp. 2711-2719. 2009.

[58] H. L. Shen, H. Zhang, S. Shao and J. H. Xin. Chromaticity-based separation of reflection components in a single image. *Pattern Recogn. 41(8),* pp. 2461-2469. 2008.

[59] H. L. Shen and Z. Zheng. Real-time highlight removal using intensity ratio. *Appl. Opt. 52(19),* pp. 4483-4493. 2013.

[60] R. Tan and K. Ikeuchi. Separating reflection components of textured surfaces using a single image. *IEEE Trans. Pattern Anal. Mach. Intell. 27(2),* pp. 178-193. 2005.

[61] Q. Yang, S. Wang and N. Ahuja. Real-time specular highlight removal using bilateral filtering. *Computer Vision-Eccv 2010, Pt Iv 6314,* pp. 87-100. 2010.

[62] B. T. Phong. Illumination for computer generated pictures. *Commun ACM 18(6),* pp. 311-317. 1975.

[63] S. Rahman and A. Robles-Kelly. An optimisation approach to the recovery of reflection parameters from a single hyperspectral image. *Comput. Vision Image Understanding 117(12),* pp. 1672-1688. 2013.

[64] A. S. Nery, N. Nedjah and F. M. G. Franca. Efficient hardware implementation of ray tracing based on an embedded software for intersection computation. *J. Syst. Archit. 59(3),* pp. 176-185. 2013.

[65] T. Lin, S. Chen and C. Liu. A Low-Error and Rom-Free Logarithmic Arithmetic Unit for Embedded 3D Graphics Applications. *Proceedings of VLSI-DAT.* 2013.

[66] T. Ichikawa, K. Yamaguchi and Y. Sakamoto. Realistic 3D image reconstruction in CGH with fourier transform optical system. *Practical Holography Xxvii: Materials and Applications 8644.* 2013

[67] F. Sheikh, S. K. Mathew, M. A. Anders, H. Kaul, S. K. Hsu, A. Agarwal, R. K. Krishnamurthy and S. Borkar. A 2.05 GVertices/s 151 mW lighting accelerator for 3D graphics vertex and pixel shading in 32 nm CMOS. *IEEE J. Solid State Circuits 48(1),* pp. 128-139. 2013.

[68] M. Oren and S. K. Nayar. Generalization of lambert's reflectance model. *Proceedings of the 21st Annual Conference on Computer Graphics and Interactive Techniques,* pp. 239. 1994

[69] L. Sharan, C. Liu, R. Rosenholtz and E. H. Adelson. Recognizing materials using perceptually inspired features. *Int. J.of Comput. Vision 103(3),* pp. 348-371. 2013.

[70] E. Angelopoulou and L. Wolff. Sign of gaussian curvature from curve orientation in photometric space. *IEEE Trans. Pattern Anal. Mach. Intell. 20(10),* pp. 1056-1066. 1998.

[71] L. Clarke and B. Werner. Synoptic imaging of nearshore bathymetric patterns. *Journal of Geophysical Research-Oceans 108(C1),* pp. 3005. 2003.

[72] M. Oren and S. K. Nayar. Generalization of the lambertian model and implications for machine vision. *Int. J.of Comput. Vision 14(3),* pp. 227-251. 1995.

[73] R. G. Kuehni and R. T. Marcus. An experiment in visual scaling of small color differences. *Color Res. Appl. 4(2),* pp. 83-91. 1979.

[74] J. H. Xin, C. C. Lam and M. R. Luo. Investigation of texture effect on CRT colour difference evaluation. *Proceedings of AIC 2003, Bangkok,* pp. 60. 2003.

[75] B. Han, G. Cui and M. Luo. Texture effect on evaluation of colour difference. *Proceedings AIC 2003, Bangkok,* pp. 176. 2003.

[76] S. G. Kandi and M. A. Tehran. Investigating the effect of texture on the performance of color difference formulae. *Color Res. Appl. 35(2),* pp. 94-100. 2010.

[77] E. Montag and R. Berns. Lightness dependencies and the effect of texture on suprathreshold lightness tolerances. *Color Res. Appl. 25(4),* pp. 241-249. 2000.

[78] R. Huertas, M. J. Rivas, A. Yebra, M. Del Mar Pérez, M. Melgosa, M. Sánchez-Marañón and E. Hita. Investigation of simulated texture effect on perceived color differences. *Proceedings of AIC 2004, Porto Alegre,* pp.56. 2004.

[79] R. Huertas, M. Melgosa and E. Hita. Parametric factors for colour differences of samples with simulated texture. *Proceedings of AIC 2005, Granada,* pp. 587. 2005.

[80] R. Huertas, M. Melgosa and E. Hita. Influence of random-dot textures on perception of suprathreshold color differences. *J. Opt. Soc. Am. A 23(9),* pp. 2067-2076. 2006.

[81] L. Luo, K. M. Tsang, S. J. Shao and J. H. Xin. How the surface texture of a textile affects its colour. *Proceedings of AIC 2013, Newcastle*. pp. 1329-332. 2013

[82] H. Trussell, J. Lin and R. Shamey. Effects of texture on color perception. *Presented at IVMSP Workshop, 2011 IEEE 10th*. 2011.

[83] AATCC. Evaluation Procedure 1-2007.

[84] S. G. Kandi. The effect of spectrophotometer geometry on the measured colors for textile samples with different textures. *J. Eng. Fiber. Fabr. 6(4),* 2011.

[85] J. C. Bezdek. *Pattern Recognition with Fuzzy Objective Function Algoritms.* New York: Plenum Press, 1981..

[86] J. C. Dunn. A fuzzy relative of the ISODATA process and its use in detecting compact well-separated clusters. *Journal of Cybernetics* (3), pp. 32-57. 1973.

[87] R. Pan, W. Gao and J. Liu. Color clustering analysis of yarn-dyed fabric in HSL color space. *Presented at Software Engineering, 2009. WCSE'09. WRI World Congress on*. 2009.

[88] R. Pan, W. Gao, J. Liu and H. Wang. Automatic detection of the layout of color yarns for yarn dyed fabric via a FCM algorithm. *Text. Res. J. 80(12),* pp. 1222-1231. 2010.

[89] C. Kuo, C. Shih, C. Kao and J. Lee. Color and pattern analysis of printed fabric by an unsupervised clustering method. *Text. Res. J. 75(1),* pp. 9-12. 2005.

[90] H. Cheng, X. Jiang and J. Wang. Color image segmentation based on homogram thresholding and region merging. *Pattern Recogn. 35(2),* pp. 373-393. 2002.

[91] K. Chenaoua, A. Bouridane and F. Kurugollu. Unsupervised histogram based color image segmentation. *Proceedings of ICECS 2003.* 2003.

[92] R. Adams and L. Bischof. Seeded region growing. *IEEE Trans. Pattern Anal. Mach. Intell. 16(6),* pp. 641-647. 1994.

[93] Y. Chang and X. Li. Adaptive image region-growing. *IEEE Trans. Image Process. 3(6),* pp. 868-872. 1994.

[94] M. Spann and R. Wilson. A quad-tree approach to image segmentation which combines statistical and spatial information. *Pattern Recogn. 18(3-4),* pp. 257-269. 1985.

[95] L. Vincent and P. Soille. Watersheds in digital spaces - an efficient algorithm based on immersion simulations. *IEEE Trans. Pattern Anal. Mach. Intell. 13(6),* pp. 583-598. 1991.

[96] L. Najman and M. Schmitt. Geodesic saliency of watershed contours and hierarchical segmentation. *IEEE Trans. Pattern Anal. Mach. Intell. 18(12),* pp. 1163-1173. 1996.

[97] W. Ma and B. Manjunath. EdgeFlow: A technique for boundary detection and image segmentation. *IEEE Trans. Image Process. 9(8),* pp. 1375-1388. 2000.

[98] G. Iannizzotto and L. Vita. Fast and accurate edge-based segmentation with no contour smoothing in 2-D real images. *IEEE Trans. Image Process. 9(7),* pp. 1232-1237. 2000.

[99] J. Gauch. Image segmentation and analysis via multiscale gradient watershed hierarchies. *IEEE Trans. Image Process. 8(1),* pp. 69-79. 1999.

[100] J. Fan, D. Yau, A. Elmagarmid and W. Aref. Automatic image segmentation by integrating color-edge extraction and seeded region growing. *IEEE Trans. Image Process. 10(10),* pp. 1454-1466. 2001.

[101] T. Gevers. Adaptive image segmentation by combining photometric invariant region and edge information. *IEEE Trans. Pattern Anal. Mach. Intell. 24(6),* pp. 848-852. 2002.

[102] J. Fan, X. Zhu and L. Wu. Automatic model-based semantic object extraction algorithm. *IEEE T. Circ. Syst. Vid. 11(10),* pp. 1073-1084. 2001.

[103] A. Tremeau and P. Colantoni. Regions adjacency graph applied to color image segmentation. *IEEE Trans. Image Process. 9(4),* pp. 735-744. 2000.

[104] P. Felzenszwalb and D. Huttenlocher. Efficient graph-based image segmentation. *Int. J.of Comput. Vision 59(2),* pp. 167-181. 2004.

[105] Maria Pertou and Panagiota Bosdogianni. *Image Processing the Fundamentals.* Wiley, 1999.

[106] Maria Pertou and Costas Petrou. *Image Processing the Fundamentals.* Wiley, 2010.

[107] T. Lindeberg. "Edge detection," in *Encyclopedia of Mathematics*, M. Hazewinkel, Ed. Springer, 2001.

[108] T. Lindeberg. Edge detection and ridge detection with automatic scale selection. *Int. J.of Comput. Vision 30(2),* pp. 117-154. 1998.

[109] Committee RA36, Color Measurement Test Methods American Association of Textile Chemists and Colorists, *COLOR TECHNOLOGY in the Textile Industry*. American Association of Textile Chemists and Colorists, 1997.

[110] P. Kubelka and F. Munk, Reflection characteristics of paints, *Zeitschrift Fur Technische Physik* (12), pp. 593-601, 1931.

[111] L. Wilen and B. R. Dasgupta. Spectral bidirectional reflectance distribution function measurements on well-defined textured surfaces: Direct observation of

shadowing, masking, inter-reflection, and transparency effects. *J. Opt. Soc. Am. A 28(11),* pp. 2414-2427. 2011.

[112] B. Funt, M. Drew and J. Ho. Color constancy from mutual reflection. *Int. J. Comput. Vision 6(1),* pp. 5-24. 1991.

[113] K. E. Torrance and E. M. Sparrow. Theory for off-specular reflection from roughened surfaces. *J. Opt. Soc. Am. A 57(9),* pp. 1105-1112. 1967.

[114] J. Xin, H. Shen and C. Lam. Investigation of texture effect on visual colour difference evaluation. *Color Res. Appl. 30(5),* pp. 341-347. 2005.

[115] S. G. Kandi, M. A. Tehran and M. Rahmati. Colour dependency of textile samples on the surface texture. *Color. Technol. 124(6),* pp. 348-354. 2008..

[116] S. Kitaguchi, S. Westland and M. R. Luo. Suitability of texture analysis methods for perceptual texture. *Proceedings of AIC 2005, Granada,* pp. 923. 2005.

[117] S. Shao, J. H. Xin, Y. Zhang and L. M. Zhang. The effect of texture structure on instrumental and visual color difference evaluation. *AATCC Rev. 6(10),* pp. 42-48. 2006.

[118] R. Hunter and R. Harold. *The Measurement of Appearance.* New York: Wiley, 1987

[119] D. Malacara. *Physical Optics and Light Measurements.* Boston: Academic Press, 1988.

[120] T. Akenine-Moller, E. Haines and N. Hoffman. *Real-Time Rendering.* A K Peters/CRC Press, 2008.

[121] A. Kemp. An extension of peirce's cloth geometry to the treatment of non-circular threads. *J. Text. Inst. (49),* pp. 44-48. 1958.

[122] W. Shanahan and J. Hearle, An energy method for calculations in fabric mechanics, part ii: examples of application of the method to woven fabrics, *J. Text. Inst (4),* pp. 92-100, 1978.

[123] J. Sui, L. Ding and C. Song. The discussion of the yarn cross-section shape of woven fabrics. *Silk: Inheritance and Innovation - Modern Silk Road 175-176* pp. 402-407. 2011.

[124] R. McDonald. *Color Physics for Industry.* Society of Dyers and Colorists, 1997

[125] S. Westland, C. Ripamonti and V. Cheung. *Computational Color Science using MATLAB.* Wiley, 2012.

[126] A. R. Robertson. CIE guidelines for coordinated research on colour-difference evaluation. *Color Res. Appl.* 3, pp. 149–151. 1978.

[127] S. Banerjee and A. Roy. *Linear algebra and matrix analysis for statistics*. CRC Press, 2014.

[128] K. Prakash, O. P. Chug and R. S. Dahiya. *Topics in Vector Analysis*. Firewall Media, 2006.

[129] A. Bjorck. *Numerical Methods for Least Squares Problems.* SIAM, 1996.

[130] S. Ghahramani. *Fundamentals of Probability.* Prentice Hall: New Jersey, 1999.

[131] R. John. *Mathematical Statistics and Data Analysis.* Duxbury Press, 1995.

[132] M. L. Eaton. *Multivariate Statistics: A Vector Space Approach,* 53 (2007) 103

[133] F. Kurugollu, B. Sankur and A. Harmanci. Color image segmentation using histogram multithresholding and fusion. *Image Vision Comput. 19(13),* pp. 915-928. 2001.

[134] H. C. Lee. *Introduction to Colour Imaging Science.* Cambridge University Press, 2009

[135] C. Wohler. *3D Computer Vision: Efficient Methods and Applications.* Springer, 2009.

[136] P. Dattalo. *Analysis of Multiple Dependent Variables,* Oxford University Press, 2013

[137] L. Fahrmeir, T Kneib, S Lang and B Marx. *Regression: Models, Methods and Applications*, Springer, 2013

[138] C. M. Bishop. *Pattern Recognition and Machine Learning*. Springer, 2006.

[139] S. Adanur, *Wellington Sears Handbook of Industrial Textiles.* CRC Press, 1995.

[140] D. MacKay. *Information Theory, Inference and Learning Algorithms.* Cambridge University Press, 2003.

[141] G. Hamerly and C. Elkan. Alternatives to the k-means algorithm that find better clusterings. *Proceedings of the Eleventh International Conference on Information and Knowledge Management (CIKM '02),* New York, USA, pp. 600-607. 2002.

[142] B. Mirkin. *Clustering: A Data Recovery Approach.* CRC Press, 2012.

[143] B. Everitt, S. Landau, M. Leese and D. Stahl. *Cluster Analysis.* WILEY, 2011.

[144] M. Honarkhah and J. Caers. Stochastic simulation of patterns using distance-based pattern modeling. *Math Geosci. 42(5),* pp. 487-517. 2010

[145] R. Lleti, M. Ortiz, L. Sarabia and M. Sanchez. Selecting variables for k-means cluster analysis by using a genetic algorithm that optimises the silhouettes. *Anal. Chim. Acta 515(1),* pp. 87-100. 2004.

[146] A. C. Sugar and M. G. James. Finding the number of clusters in a data set: An information theoretic approach. *J. Am. Stat. Assoc.*, pp. 750-763, 2003.

[147] M. Akgun, B. Becerir and H. R. Alpay. Reflectance prediction of colored polyester fabrics by a novel formula. *Fiber. Polym. 15(1),* pp. 126-137. 2014

[148] K. Mathur, A. M. Seyam, D. Hinks and R. A. Donaldson. Towards automation of colour/weave selection in jacquard designs: Model verification through visual assessment. *Color. Technol. 124(1),* pp. 48-55. 2008

[149] H. Gabrijelcic and K. Dimitrovski. Influence of yarn count and warp and weft thread density on colour values of woven surface. *Fibres Text. East. Eur. 12(1),* pp. 32-39. 2004.

[150] H. Gabrijelcic and K. Dimitrovski. Use of regression methods for determining the relation between theoretical-linear and spectrophotometrical colour values of bicolour woven structures. *Color. Technol. 125(2),* pp. 74-85. 2009.

[151] L. Luo, K. M. TSANG, H. L. Shen ,S. J. Shao and J. H. Xin. An investigation of how the texture surface of a fabric influences its instrumental color. *Color Res. Appl.* (submitted)

[152] J, C. Russ. *The Image Processing Handbook,* Fifth Edition. CRC Press, 2006

[153] K. Nassau. *Color for Science, Art and Technology.* North Holland, 1998

[154] G. A. Klein. *Industrial Color Physics*. Springer, 2010.

[155] G. B. Dantzig. Maximization of a linear function of variables subject to linear inequalities. In*: Activity analysis of production and allocation*. Wiley, New York, pp.339–347, 1951

[156] G. B. Dantzig and M. N. Thapa. *Linear programming, 1: introduction*. Springer, New York. 1997

[157] K. G. Murty. *Linear programming*. John Wiley & Sons Inc. 1983

[158] G. B. Dantzig and M. N. Thapa. *Linear Programming 2: Theory and Extensions*. Springer-Verlag. 2003.

[159] M. A. Treiber. *Optimization for Computer Vision: An Introduction to Core Concepts and Methods.* Springer, 2013.